

UCSUS/8.10/279
c.1



COMPONENTS OF INFRARED NET RADIATION IN A MOUNTAIN VALLEY

by

Thomas B. McKee

C. David Whiteman



Atmospheric Science

PAPER NO.

279

CLIMATOLOGY REPORT NO. 77-5

US ISSN 0067-0340

DEPARTMENT OF ATMOSPHERIC SCIENCE
COLORADO STATE UNIVERSITY
FORT COLLINS, COLORADO



" COMPONENTS OF INFRARED NET RADIATION
IN A MOUNTAIN VALLEY "

By

Thomas B. McKee and C. David Whiteman

This report was prepared with support from
Cooperative Agreement No. 16-629-CA with
the U.S. Forest Service, Rocky Mountain
Forest and Range Experiment Station.

Department of Atmospheric Science
Colorado State University
Fort Collins, Colorado 80523

October, 1977

Atmospheric Science Paper No. 279

2

ABSTRACT

The infrared components of the surface radiation budget in a mountain valley have been investigated theoretically. Calculations were based on a set of winter and summer atmospheric soundings specifying temperature and moisture content and for two valley models including a linear valley model and a circularly symmetric valley model. Radiance and irradiance calculations are compared with similar calculations for flat terrain. Downward irradiances at the valley center were shown to be higher than for flat terrain and were due to radiation from the valley sidewalls. The largest effect was obtained for a dry winter atmosphere with the sidewalls warmer than the valley bottom. Downward irradiance was increased by 16% over the flat terrain case and the net irradiance at the valley center was decreased by 24% which would lead to a decreased surface cooling.

Calculations were made for five spectral intervals including the 6.5 micron water band ($4.4 - 7.8\mu$), the water vapor continuum or atmospheric window ($7.8 - 13.4\mu$), the 15 micron carbon dioxide band ($13.4 - 16.3\mu$), a small window ($16.3 - 20.2\mu$), and the rotational water bands ($20.2 - 48.8\mu$). Only the two bands described as windows contribute significantly to the changes in downward irradiance. The remaining three spectral intervals are nearly opaque to transmission of radiation from the valley sidewalls to the valley center.

TABLE OF CONTENTS

	<u>Page</u>
I. INTRODUCTION.....	1
II. RADIATION BACKGROUND.....	4
III. RADIATION ON FLAT TERRAIN.....	7
A. Irradiance Field.....	7
B. Radiance Field.....	19
IV. RADIATION FOR MOUNTAIN VALLEYS.....	30
A. Radiance and Irradiance Field Components for Mountain Valleys.....	30
B. Components of IR Radiation Budget at the Surface.....	54
C. Radiative Cooling in Valley Atmospheres.....	58
V. SUMMARY AND CONCLUSIONS.....	62
VI. REFERENCES.....	67
APPENDICES.....	68
APPENDIX A - Standard Soundings.....	68
1. VAIL DEC ISO.....	68
2. NAVAIR Soundings.....	69
2.1 NAVAIR GJT JAN AVG.....	69
2.2 NAVAIR GJT JAN-3S.....	72
2.3 NAVAIR GJT JAN SAT.....	74
2.4 NAVAIR GJT JUL AVG.....	76
2.5 NAVAIR GJT JUL-3S.....	78
2.6 NAVAIR GJT JUL SAT.....	80
APPENDIX B - Computer Programs.....	82
1. Irradiance Program.....	82
2. Radiance Program.....	84
3. Blackbody Flux Program.....	87
APPENDIX C - Interim Progress Report.....	91

I. INTRODUCTION

Diurnal temperature and wind structure in mountainous terrain are strongly affected by diabatic processes of radiation, conduction, and evaporation. The radiative component is active at the surface and in the free air. The radiative budget at the surface is especially important, since surface temperature affects both conduction and evaporation. Any attempt to predict or understand diurnal temperature changes close to the ground demands a specification of the energy exchanges at the surface. Energy components include infrared and solar irradiances, conduction by the ground, conduction or convection by the atmosphere, and evaporation at the surface. The work of the current effort is to specify and bound the upward and downward infrared irradiances.

The specific objectives of this study are:

1. To conduct a theoretical study of the infrared components of the surface radiation budget in mountainous terrain. The components will be considered for different atmospheric constituents and topographic features.
2. To calculate the magnitude of the atmospheric radiative cooling under winter conditions in a mountain valley.

The method used to attain the first objective consisted of several steps. First--upward and downward infrared irradiances were calculated for flat terrain using an infrared radiative transfer computer program that considers the atmosphere to consist of a number of plane parallel layers of infinite extent. Each calculation requires an atmospheric

temperature, moisture, and CO₂ concentration profile, as well as a surface temperature. Calculations were made using average January and July temperature soundings, a fixed CO₂ mixing ratio, and variable moisture conditions to allow a determination of the limits of the infrared energy components and their variability with moisture content over flat terrain.

Second--once irradiance calculations were obtained for a horizontally homogeneous atmosphere, the infrared irradiance fields for a representative mountain valley were obtained for comparison. In this way the magnitude of the effect of a mountain valley on irradiance fields can be directly compared to a known standard (flat terrain) and the conditions under which the effect is maximized can be obtained.

It is immediately apparent that the horizontal inhomogeneity (i.e., non-finite extent) of air layers within a valley will require irradiances to be calculated from first principles--i.e., they must be calculated from radiance fields. The choice of a symmetrically configured valley greatly reduced the complexity of these calculations. Additionally, irradiance calculations for a mountain valley differed in one important aspect from those over flat terrain; they included a contribution from an extra source--radiating sidewalls. In order to calculate the contribution from this source it was necessary to specify the actual temperature profile along the sidewalls and the transmissivity between the sidewalls and the point where irradiances are desired. Such computations of components to radiance fields naturally require a great deal more computing time and data handling than are required in irradiance calculations, but the results allow a determination of the wavelength dependence and angular dependence of the radiation fields.

Third--combination of the contributions to downward irradiance at the valley floor from the three components:

- (1) the radiating sidewalls
- (2) the air within the valley, and
- (3) the air above the valley

then lead to a total downward irradiance at the valley floor. The infrared energy balance at the surface was then constructed from the component parts to determine downward, upward, and net infrared radiation streams given sidewalls with different radiating temperatures.

The second objective--that of determining the magnitude of atmospheric radiative cooling under winter conditions in a mountain valley--was accomplished qualitatively by calculating atmospheric cooling rates over flat terrain and considering the effect of the addition of mountain sidewalls in producing changes in surface net radiation.

II. RADIATION BACKGROUND

Net radiation at the earth's surface, H_N , is the sum of four components ($SWH\downarrow - SWH\uparrow + LWH\downarrow - LWH\uparrow$) where irradiance, H , is the power per unit area denoted as up or down by arrows and preceded by short wave, SW, or long wave, LW. A positive value for the sum results in surface heating and a negative value in cooling. Irradiances used to determine the net radiation are normally calculated using the theory of radiative transfer with several approximations included. The intent of the current study is to examine the long wave component, particularly the downward long wave component, of the net radiation; consequently the study must begin with the equation of radiative transfer.

Spectral radiance, N_ν , is the radiant energy in a specified wave number interval ($\nu, \nu+d\nu$) which is transported across an element of area ($d\sigma$) in directions confined to an element of solid angle ($d\omega$) during a time period (dt). The energy increment dE_ν is given by

$$dE_\nu = N_\nu d\nu d\sigma d\omega dt \quad (1)$$

and the units of N_ν are joules $\text{cm}^2 \text{sr}^{-1} \text{sec}^{-1}$ which is power per unit wave number per unit area per unit solid angle. Thus radiance is a field property of radiation describing the radiation in a narrow beam in a specified direction. The defining equation for spectral radiance (Goody, 1964) is illustrated in Fig. 1 and given by

$$N_\nu(s) = J_\nu(s_0) \tau_\nu(s, s_0) - \int_{s'=0}^{s'=s_0} J_\nu(s') \frac{\partial \tau_\nu}{\partial s}(s, s') ds' \quad (2)$$

where J_ν is the source term, τ_ν is the transmittance, and s is distance along the path of integration. For infrared long wave calculations in

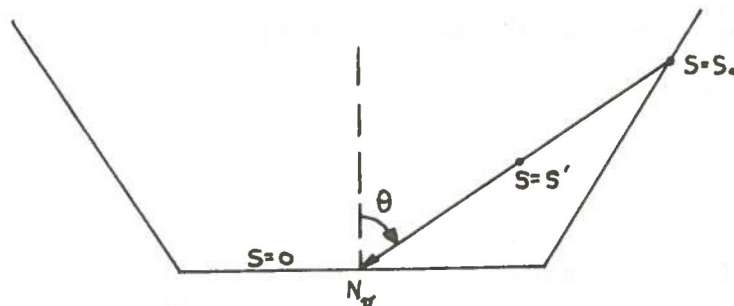


Fig. 1 Radiance in mountain valley.

which scattering and ground reflection are neglected the source term becomes the Planck black body function which is only dependent on temperature.

$$N_\nu(s) = N_\nu(T_0)\tau_\nu(s, s_0) - \int_{s'=0}^{s'=s_0} N_\nu(T) \frac{\partial \tau_\nu}{\partial s'}(s, s') ds' \quad (3)$$

The radiance arriving at the bottom of a valley as depicted in Fig. 1 is composed of two terms. The integral term accounts for the radiation originating in the atmosphere between $s = 0$ and $s = s_0$ from the gases CO_2 and H_2O . The second term is a boundary term which accounts for the radiation emitted by the valley sidewall and transmitted to the valley bottom. For a line of sight which does not intersect the sidewall the boundary term is zero. Radiance calculations at a variety of zenith angles reveal the quantity and origin of radiation reaching the valley bottom.

The definition of spectral irradiance is given in terms of radiance by

$$H_{\nu} = \int N_{\nu} \cos\theta \, d\omega \quad (4)$$

where θ and ω are zenith angle and solid angle. Solid angle is specified by

$$d\omega = \sin\theta \, d\theta \, d\phi \quad (5)$$

with ϕ being an azimuth angle. Spectral irradiance is then a result of integrating spectral radiance over solid angle and is given by

$$H_{\nu} = \int N_{\nu}(T_o) \tau_{\nu}(s, s_o) \cos\theta \, d\omega - \int_{s'=0}^{s'=s_o} \int N_{\nu}(T) \frac{\partial \tau_{\nu}}{\partial s'}(s, s') \, ds' \, d\omega \quad (6)$$

Total irradiance is obtained by integrating spectral irradiance over wave number as

$$H = \int_0^{\infty} H_{\nu} \, d\nu \quad (7)$$

Calculations presented in following sections include spectral radiances, spectral irradiance, and total irradiances which illustrate the changes in the radiation field due to the valley topography.

III. RADIATION ON FLAT TERRAIN

As a first step in determining the effect of a mountain valley on components of infrared net radiation, a set of mean January and July atmospheric soundings were obtained and utilized in a radiative transfer computer program that calculated irradiance fields over flat terrain. Subsequently, using another radiative transfer program, longwave spectral radiances were resolved from this irradiance field in order to investigate the angular and spectral components. In this section we present the results of an analysis of the radiance and irradiance fields over flat terrain; in subsequent sections these calculations will be used as a standard against which we can determine the effect of introducing valley topography into the radiation model.

A. Irradiance Field

First, irradiances were calculated for a horizontally homogeneous atmosphere for 6 specified soundings obtained from averaged Grand Junction, Colorado radiosonde data. The soundings included a mean January and July sounding, a dry January and July sounding, and a saturated January and July sounding. The soundings, consisting of temperature and water vapor mixing ratio curves as a function of pressure, are presented in Appendix A. Details of the computer program used to calculate irradiances was described by Cox et al. (1976) and is summarized in Appendix B. The results of the calculations are shown in Figs. 2-7, including information on the longwave downward and upward fluxes, the net longwave flux, and the atmospheric heating rate in degrees Celsius per day. Computer printouts of the actual computer-generated data are presented in Tables 1-6.

NAVAIR JAN GJT AVG

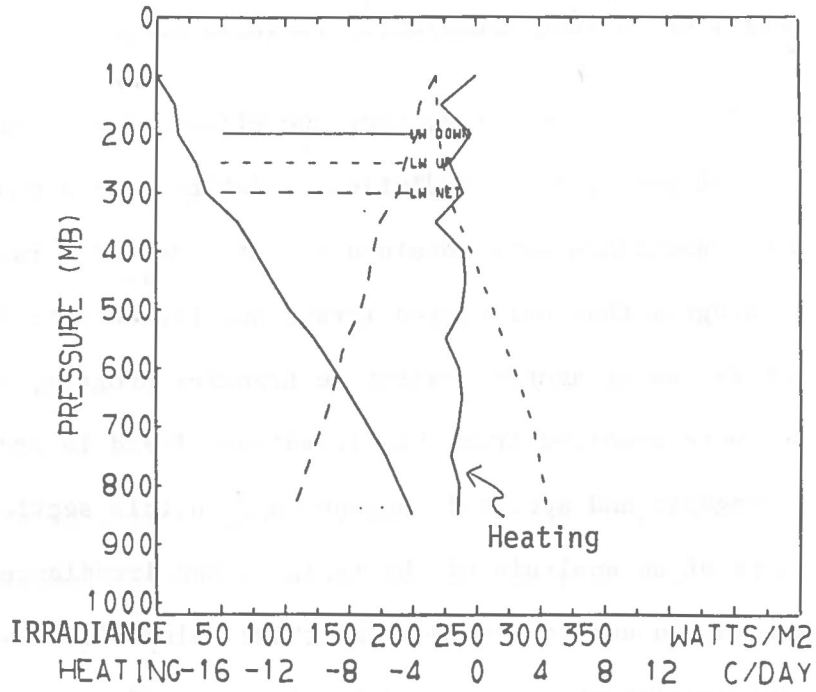


Fig. 2 Program IRRADLON results for average January Grand Junction sounding.

NAVAIR JAN GJT -3S

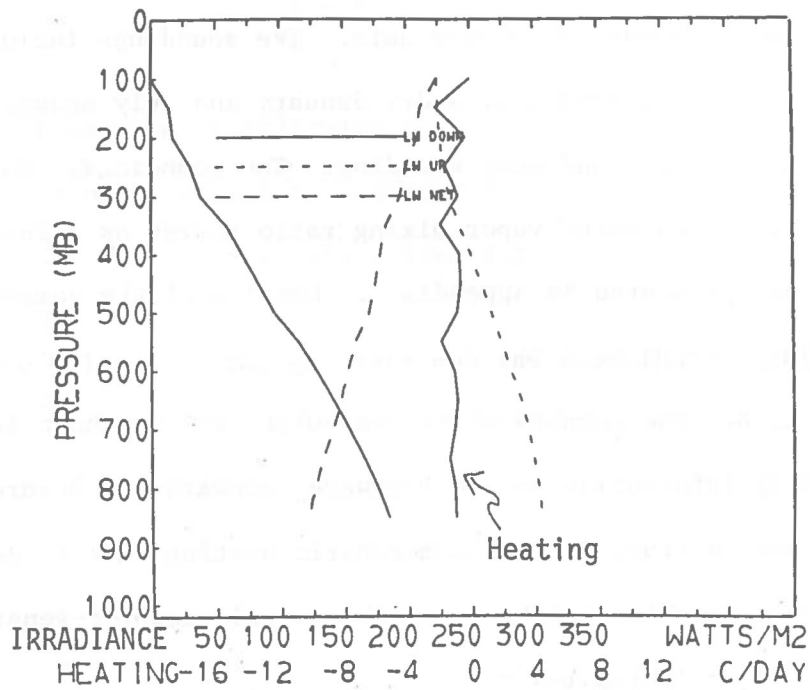


Fig. 3 Program IRRADLON results for dry January Grand Junction sounding.

NAVAIR JAN GJT SAT

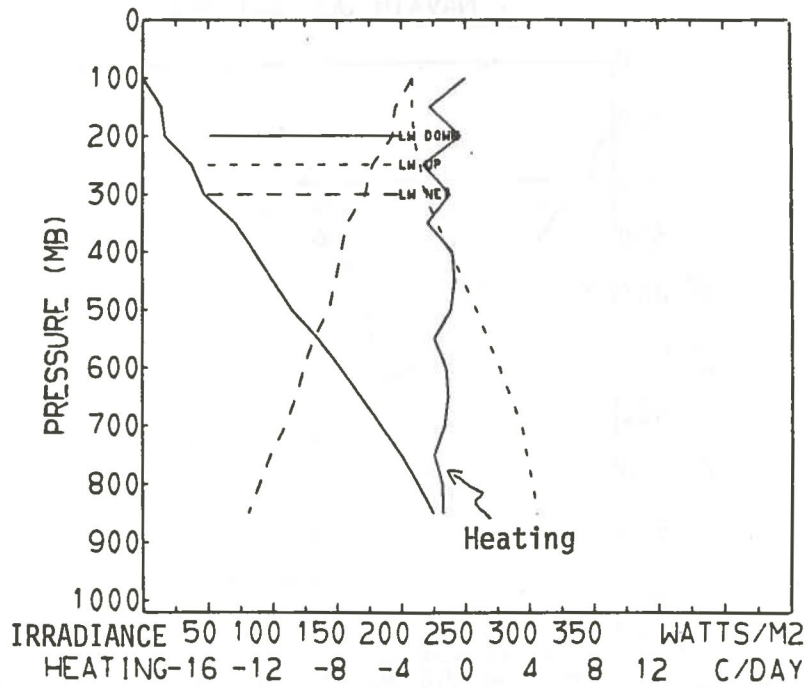


Fig. 4 Program IRRADLON results for saturated January Grand Junction sounding.

ing.

ling.

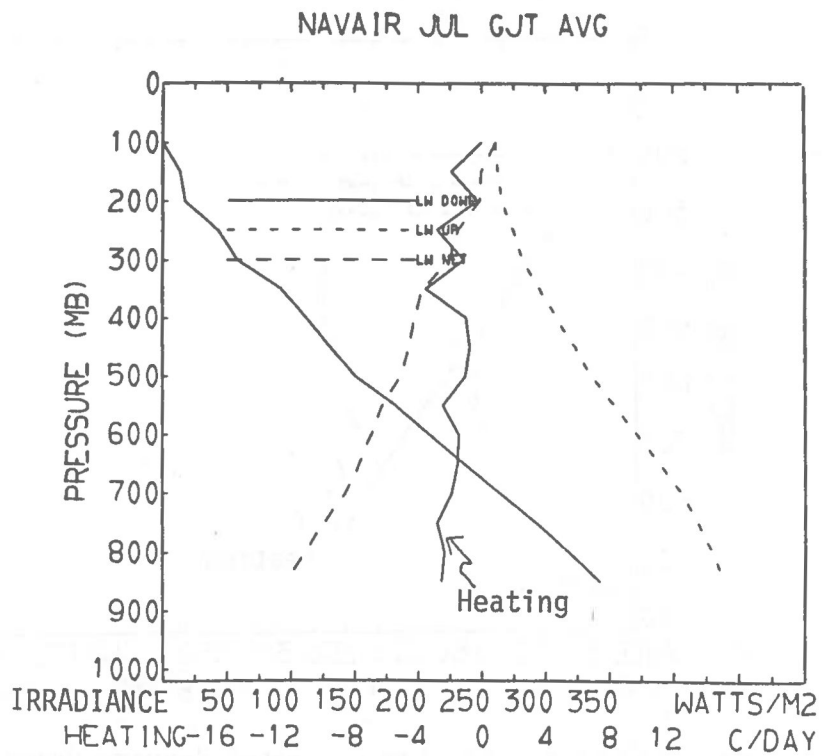


Fig. 5 Program IRRADLON results for average July Grand Junction sounding.

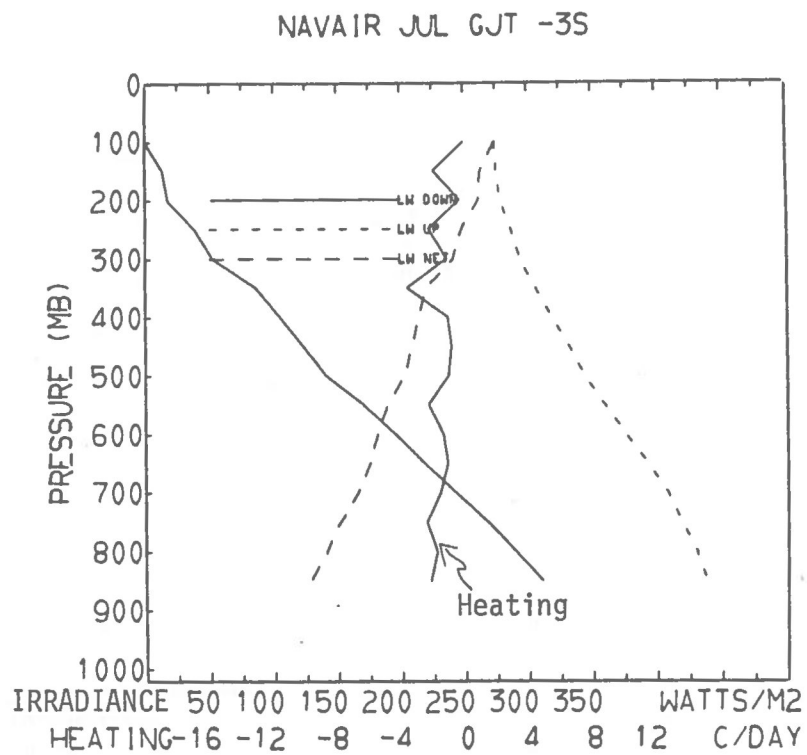


Fig. 6 Program IRRADLON results for dry July Grand Junction sounding.

NAVAIR JUL GJT SAT

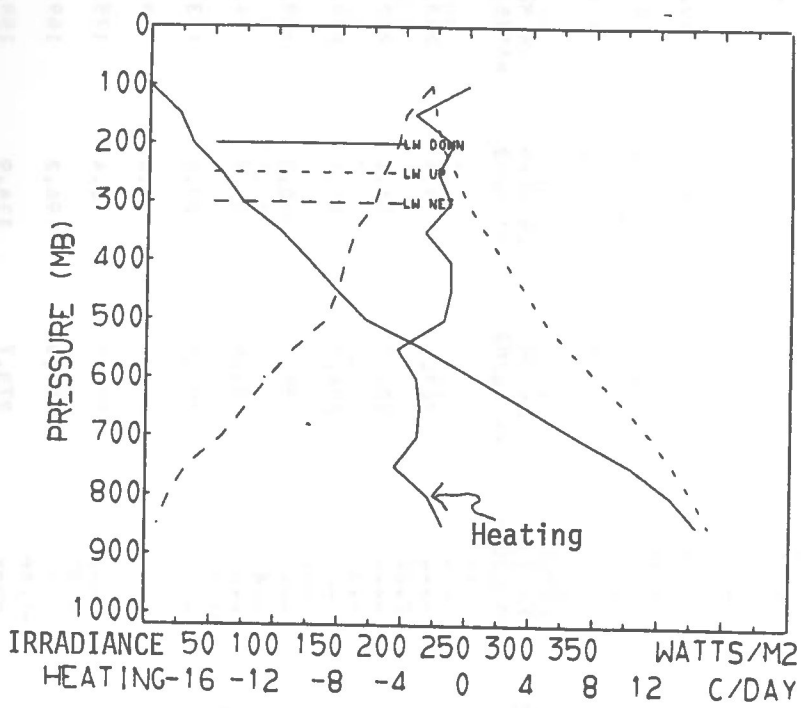


Fig. 7 Program IRRADLON results for saturated July Grand Junction sounding.

ing.

Table 1.

NAVAID JAN GJT -3S			INPUT DATA		
PRESSURE MB	TEMPERATURE DEG C	W H2O G/KG	W O3 UG/G	W CO2 G/KG	U H2O ATM CM
100.0	-61.0	.001	-0.000	.486	0.000
200.0	-57.4	.001	-0.000	.486	.000
300.0	-47.2	.050	-0.000	.486	.000
500.0	-22.2	.330	-0.000	.486	.041
700.0	-7.0	1.000	-0.000	.486	.177
850.0	-2.2	1.200	-0.000	.486	.233

12

HEIGHT METERS	TEMPERATURE DEG C	W H2O G/KG	W O3 UG/G	W CO2 G/KG	U H2O ATM CM
14581.0	-61.0	.001	-0.000	.486	0.000
12051.7	-59.2	.001	0.000	.486	.000
10241.7	-57.4	.001	-0.000	.486	.000
8815.6	-52.3	.025	0.000	.486	.001
7623.3	-47.2	.050	-0.000	.486	.003
6589.6	-41.0	.120	0.000	.486	.012
5669.6	-34.7	.190	0.000	.486	.022
4836.5	-28.5	.260	0.000	.486	.032
4072.0	-22.2	.330	-0.000	.486	.041
3366.2	-18.4	.497	0.000	.486	.075
2712.1	-14.6	.665	0.000	.486	.109
2101.4	-10.8	.832	0.000	.486	.143
1527.7	-7.0	1.000	-0.000	.486	.177
988.0	-5.4	1.067	0.000	.486	.233
480.0	-3.8	1.133	0.000	.486	.289
0.0	-2.2	1.200	-0.000	.486	.346

Table 2.

IRADLON

06/02/77

PRESSURE MB	LAYER HEATING DEG C/DAY	LW UP WATTS/M2	LW DOWN WATTS/M2	LW NET WATTS/M2
100.0	----	223.8	0.0	223.8
150.0	-2.20	224.7	14.0	210.8
200.0	-.31	226.0	17.1	208.9
250.0	-1.61	229.7	30.3	199.4
300.0	-.80	233.4	38.7	194.6
350.0	-1.91	241.5	58.2	183.3
400.0	-.73	250.0	71.0	178.9
450.0	-.65	258.5	83.4	175.1
500.0	-.89	266.0	96.2	169.8
550.0	-1.86	273.7	114.9	158.8
600.0	-1.06	281.5	129.0	152.5
650.0	-.87	289.1	141.8	147.3
700.0	-1.05	295.6	154.5	141.1
750.0	-1.39	299.5	166.6	132.9
800.0	-1.04	303.1	176.4	126.7
850.0	-.99	305.9	185.0	120.9

480.0	-3.8	1.133	0.000	.486	.284
0.0	-2.2	1.200	-0.000	.486	.346

Table 2.

NAVAID JAN GJT AVG

INPUT DATA

PRESSURE MB	TEMPERATURE DEG C	W H2O G/KG	W O3 UG/G	W CO2 G/KG
100.0	-61.0	.001	-0.000	.486
200.0	-57.4	.001	-0.000	.486
300.0	-47.2	.050	-0.000	.486
500.0	-22.2	.600	-0.000	.486
700.0	-7.0	1.700	-0.000	.486
850.0	-2.2	2.400	-0.000	.486

13

HEIGHT METERS	TEMPERATURE DEG C	W H2O G/KG	W O3 UG/G	W CO2 G/KG	U H2O ATM CM
14582.9	-61.0	.001	-0.000	.486	0.000
12053.6	-59.2	.001	0.000	.486	.000
10243.6	-57.4	.001	-0.000	.486	.000
8817.5	-52.3	.025	0.000	.486	.001
7625.1	-47.2	.050	-0.000	.486	.003
6591.4	-41.0	.188	0.000	.486	.019
5671.4	-34.7	.325	0.000	.486	.036
4838.3	-28.5	.462	0.000	.486	.052
4073.6	-22.2	.600	-0.000	.486	.069
3367.7	-18.4	.875	0.000	.486	.128
2713.4	-14.6	1.150	0.000	.486	.186
2102.5	-10.8	1.425	0.000	.486	.245
1528.5	-7.0	1.700	-0.000	.486	.304
988.6	-5.4	1.933	0.000	.486	.408
480.4	-3.8	2.167	0.000	.486	.513
0.0	-2.2	2.400	-0.000	.486	.617

000.0

-.99

305.9

185.0

120.9

850.0

IRADLON

06/02/77

PRESSURE MB	LAYER HEATING DEG C/DAY	LW UP WATTS/M2	LW DOWN WATTS/M2	LW NET WATTS/M2
100.0	----	218.8	0.0	218.8
150.0	-2.20	219.7	14.0	205.7
200.0	-.32	220.9	17.1	203.8
250.0	-1.63	224.5	30.3	194.1
300.0	-.84	227.9	38.7	189.2
350.0	-2.53	236.6	62.5	174.2
400.0	-.83	245.7	76.5	169.3
450.0	-.70	254.9	89.8	165.1
500.0	-.90	262.9	103.2	159.8
550.0	-1.94	271.1	122.9	148.3
600.0	-1.09	279.5	137.7	141.8
650.0	-.93	287.7	151.4	136.3
700.0	-1.12	294.7	165.0	129.6
750.0	-1.60	298.9	178.7	120.2
800.0	-1.12	302.9	189.3	113.5
850.0	-1.20	305.9	199.5	106.4

Table 3.

NAVAID JAN GJT SAT			INPUT DATA		
PRESSURE MB	TEMPERATURE DEG C	W H2O G/KG	W O3 UG/G	W CO2 G/KG	
100.0	-61.0	.001	-0.000	.486	.486
200.0	-57.4	.001	-0.000	.486	.486
300.0	-47.2	.150	-0.000	.486	.486
500.0	-22.2	1.300	-0.000	.486	.486
700.0	-7.0	3.200	-0.000	.486	.486
850.0	-2.2	3.700	-0.000	.486	.486

14

HEIGHT METERS	TEMPERATURE DEG C	W H2O G/KG	W O3 UG/G	W CO2 G/KG	U H2O ATM CM
14586.8	-61.0	.001	-0.000	.486	0.000
12057.4	-59.2	.001	0.000	.486	.000
10247.4	-57.4	.001	-0.000	.486	.000
8821.3	-52.3	.075	0.000	.486	.004
7628.9	-47.2	.150	-0.000	.486	.008
6595.1	-41.0	.437	0.000	.486	.045
5674.9	-34.7	.725	0.000	.486	.082
4841.5	-28.5	1.012	0.000	.486	.119
4076.6	-22.2	1.300	-0.000	.486	.156
3370.3	-18.4	1.775	0.000	.486	.271
2715.6	-14.6	2.250	0.000	.486	.385
2104.3	-10.8	2.725	0.000	.486	.500
1529.8	-7.0	3.200	-0.000	.486	.615
989.4	-5.4	3.367	0.000	.486	.791
480.8	-3.8	3.533	0.000	.486	.967
0.0	-2.2	3.700	-0.000	.486	1.143

Table 4.

IRADLON

06/02/77

PRESSURE MB	LAYER HEATING DEG C/DAY	LW UP WATTS/M2	LW DOWN WATTS/M2	LW NET WATTS/M2
100.0	----	208.4	0.0	208.4
	-2.21			
150.0	----	209.2	14.0	195.3
	-.33			
200.0	----	210.4	17.1	193.3
	-2.66			
250.0	----	214.7	37.2	177.5
	-.96			
300.0	----	218.8	47.0	171.8
	-2.36			
350.0	----	228.5	70.6	157.9
	-.81			
400.0	----	238.7	85.6	153.1
	-.69			
450.0	----	249.0	100.0	149.0
	-.94			
500.0	----	258.2	114.8	143.4
	-1.94			
550.0	----	267.3	135.4	131.9
	-1.25			
600.0	----	276.5	152.1	124.5
	-1.11			
650.0	----	285.7	167.8	117.9
	-1.34			
700.0	----	293.6	183.7	109.9
	-1.95			
750.0	----	298.2	199.9	98.4
	-1.47			
800.0	----	302.6	212.9	89.7
	-1.43			
850.0	----	305.9	224.7	81.2

480.8

-3.0

3.700

-0.000

.486

1.143

0.0

-2.2

Table 4.

NAVAID JUL GJT -3S

INPUT DATA

PRESSURE MB	TEMPERATURE DEG C	W H2O G/KG	W O3 UG/G	W CO2 G/KG
100.0	-66.1	.001	-0.000	.486
200.0	-53.8	.001	-0.000	.486
300.0	-34.4	.110	-0.000	.486
500.0	-8.1	1.400	-0.000	.486
700.0	14.1	4.000	-0.000	.486
850.0	23.5	5.400	-0.000	.486

15

HEIGHT METERS	TEMPERATURE DEG C	W H2O G/KG	W O3 UG/G	W CO2 G/KG	U H2O ATM CM
15162.3	-66.1	.001	-0.000	.486	0.000
12669.7	-60.0	.001	0.000	.486	.000
10848.7	-53.8	.001	-0.000	.486	.000
9384.5	-44.1	.055	0.000	.486	.003
8136.2	-34.4	.110	-0.000	.486	.006
7043.7	-27.8	.432	0.000	.486	.044
6071.4	-21.3	.755	0.000	.486	.083
5190.9	-14.7	1.077	0.000	.486	.121
4382.9	-8.1	1.400	-0.000	.486	.160
3634.7	-2.6	2.050	0.000	.486	.298
2937.2	3.0	2.700	0.000	.486	.435
2282.3	8.5	3.350	0.000	.486	.573
1663.7	14.1	4.000	-0.000	.486	.711
1078.7	17.2	4.467	0.000	.486	.951
525.5	20.3	4.933	0.000	.486	1.190
0.0	23.4	5.400	-0.000	.486	1.430

IRADLON

06/02/77

PRESSURE MB	LAYER HEATING DEG C/DAY	LW UP WATTS/M2	LW DOWN WATTS/M2	LW NET WATTS/M2
100.0	----	274.2	0.0	274.2
	-1.91			
150.0	----	276.3	13.5	262.9
	-.26			
200.0	----	279.1	17.7	261.4
	-2.22			
250.0	----	287.0	38.7	248.2
	-1.12			
300.0	----	294.0	52.4	241.6
	-3.61			
350.0	----	306.2	86.0	220.2
	-1.06			
400.0	----	319.0	105.0	213.9
	-.80			
450.0	----	332.1	122.9	209.2
	-.99			
500.0	----	344.3	141.0	203.3
	-2.28			
550.0	----	360.2	170.4	189.8
	-1.37			
600.0	----	376.8	195.1	181.7
	-1.09			
650.0	----	393.5	218.3	175.2
	-1.55			
700.0	----	408.5	242.5	166.0
	-2.42			
750.0	----	419.7	268.1	151.6
	-1.80			
800.0	----	430.5	289.5	141.0
	-2.21			
850.0	----	438.9	311.0	127.9

Table 5.

NAVAID JUL GJT AVG			INPUT DATA	
PRESSURE MB	TEMPERATURE DEG C	W H2O G/KG	W O3 UG/G	W CO2 G/KG
100.0	-66.1	.001	-0.000	.486
200.0	-53.8	.001	-0.000	.486
300.0	-34.4	.200	-0.000	.486
500.0	-8.1	2.200	-0.000	.486
700.0	14.1	6.000	-0.000	.486
850.0	23.5	7.300	-0.000	.486

9T

HFIGHT METERS	TEMPERATURE DEG C	W H2O G/KG	W O3 UG/G	W CO2 G/KG	U H2O ATM CM
15167.6	-66.1	.001	-0.000	.486	0.000
12674.9	-60.0	.001	0.000	.486	.000
10853.9	-53.8	.001	-0.000	.486	.000
9389.7	-44.1	.100	0.000	.486	.005
8141.4	-34.4	.200	-0.000	.486	.010
7048.8	-27.8	.700	0.000	.486	.072
6076.3	-21.3	1.200	0.000	.486	.133
5195.5	-14.7	1.700	0.000	.486	.194
4387.1	-8.1	2.200	-0.000	.486	.255
3638.5	-2.6	3.150	0.000	.486	.464
2940.5	3.0	4.100	0.000	.486	.674
2285.0	8.5	5.050	0.000	.486	.883
1665.6	14.1	6.000	-0.000	.486	1.092
1080.0	17.2	6.433	0.000	.486	1.431
526.1	20.3	6.867	0.000	.486	1.771
0.0	23.4	7.300	-0.000	.486	2.110

Table 6

NAVAID JUL GJT SAT

INPUT DATA

PRESSURE MB	LAYER HEATING DEG C/DAY	LW UP WATTS/M2	LW DOWN WATTS/M2	LW NET WATTS/M2
100.0	----	260.9	0.0	260.9
150.0	-1.91	263.0	13.5	249.6
200.0	-.27	265.7	17.7	248.0
250.0	-2.84	274.5	43.3	231.1
300.0	-1.16	282.3	58.1	224.2
350.0	-3.53	295.3	92.0	203.3
400.0	-1.03	309.1	111.9	197.2
450.0	-.80	323.2	130.8	192.4
500.0	-1.06	336.4	150.2	186.1
550.0	-2.46	353.7	182.2	171.5
600.0	-1.45	371.7	208.8	162.9
650.0	-1.54	389.9	236.2	153.7
700.0	-1.93	406.3	264.0	142.3
750.0	-2.83	418.4	292.9	125.5
800.0	-2.38	430.0	318.5	111.5
850.0	-2.55	438.9	342.5	96.3

0.0

23.4

7.300

-0.000

.486

2.110

Table 6.

NAVAID JUL GJT SAT

INPUT DATA

```

*****
PRESSURE      TEMPERATURE      W H2O      W O3      W CO2
  MB           DEG C           G/KG       UG/G       G/KG
100.0         -66.1           .001       -0.000     .486
200.0         -53.8           .100       -0.000     .486
300.0         -34.4           .700       -0.000     .486
500.0          -8.1           4.200      -0.000     .486
700.0          14.1          15.000     -0.000     .486
850.0          23.5          22.100     -0.000     .486

```

```

HEIGHT      TEMPERATURE      W H2O      W O3      W CO2      U H2O
METERS      DEG C           G/KG       UG/G       G/KG       ATM CM
15191.2     -66.1           .001       -0.000     .486       0.000
12698.6     -60.0           .050       0.000     .486       .003
10877.5     -53.8           .100       -0.000     .486       .005
 9413.1     -44.1           .400       0.000     .486       .026
 8164.5     -34.4           .700       -0.000     .486       .046
 7071.4     -27.8           1.575      0.000     .486       .171
 6098.3     -21.3           2.450      0.000     .486       .296
 5216.7     -14.7           3.325      0.000     .486       .421
 4407.4      -8.1           4.200     -0.000     .486       .546
 3657.5      -2.6           6.900      0.000     .486       1.036
 2957.6       3.0           9.600      0.000     .486       1.526
 2299.6       8.5          12.300      0.000     .486       2.015
 1677.3      14.1          15.000     -0.000     .486       2.505
 1088.2      17.2          17.367      0.000     .486       3.452
  530.3      20.3          19.733      0.000     .486       4.398
   0.0      23.4          22.100     -0.000     .486       5.344

```

IRADLON

06/02/77

PRESSURE MB	LAYER HEATING DEG C/DAY	LW UP WATTS/M2	LW DOWN WATTS/M2	LW NET WATTS/M2
100.0	----- -3.38	220.3	0.0	220.3
150.0	----- -.94	224.3	23.9	200.3
200.0	----- -1.90	228.5	33.8	194.7
250.0	----- -1.12	239.7	56.2	183.5
300.0	----- -2.67	249.9	73.1	176.8
350.0	----- -1.10	264.4	103.4	161.0
400.0	----- -1.05	279.7	125.2	154.5
450.0	----- -1.47	295.4	147.1	148.3
500.0	----- -4.35	309.9	170.3	139.6
550.0	----- -3.20	330.6	216.8	113.8
600.0	----- -2.94	352.7	257.9	94.9
650.0	----- -3.11	375.2	297.8	77.4
700.0	----- -4.51	395.1	336.2	59.0
750.0	----- -2.42	411.4	379.1	32.2
800.0	----- -1.48	427.1	409.3	17.8
850.0	-----	438.9	429.8	9.1

Summarizing the results of the computer runs we see that, in winter, downward irradiances at the surface range from 185 to 225 Wm^{-2} while in summer, they range from 311 to 439 Wm^{-2} . The highest seasonal downward irradiances are associated with the moister soundings. Since a drier atmosphere is less opaque, more of the downward-coming radiation originates higher in the atmosphere, where temperatures are colder. These result in relatively low downward irradiances. It is apparent from the calculations that the maximum differences in downward irradiances between a mountain valley case and a flat terrain case will occur with the drier soundings since, in this case, a larger relative contribution can come from the radiating sidewalls, and the contribution from the air mass within the valley is minimized.

Upward irradiances at the surface remain fixed for the January and July soundings by virtue of the fixed radiating temperature of the ground surface. In both the January and July soundings the upward irradiances (fluxes) decrease with height. This decrease is more rapid in the moister soundings but is much less pronounced in the winter soundings where precipitable water values are low. Note that precipitable water values are given for each of the soundings in Appendix A.

As a result of the near-uniform rates of decrease of upward and downward irradiances as a function of height, net radiation is a near-linear increasing function of height. Surface values of net radiation as calculated by the computer program for the winter soundings range from 81 to 121 Wm^{-2} . In summer they range from 9 to 128 Wm^{-2} . The biggest relative changes in net radiation at the surface from summer to winter occur with the relatively unrealistic saturated soundings. Note

that the soundings utilized in the radiative transfer programs do not contain clouds; calculations are for clear atmospheres only.

Atmospheric cooling rates in the reference atmospheres are generally about 1°C/day at all levels in the winter soundings and 2°C/day in the summer soundings. Enhanced cooling of the lower levels of the soundings, however, occur when water vapor contents are high.

B. Radiance Field

In order to ascertain the contributions from various spectral intervals, zenith angles, and layers of the atmosphere to the surface irradiance over flat terrain, the average and dry January and July soundings were utilized in a second radiative transfer program called PROGRAM RADLON. A description of this program has been given by Cox et al. (1976) and their description is summarized in Appendix B. In short, the computer program is a spectral infrared radiative transfer program that allows radiances to be calculated for any zenith angle and spectral interval of interest. The spectral intervals chosen for these calculations correspond to major absorption bands of CO₂ and water vapor and are presented below in Table 7. The actual delineation of the edges of the individual bands was accomplished in mountain valley calculations for a special isothermal atmosphere, as described later in this report.

Results of the calculations are illustrated in Figs. 8 through 27. In these figures cumulative energy fraction is plotted against pressure for the January and July average and dry soundings, the 5 spectral bands and 4 viewing angles. The abscissas of the figures, labeled cumulative energy fraction, enable one to determine the fraction of the radiance arriving at the ground from various viewing angles that comes from

Table 7. Spectral Intervals Utilized in Calculations

Band No.	Wavelength (microns)	Wavenumber (cm ⁻¹)	Band
1	4.4- 7.8	1285-2265	H ₂ O
2	7.8-13.4	745-1285	H ₂ O continuum
3	13.4-16.3	615-745	CO ₂
4	16.3-20.2	495-615	Small window
5	20.2-48.8	205-495	H ₂ O rotation
All	4.4-48.8	205-2265	--

different layers of the atmosphere. An example of the use of these figures is provided by Fig. 11. Here for an average January sounding we see that for an 80° viewing angle approximately 90% of the energy reaching the surface in the 16.3 - 20.2 micron band comes from the layer extending from the surface to about 780 mb. Thus most of the energy at this viewing angle comes from the lowest 70 mb of the atmosphere. For the 0° viewing angle (i.e., looking straight up) 90% of the radiance reaching the surface comes from the layer extending from the surface to 675 mb, i.e., the lowest 175 mb of the sounding. In bands 1, 3, and 5 (Figs 8, 10 and 12) most of the radiance reaching the surface comes from the 100 mb layer nearest the surface. Bands 2 and 4 have significant percentages of their radiance come from higher levels of the atmosphere-- i.e., atmospheric transmittance is greater in these bands. In the drier soundings, e.g. compare Figs. 13 - 17, more of the radiation reaching the surface in all bands comes from higher atmospheric levels. The figures suggest that, in future computations of radiance fields within mountain valleys, atmospheric characteristics within the valley will be of

primary importance and the contribution to radiance fields from high atmospheric levels will be slight.

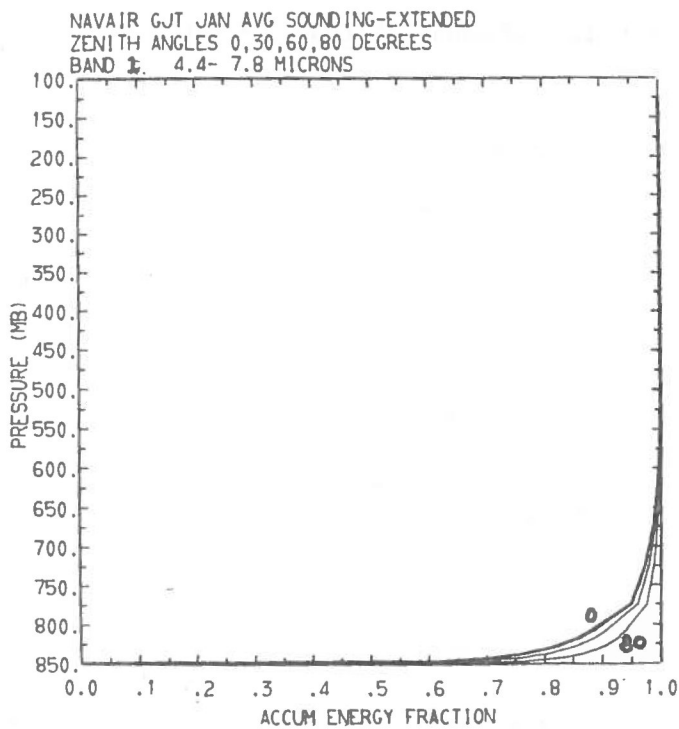


Fig. 8 Cumulative fraction of energy received at the ground from various pressure levels for given zenith angles and wavelength bands.

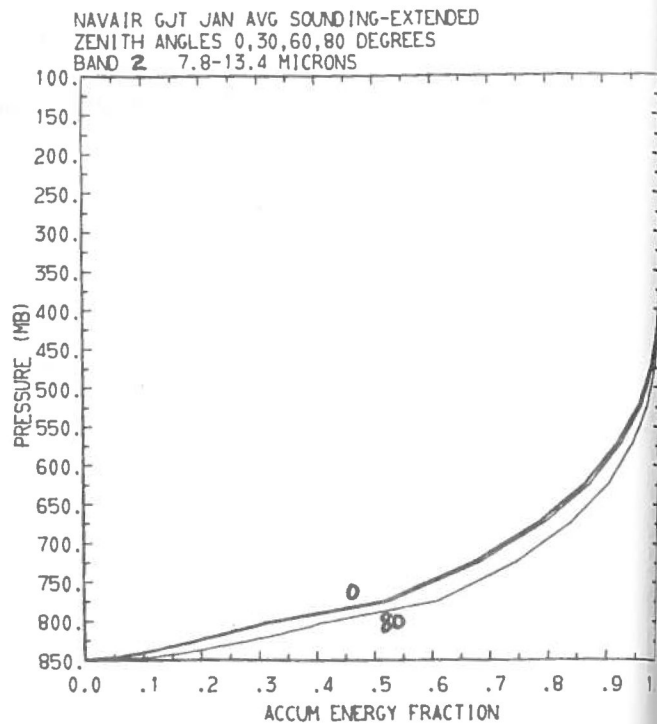


Fig. 9 Same as Fig. 8

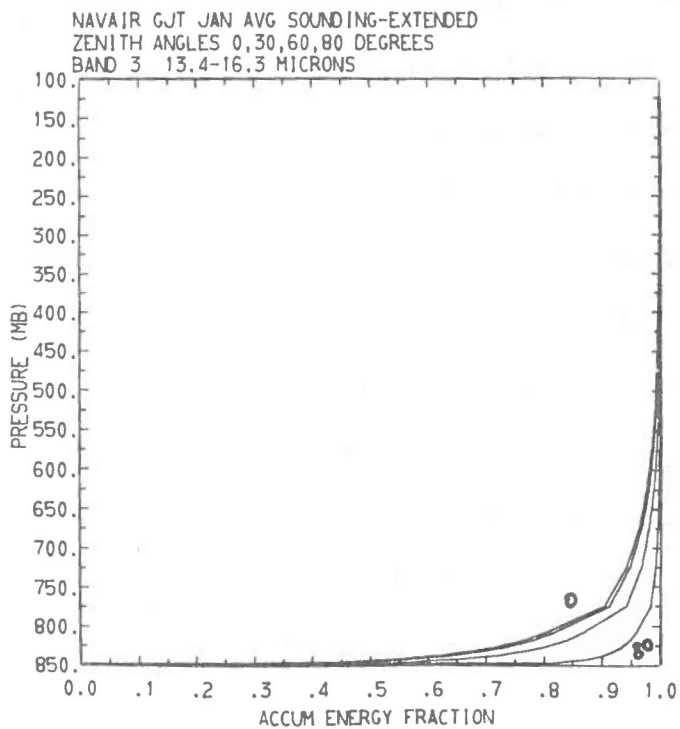


Fig. 10 Same as Fig. 8

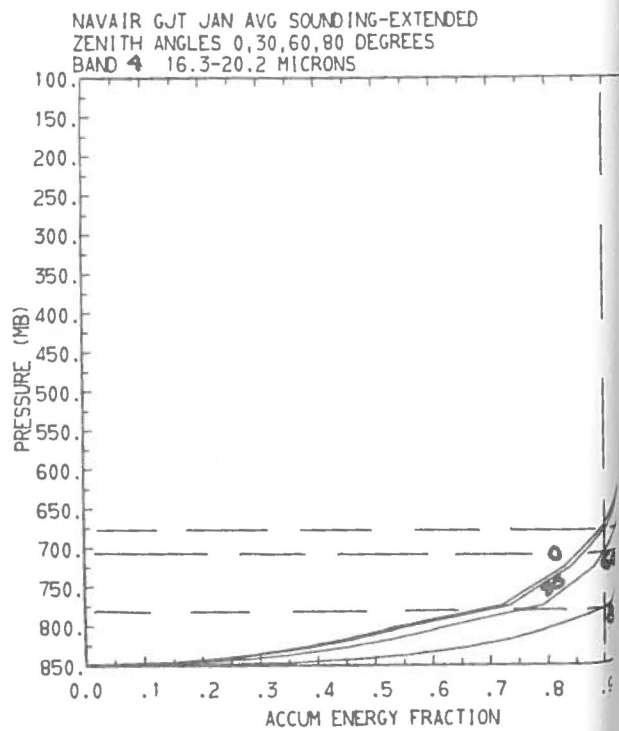


Fig. 11 Same as Fig. 8

NAVAIR GJT JAN AVG SOUNDING-EXTENDED
 ZENITH ANGLES 0,30,60,80 DEGREES
 BAND 5 20.2-48.8 MICRONS

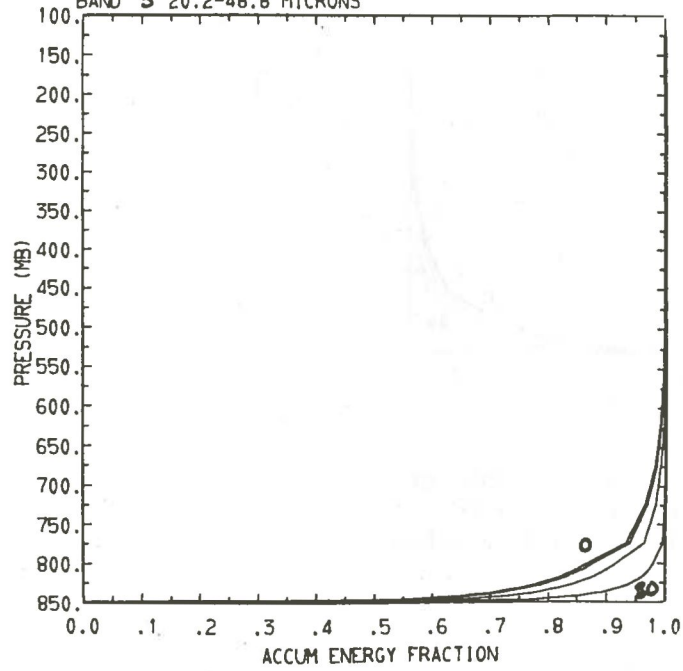


Fig. 12 Cumulative fraction of energy received at the ground from various pressure levels for given zenith angles and wavelength bands.

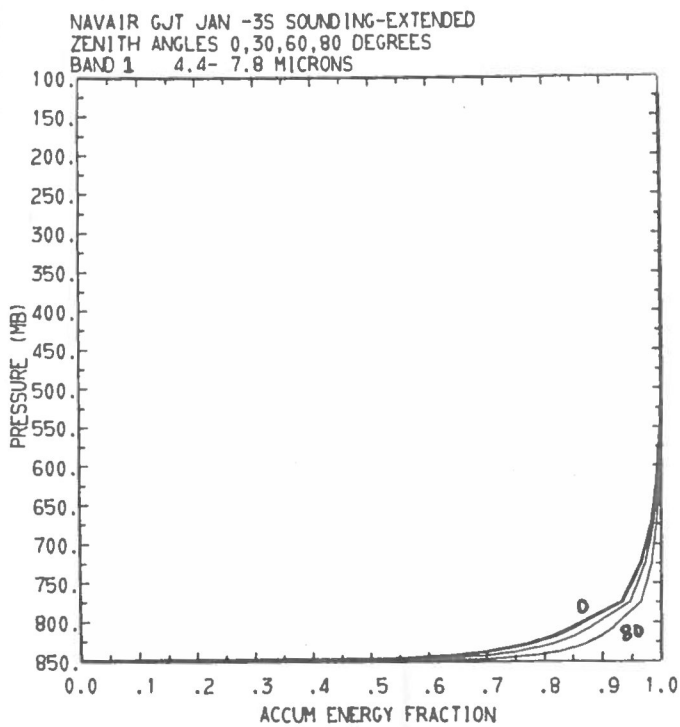


Fig. 13 Cumulative fraction of energy received at the ground from various pressure levels for given zenith angles and wavelength bands.

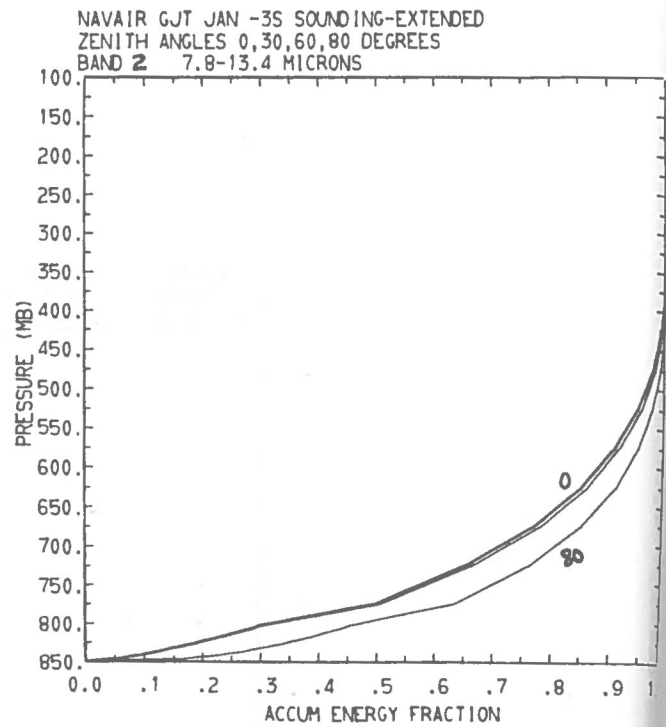


Fig. 14 Same as Fig. 13

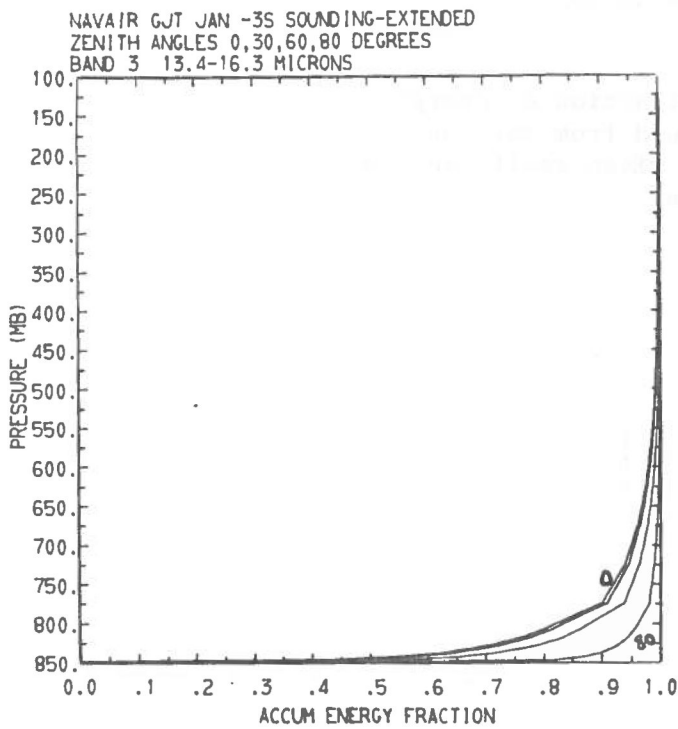


Fig.15 Same as Fig. 13

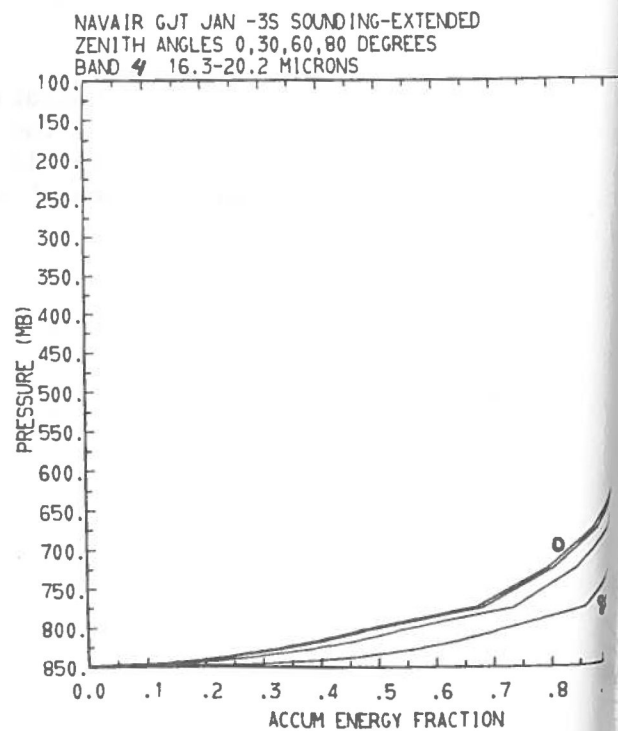


Fig. 16 Same as Fig. 13

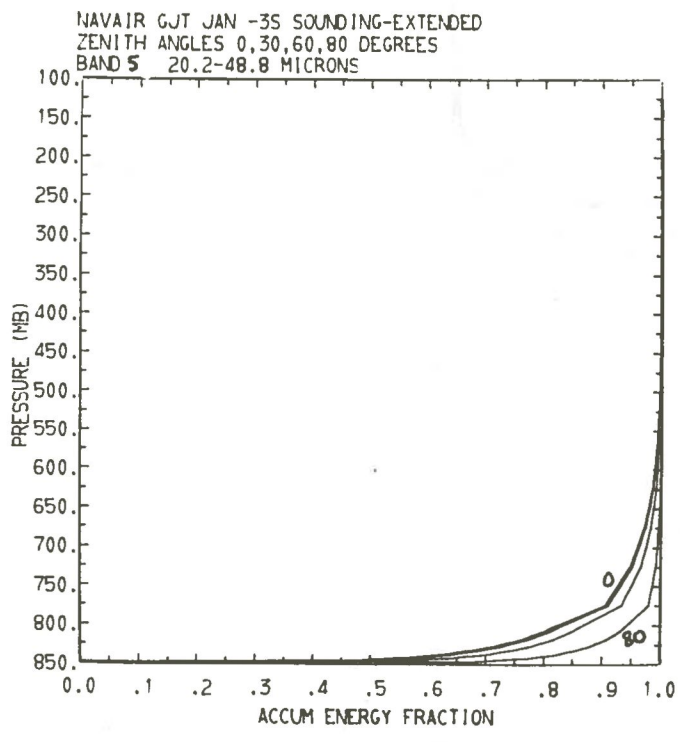


Fig. 17 Cumulative fraction of energy received at the ground from various pressure levels for given zenith angles and wavelength bands.

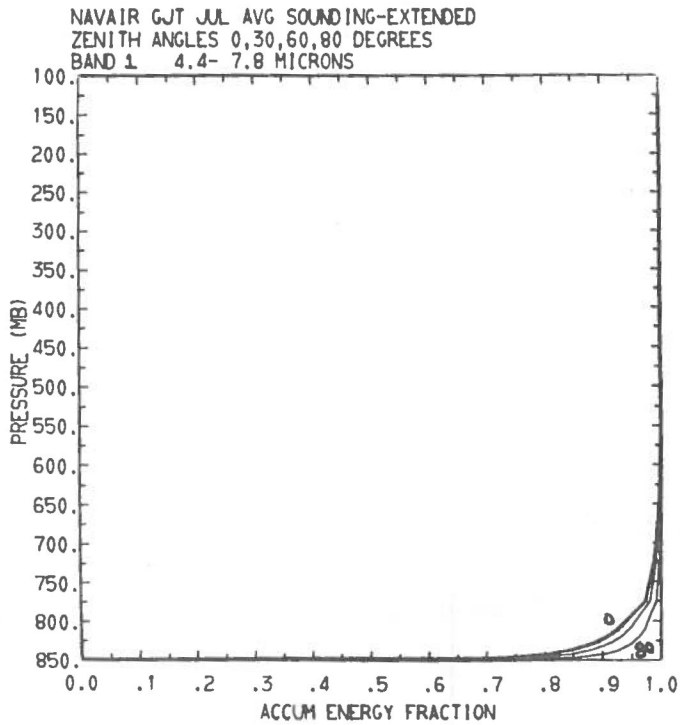


Fig. 18 Cumulative fraction of energy received at the ground from various pressure levels for given zenith angles and wavelength bands.

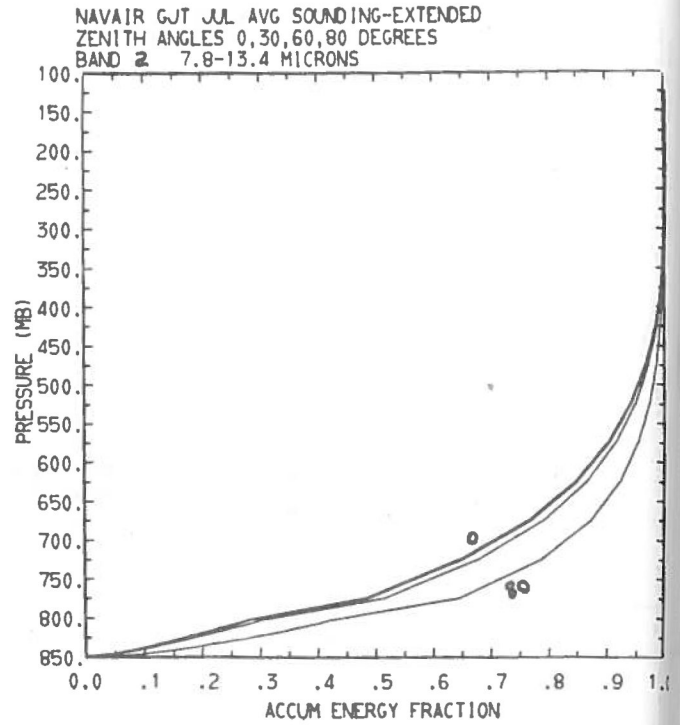


Fig. 19 Same as Fig. 18

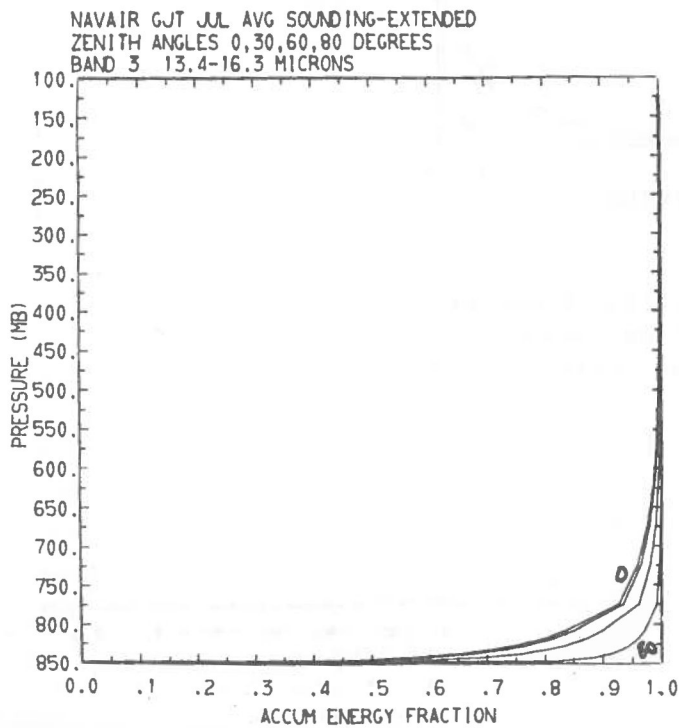


Fig. 20 Same as Fig. 18

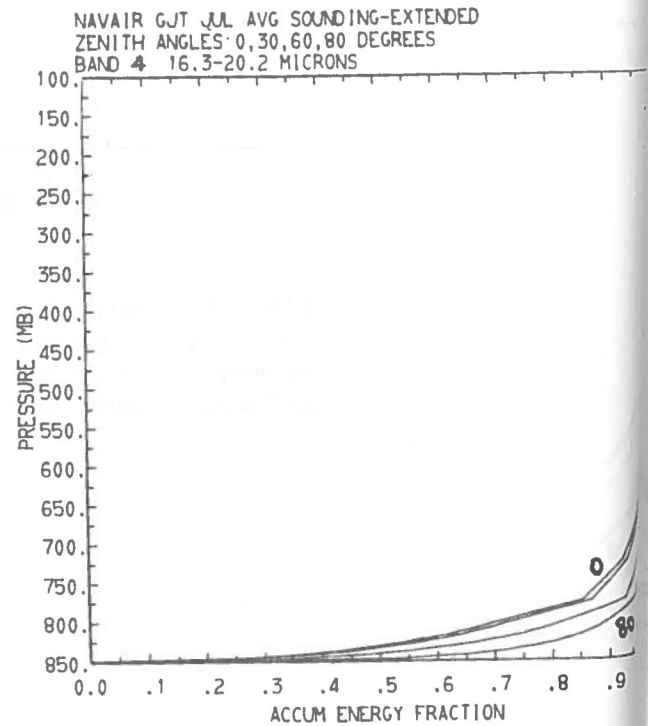


Fig. 21 Same as Fig. 18

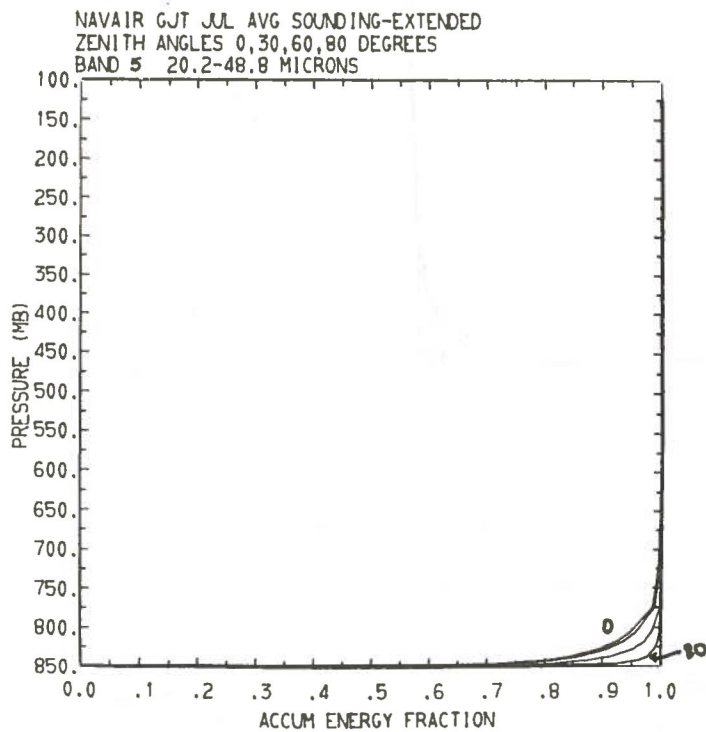


Fig. 22 Cumulative fraction of energy received at the ground from various pressure levels for given zenith angles and wavelength bands.

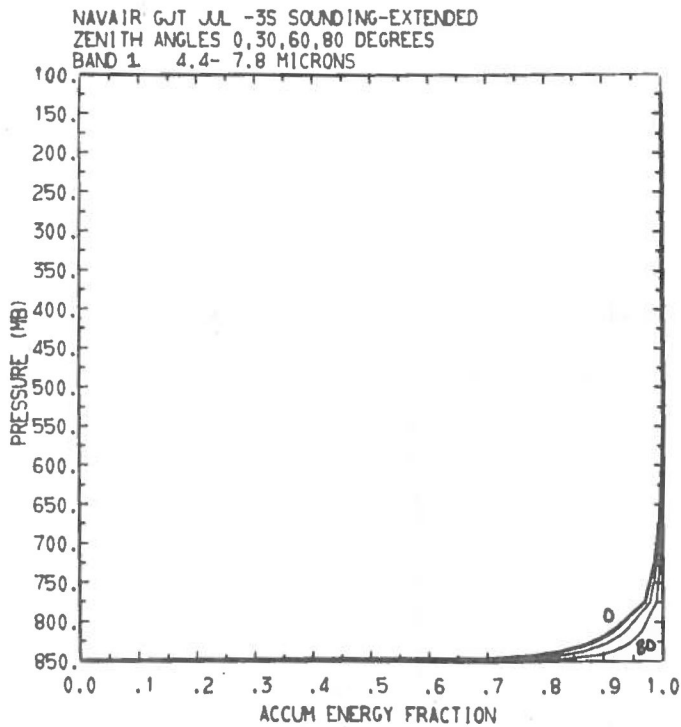


Fig. 23 Cumulative fraction of energy received at the ground from various pressure levels for given zenith angles and wavelength bands.

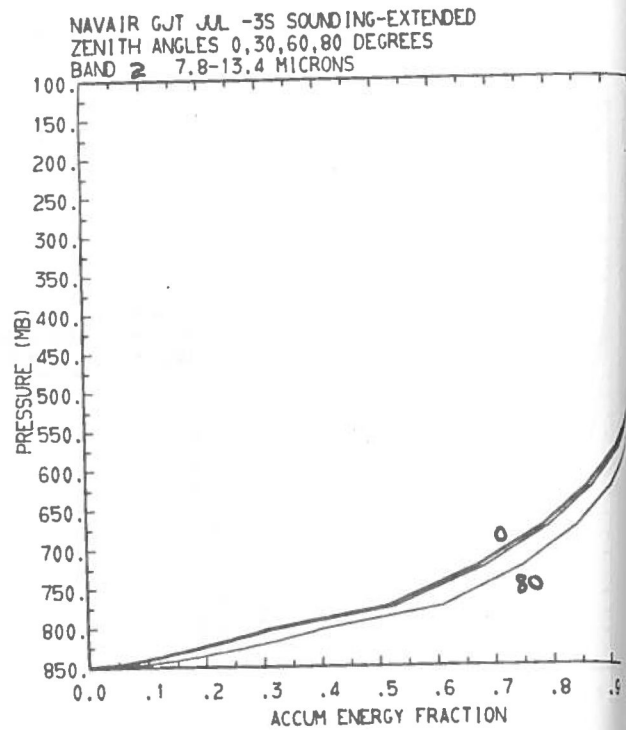


Fig. 24 Same as Fig. 23

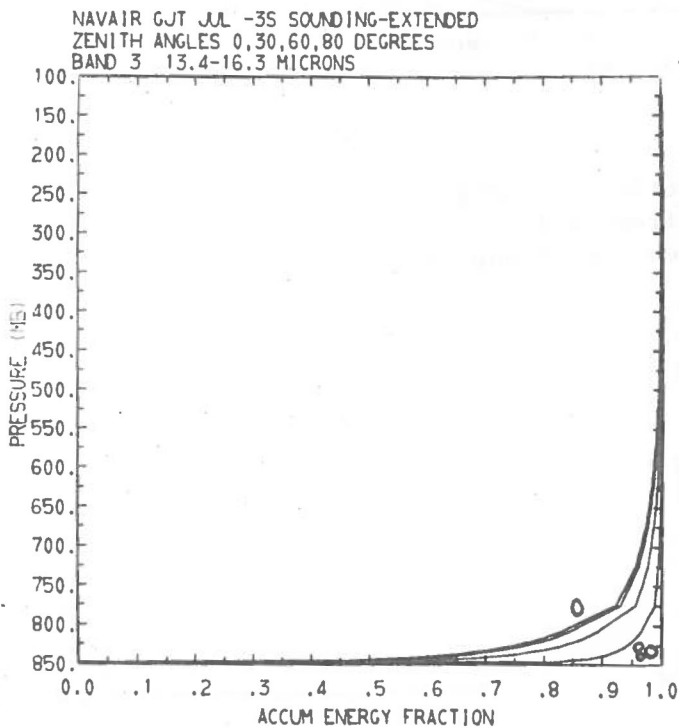


Fig. 25 Same as Fig. 23

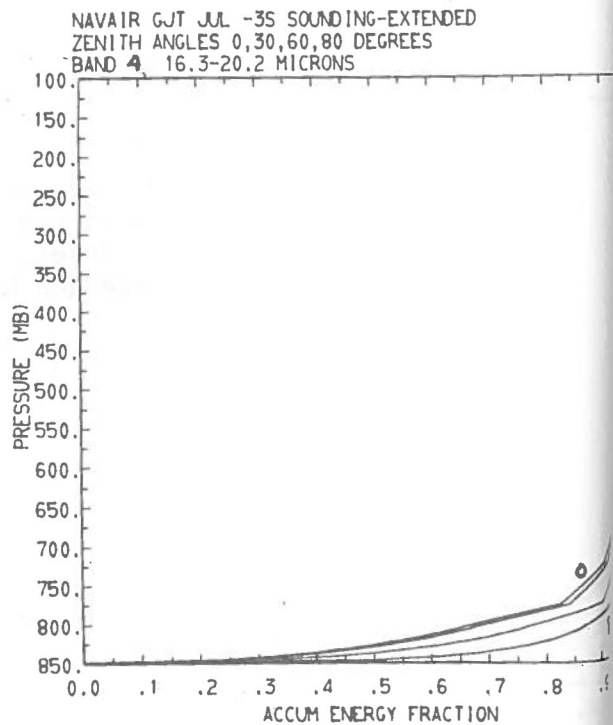


Fig. 26 Same as Fig. 23

NAVAIR GJT JUL -35 SOUNDING-EXTENDED
 ZENITH ANGLES 0, 30, 60, 80 DEGREES
 BAND 5 20.2-48.8 MICRONS

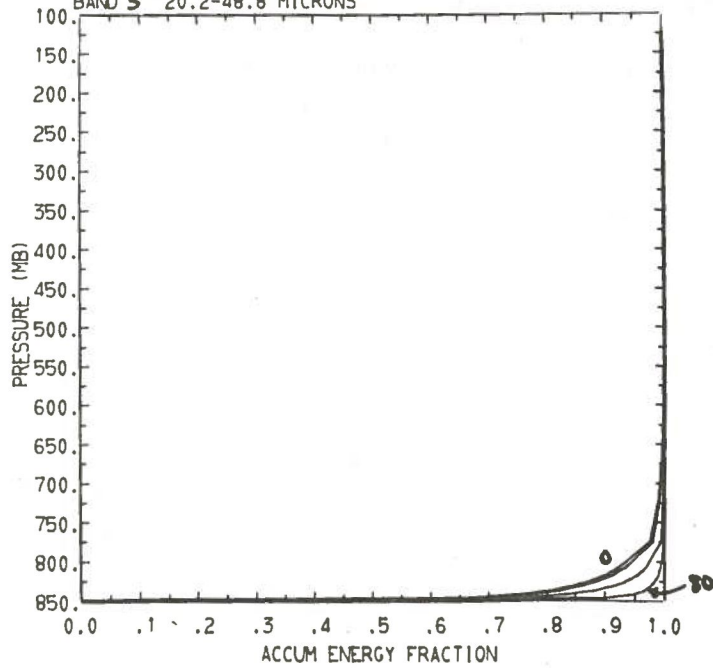


Fig. 27 Cumulative fraction of energy received at the ground from various pressure levels for given zenith angles and wavelength bands.

IV. RADIATION FOR MOUNTAIN VALLEYS

A. Radiance and Irradiance Field Components for Mountain Valleys

Two slightly different approaches were taken in calculating theoretical radiance fields within a mountain valley. In the first approach, reported in the Interim Progress Report, a linear mountain valley was envisioned (Fig. 28) in which a number of points were located on the valley sidewalls and on the valley floor.

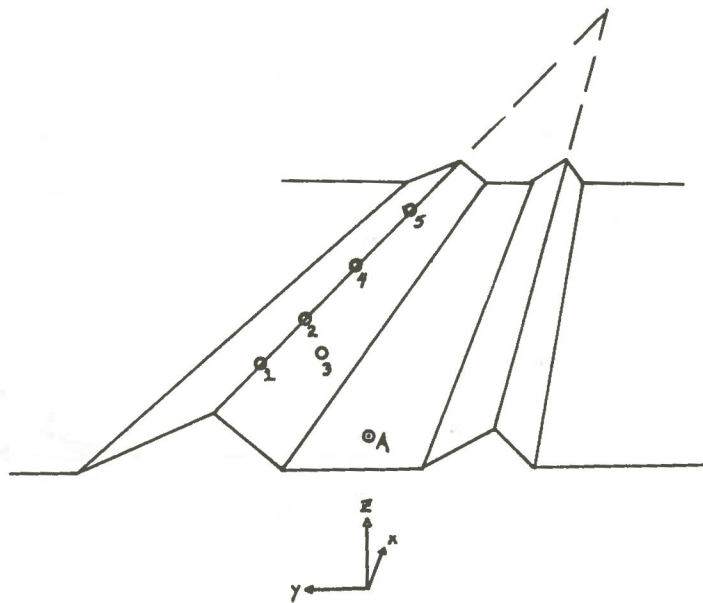


Fig. 28 Idealized valley configuration with calculation points indicated.

The desired information from this model was the following: Given two points--one on the valley floor and the other on a valley sidewall--each radiating as a black body at temperature T , what is the spectral transmissivity between the two points and what is the spectral radiance across the IR spectrum at either of the points when looking in the

direction of the other point? The spectral radiance, of course, will involve a product of the radiation at a given wavelength leaving the first point and the transmissivity of the intervening atmosphere at that wavelength between the two points. In general, another contribution will come from the atmospheric layers along the path length between the two points, which will be radiating at their respective temperatures. The radiation emitted from these layers will be partially absorbed and transmitted by intervening layers before reaching the second point.

A complete atmospheric sounding was not required for this model since the only atmospheric contribution to radiance came from within the valley. Consequently, to simplify the calculations, an isothermal sounding was specified within the valley such that the valley atmosphere had the same temperature as the sidewalls and valley floor. The atmospheric sounding is reproduced in Appendix A as the VAIL DEC ISO sounding.

The results of this analysis are presented in the form of detailed spectral radiance and transmittance calculations in the Interim Progress Report, reproduced in Appendix C. An example of the results for point 3 is reproduced in Fig. 29.

The curve labeled A in Fig. 29 represents black body radiation at point A in Fig. 28. Curve B represents the spectral radiance received at point 3 from point A when looking in the direction of point A. Since we are dealing with an isothermal atmosphere in which both points have the same radiating temperature we may equivalently say that curve B represents the spectral radiance received at point A when looking in the direction of point 3. The area between the two curves represents the loss of radiant energy due to the limited transmittance of the atmosphere

BLACK BODY (A) AND SFC RADIANCE (B)-VAIL ISO -STA 3, PHI=75, P=715

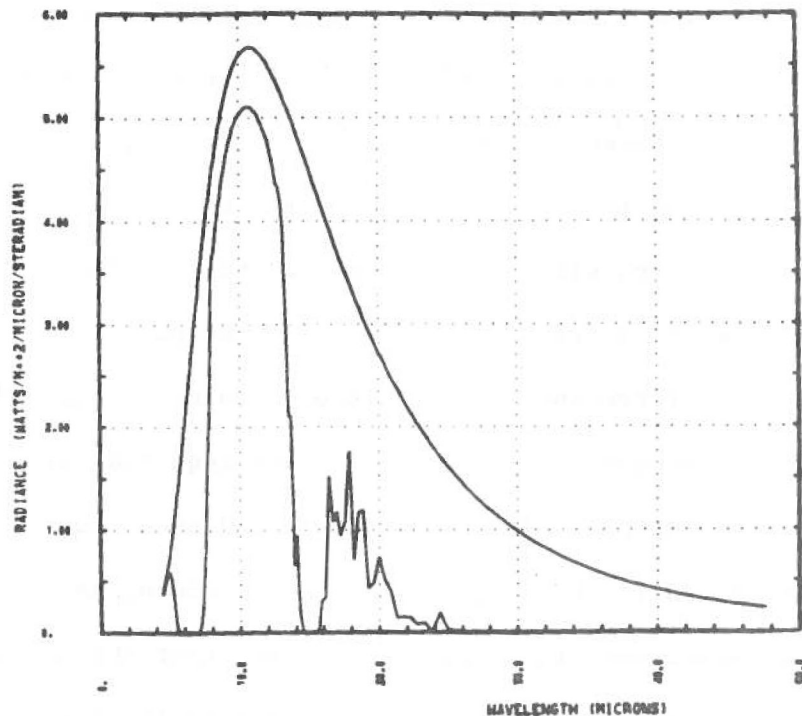


Fig. 29 Black body and surface radiance as a function of wavelength for VAIL DEC ISO sounding, Station 3.

intervening between the two points. The ratio of the areas under the two curves is .38, indicating that only 38% of the radiant energy directed from point A arrives at point 3. Point 3 is 15 degrees in elevation above the valley floor at a distance of 1.45 km from point A.

Curve B in Fig. 29 enables us to ascertain the portions of the infrared spectrum that are most effective for longwave radiation transfer within a valley, and indicates that most of the transferred radiation at point 3 occurs mainly within 2 bands. One band is centered in the water vapor continuum, or atmospheric "window", at about 8-13 microns; the other is centered around 16-20 microns in a "small window" between the carbon dioxide and rotational water absorption bands. In

future work it will be more efficient to make radiance calculations for discrete spectral bands rather than for the 10 cm^{-1} wavenumber intervals used in Fig. 29. Thus, in order to simplify further calculations of valley radiance fields the infrared spectrum was broken into 5 discrete absorption bands--the "window", the "small window", the 6.5μ water vapor band below the "window", the rotational water vapor band above the "small window", and the 15μ CO_2 band between the "window" and "small window" bands. The wavelength and wavenumber limits of the 5 bands were previously presented in Table 7.

A second and more intensive approach to calculating theoretical radiance fields within a mountain valley was accomplished by considering an idealized circularly-symmetrical valley with a flat bottom. The 3-dimensional valley was shaped like a truncated cone and a vertical cross-section through the center of the truncated cone produced the valley cross-sections shown in Figs. 30 and 31. Since calculations were to be accomplished at selected pressure levels in the computer program we chose to use slightly different "standard valleys" for the January and July cases. This was necessary since the warmer air in the summer sounding resulted in the pressure levels being farther apart within the valley. As seen in the figures each of the standard valleys are 100 mb deep. Sounding resolution is 5 mb in the lowest half of the valley, with the valley floor at 850 mb. In accordance with the goal of determining the maximum difference in the radiance and irradiance fields between the mountain case and the case of flat terrain we chose to consider a relatively steep-walled mountain valley. The slopes of the sidewalls were 31.3° and the valley was 1 km wide at the valley floor.

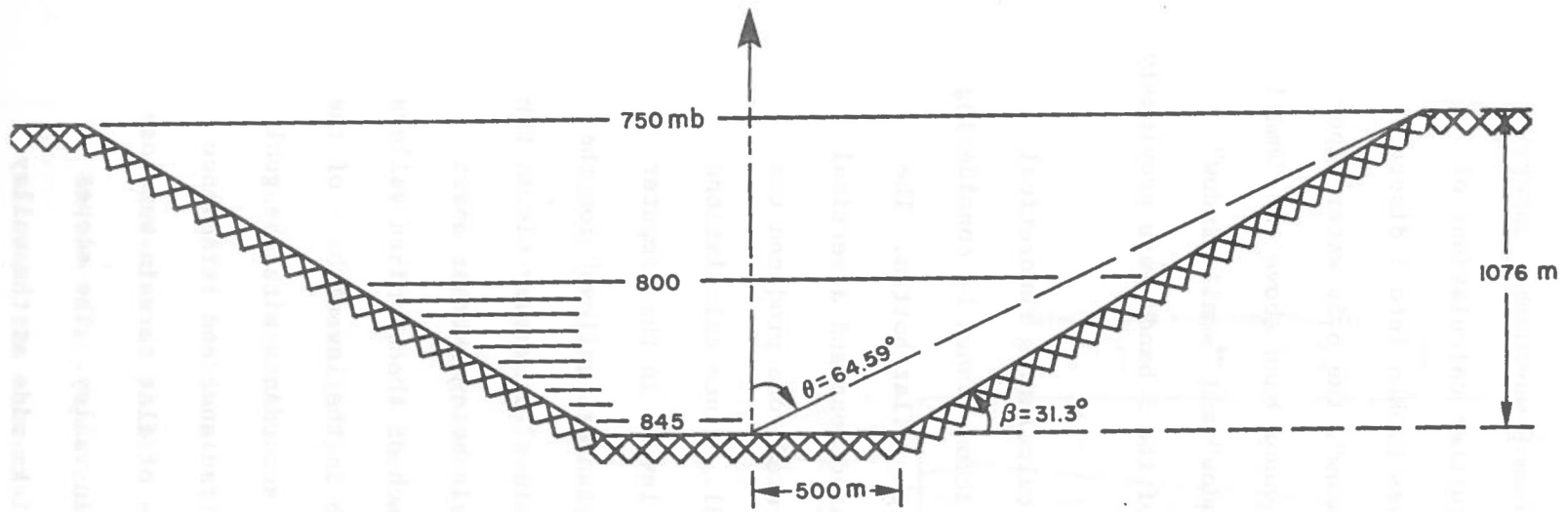


Fig. 30 Summer standard valley.

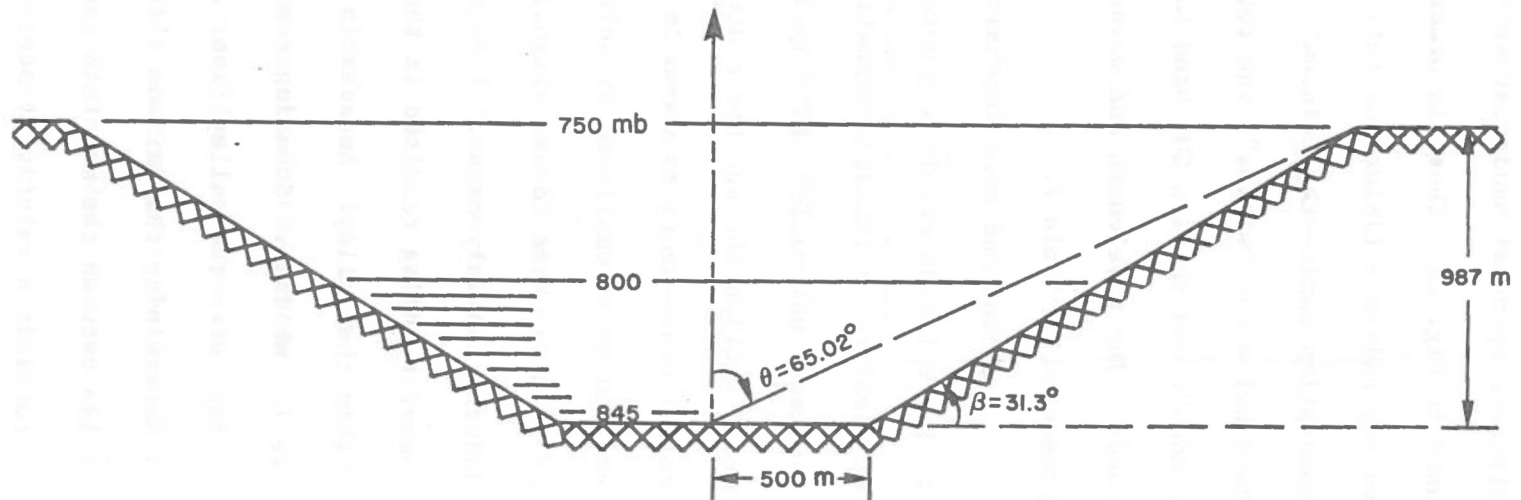


Fig. 31 Winter standard valley.

Using these valley sections calculations were made for the zenith angles to each of the intersections of pressure lines with the valley sidewalls. These zenith angles could be specified in the computer program for the desired radiance calculations. Thus we were able to specify the soundings, viewing geometry (zenith angles), and spectral intervals desired for radiance calculations. The January and July average and dry soundings listed in Appendix A, the spectral intervals listed in Table 7, and the zenith angles calculated from the respective standard valleys as depicted in Figs. 30 and 31 were then run in a modified spectral radiative transfer program (see PROGRAM RADLON description in Appendix B) to calculate radiances at the center of the valley floor. The close spacing of pressure calculation levels shown in Figs. 30 and 31 resulted in good angular resolution for the radiance calculations. For zenith angles less than the zenith angle to the ridge (i.e., elevation angles above the ridge) contributions to the radiance came from the entire depth of the atmosphere. Radiance contributions for zenith angles greater than the zenith angle of the ridge came from two sources: first, a contribution came from the limited volume of air (hereafter called the Air Wedge) enclosed by 3 surfaces: valley floor, valley sidewall, and zenith line to the ridge. Secondly, a contribution came from the radiating sidewall, considered as a black body radiator at a given temperature $T(Z)$. The radiance from the sidewall depended on its black body radiating temperature and the transmissivity along the path from sidewall to valley center. For simplicity, rather than choosing a temperature profile up the sidewalls, the sidewalls were assumed to have a constant temperature. It is stressed, however, that the

method developed can be easily applied to valleys having non-isothermal sidewalls. The calculations for a temperature profile up the sidewalls are straightforward, but require more computational effort. The general results are more easily seen in terms of calculations for several different isothermal sidewall radiating temperatures. Since IR emissivities of most naturally occurring ground materials are near 1, an emissivity of 1 was assumed. The effects of different surface materials on radiance calculations therefore appeared only in the temperature of the sidewalls.

The radiances resulting from calculations using the modified RADLON program for a point at the center of the valley floor are presented as a function of viewing geometry for the various spectral intervals and soundings in Figs. 32 through 35. Note that the radiances are not presented as simple functions of θ . Instead the figures are plotted as $N \cos \theta$ vs $\cos \theta$. This is advantageous because of the nature of the relationship between irradiance H and radiance N for the case of a circularly symmetric valley, since:

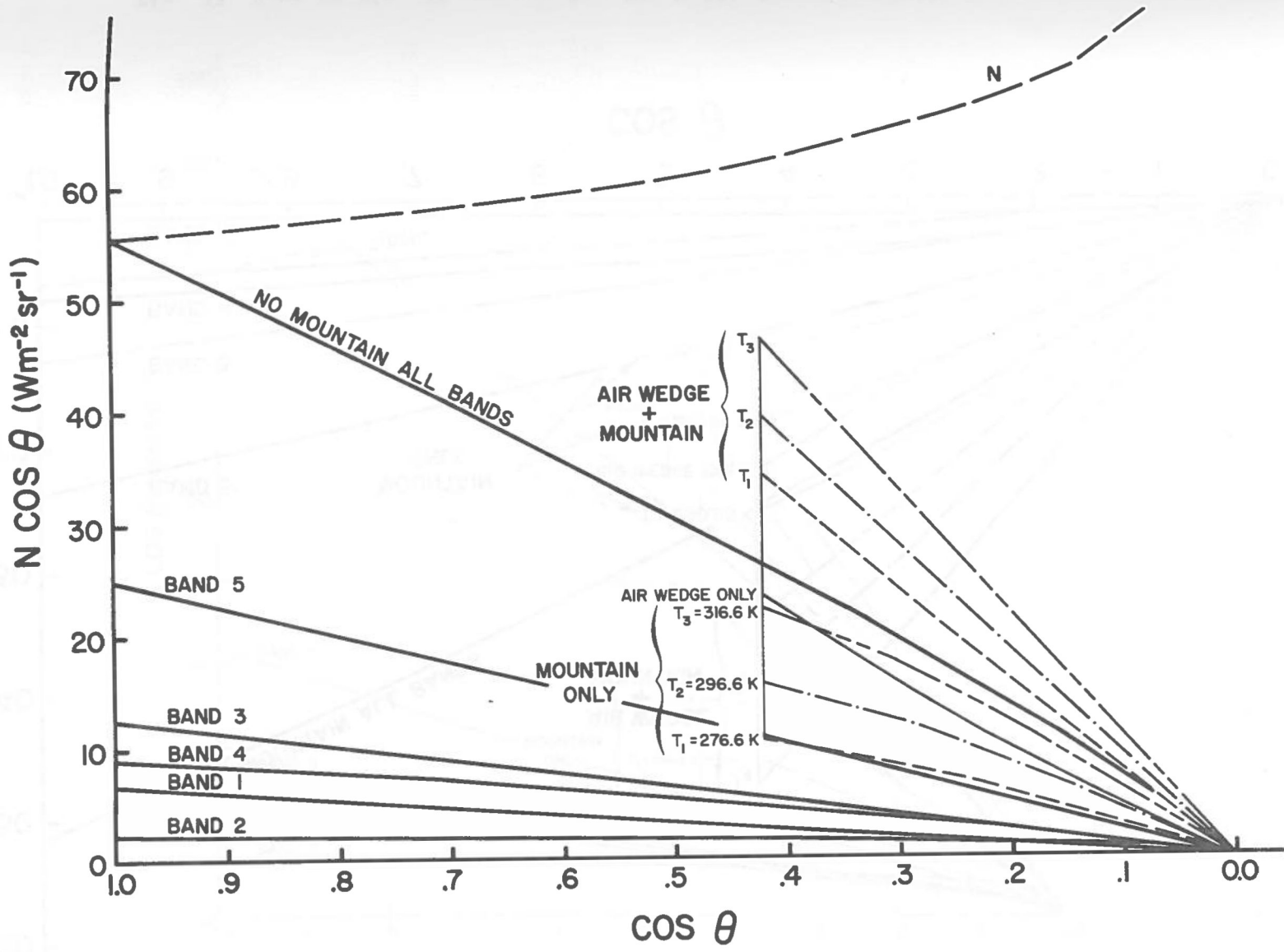
$$H_{\downarrow} = \int_0^{2\pi} \int_0^{\pi/2} N \cos \theta \, d \cos \theta \, d\theta d\phi$$

and, with the circularly-symmetrical geometry of the valley:

$$H_{\downarrow} = 2\pi \int_0^{\pi/2} N \cos \theta \, d \cos \theta \cong 2\pi \sum_{i=1}^n (N \cos \theta) \Delta \cos \theta .$$

Thus the area under the individual curves represents contributions to irradiance. Individual lines in Fig. 32, for example, are described as follows:

- i) N: The line labeled with an N shows the dependence of radiance on $\cos \theta$.



37

Fig. 32 Partitioning of radiances into spectral and topographic components using NAVAIR GJT JAN AVG sounding. Upper dashed line indicates radiance plotted against $\cos \theta$. See text for complete explanation.

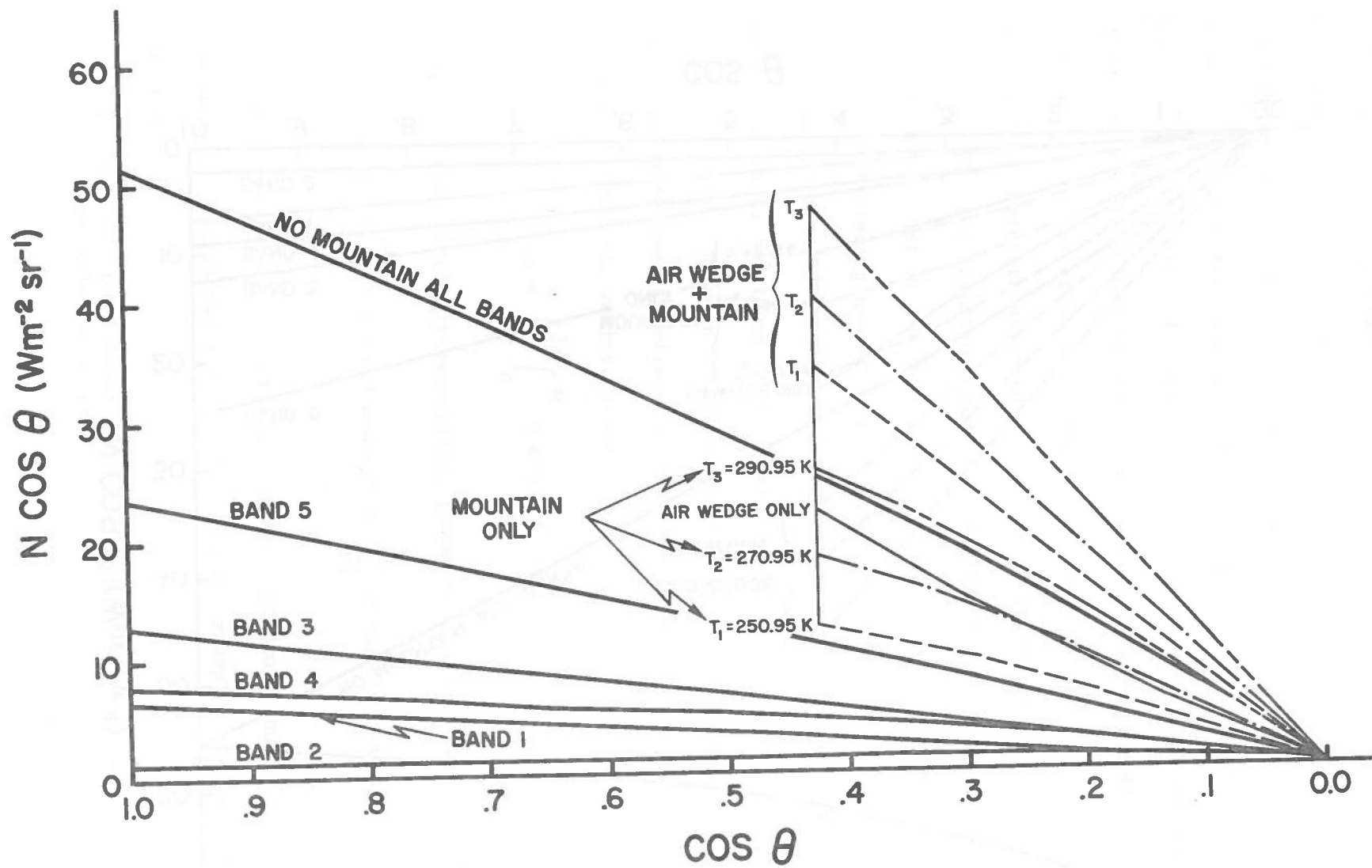


Fig. 33 Same as Fig. 32, except for dry (-3S) January sounding.

Fig. 33 Same as Fig. 32, except for dry (-3S) January sounding.

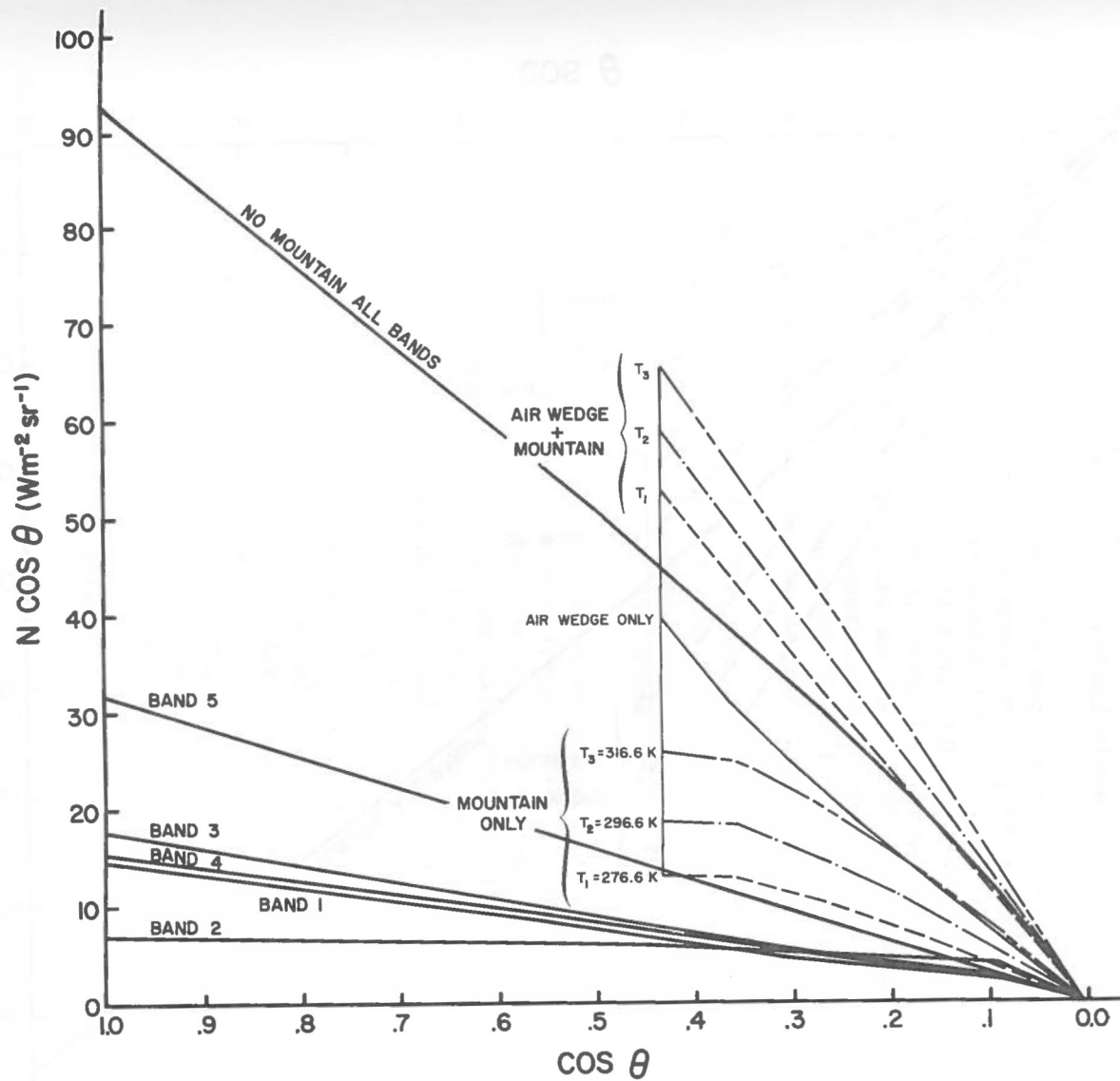


Fig. 34 Same as Fig. 32, except for July average sounding.

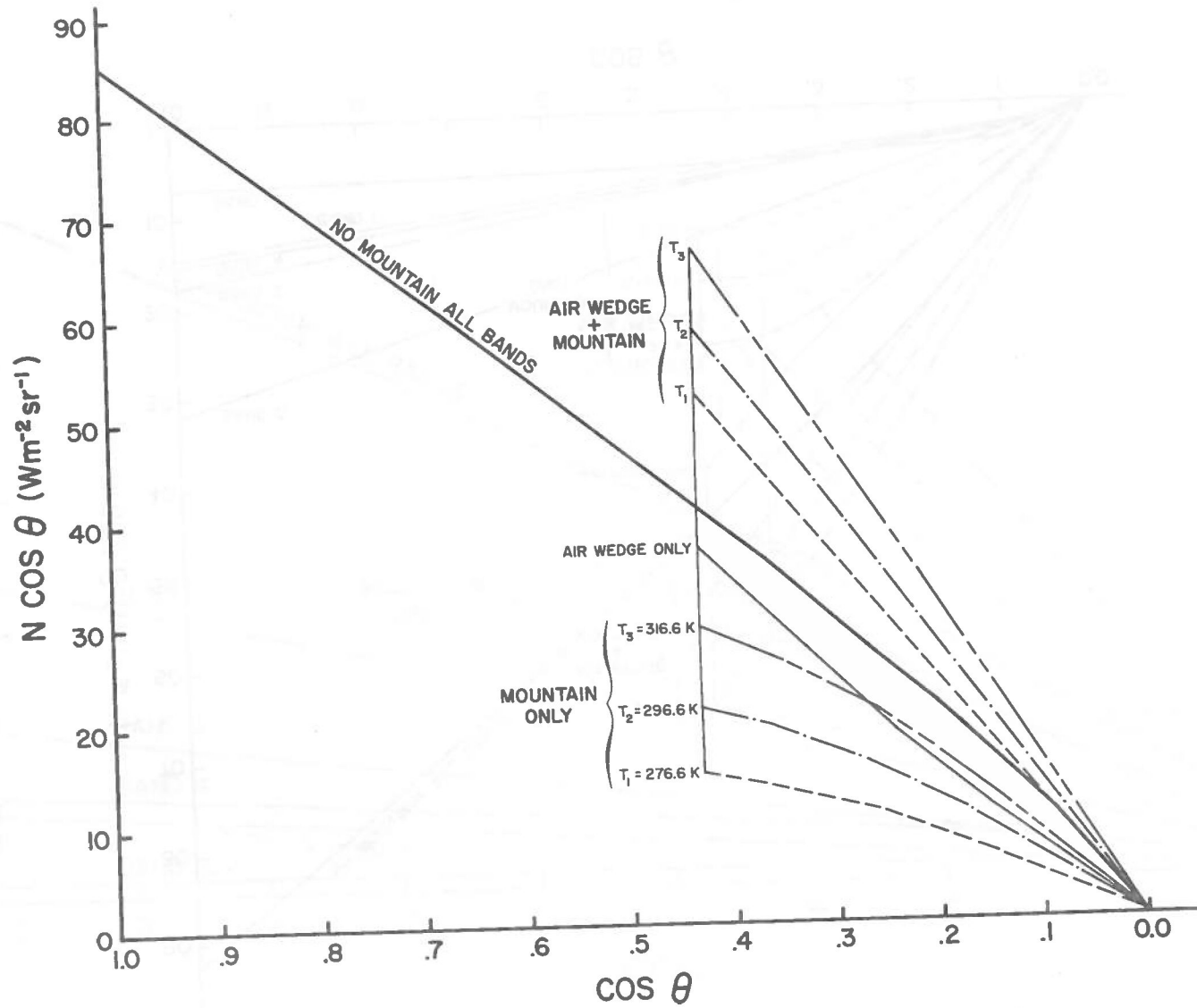


Fig. 35 Same as Fig. 32, except for July dry (-3S) sounding.

- ii) BAND 1, ..., BAND 5: The area under each of these curves represents the contribution to total irradiance over flat topography from wavelength bands 1-5, as defined in Table 7.
- iii) AIR WEDGE ONLY: The area under this curve represents the contribution to irradiance from the air wedge within the valley, as previously described in section III B 3. Note that the curve is defined only for zenith angles, θ , between 65.02° and 90° , i.e. the wedge does not extend above the ridgetops.
- iv) MOUNTAIN ONLY: The area under each of the three curves labeled with temperatures T_1 through T_3 represents the contribution to irradiance at the valley center from radiating sidewalls having the temperatures indicated. Note that temperature T_2 is the same temperature as the 850 mb temperature of the sounding. Temperatures T_1 and T_3 thus represent temperatures $\pm 20^\circ\text{C}$ different from the air temperature at the base of the sounding.
- v) AIR WEDGE + MOUNTAIN: The area under each of the three curves labeled with temperatures T_1 through T_3 represents the summed contribution to irradiance from iii) and iv) above.
- vi) NO MOUNTAIN--ALL BANDS: The area under this curve represents the downward irradiance to be expected theoretically in the case of flat terrain for the frequency spectrum of the calculations, i.e. 4.4 - 48.8 microns. Thus the curve represents the sum of the curves labeled BAND 1 through BAND 5. Note that the irradiances calculated for flat terrain in section III A will differ from the values represented here due to the differing frequency domains of the calculations. Approximately 5% of the area under a black body curve is contained at wavelengths below 4.4 microns or above 48.8 microns (see Fig. 36, following). Therefore the area under this curve does not quite represent the full irradiance over flat terrain.

To further illustrate the interpretation of the figures, we may summarize the main points of Fig. 32:

- (1) Band 5 provides the largest contribution to irradiance on flat terrain, followed in order of importance by bands 3, 4, 1, and 2. At the larger zenith angles band 2, and

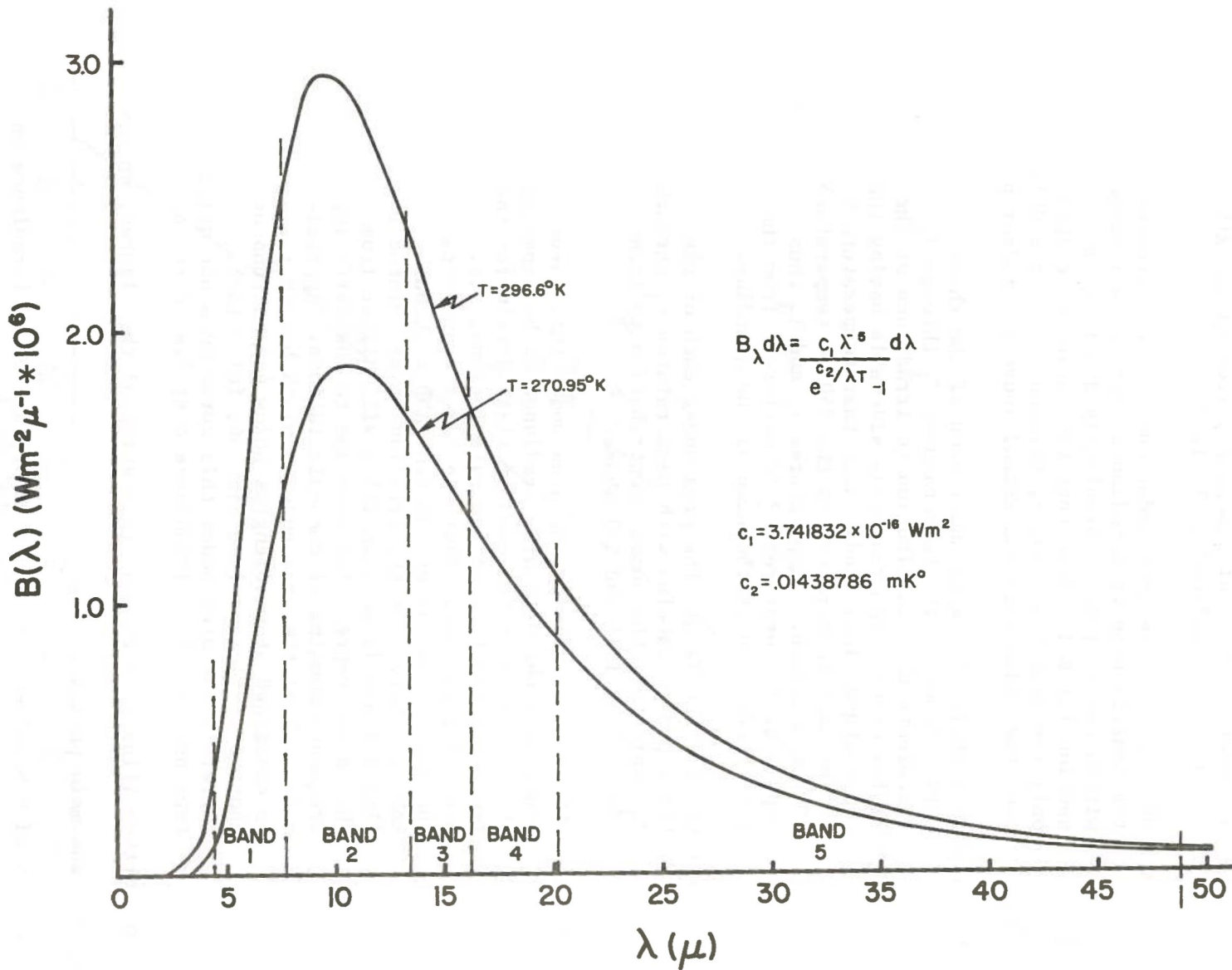


Fig. 36 Blackbody curves for two temperatures, indicating the bandwidths and locations of the various bands considered in the analysis. The indicated temperatures correspond to the temperatures at the bases of the summer and winter soundings utilized in the

Fig. 36 Blackbody curves for two temperatures, indicating the bandwidths and localities of the various bands considered in the analysis. The indicated temperatures correspond to the temperatures at the bases of the summer and winter soundings utilized in the

to a lesser extent band 4, assume more relative importance. The bands of importance in transmissions from the sidewalls (not indicated on the figure) are bands 2 and 4, as previously indicated.

- (2) Considering our "standard" mountain valley, if we assume the sidewalls do not radiate, the irradiance at valley bottom comes from the area under the NO MOUNTAIN--ALL BANDS curve to $\cos \theta = .422$ and then from the area under the AIR WEDGE ONLY curve for $0 < \cos \theta < .422$. This total area differs little from the total area under the NO MOUNTAIN--ALL BANDS curve. Thus, any major difference in the irradiance field over a mountain valley as compared to the irradiance field over flat terrain comes mainly from the effect of radiating sidewalls.
- (3) Neglect of the effect of the air wedge and consideration of the radiating sidewalls only (MOUNTAIN ONLY curve) would result in an irradiance field that would be less than that expected over flat terrain. Proper consideration of the contributions by the air wedge and the radiating sidewalls results in a valley irradiance field larger in magnitude than that expected over flat terrain. The magnitude of the difference depends on the temperature of the sidewalls--the higher the temperature the greater the irradiation.

In order to determine the effect of a drier atmosphere we may compare Figs. 32 and 33. From Fig. 33 we see that, for a drier atmosphere, the total irradiance over flat terrain is expected to be reduced slightly. The relative effect of valley sidewalls is seen to be most important for

this case. In other words, the effect of radiating sidewalls is most important for dry winter soundings. Even when sidewall temperatures are 20°C lower than those in the sounding, the irradiance field in the valley is greater in magnitude than that observed over flat terrain.

Turning to Figs. 34 and 35, the relative effect of radiating sidewalls is less in the summer case than in the winter case, especially for an average sounding, as opposed to a dry sounding case. When the atmosphere is "dry" the sidewalls assume more importance, although they have less relative importance than in the winter case.

Due to the limitations of space on Figs. 32-35 the spectral contributions to irradiance components could not be shown for zenith angles greater than the angle to the ridge, θ_r . This situation is remedied in Figs. 37-39, where the contributions are presented for the average January sounding only. In Fig. 37 the downward irradiance over flat terrain (NO MOUNTAIN--ALL BANDS) is seen to consist of contributions from bands 5, 3, 4, 1, 2, as listed in order of importance. When the winter "standard valley" is introduced, the sidewalls have the effect of cutting off part of the atmospheric contribution to the downward irradiance at valley center. In fact the only atmospheric contribution left at zenith angles greater than θ_r is the contribution from the air left within the valley, termed the AIR WEDGE. When the effect of radiating sidewalls is ignored (i.e. we consider the AIR WEDGE ONLY) the irradiance from the air wedge is less than that from the full atmosphere over flat terrain. Thus the AIR WEDGE ONLY--ALL BANDS curve lies below the NO MOUNTAIN--ALL BANDS curve. Each of these curves, however, is composed of spectral components. The effect of introducing the valley

ist
is
the
1.
side-
ly
the
they
con-
angles
ed in
e
at
ns
the
fect
d
ution
air
(Y) the
osphere
below
is
alley

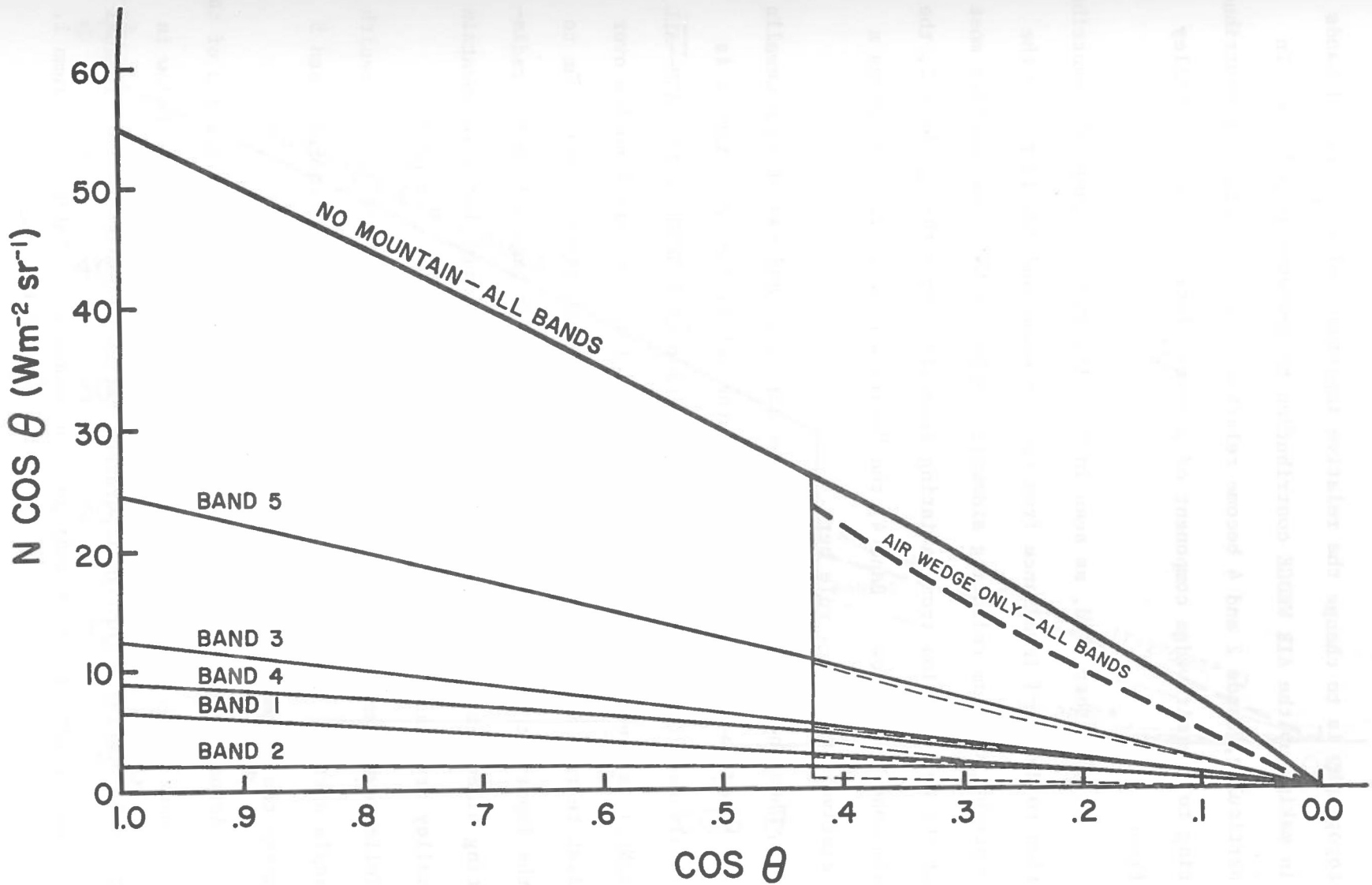


Fig. 37 Dependence of radiance on zenith angle for the average January GJT sounding, illustrating the spectral composition of the irradiance contribution from the air wedge for the valley case, and from the entire atmosphere for the flat terrain case. $\cos \theta_r = .422$.

topography is to change the relative importance of the spectral bands in making up the AIR WEDGE contribution to downward irradiance. In particular, bands 2 and 4 become relatively less important in contributing to the air wedge component of downward irradiance at the valley floor.

On the other hand, as seen in Fig. 38, when we ignore the contribution to downward irradiance from the air wedge and consider only the contribution from radiating sidewalls (MOUNTAIN ONLY) we see that most of the contribution from radiating sidewalls comes through band 2, the atmospheric "window". Band 4, the "small window", similarly plays a relatively important role here.

When the contributions from the air wedge and radiating sidewalls are added to get the total effect of the valley configuration it is easily seen (Fig. 39) that the contribution (AIR WEDGE + MOUNTAIN--ALL BANDS) is greater than that expected from the same zenith angles over flat terrain (extension of the NO MOUNTAIN--ALL BANDS curve). Due to the important contribution of radiation through band 2 from the radiating sidewalls, band 2 is the most significant contributor to mountain valley irradiance from zenith angles greater than θ_r . Band 2 is followed by bands 5, 3, 4, and 1 in order of importance in this zenith angle sector. Overall, when all zenith angles are considered, band 5 makes the biggest contribution to downward irradiance.

Actual irradiances (Wm^{-2}), obtained by numerical integration of the area under each of the curves in Figs. 32 - 35, are presented below in Table 8. Tables 9 through 12 present ratios of areas under individual curves for each of the soundings. For example, in Table 10, Column 1,

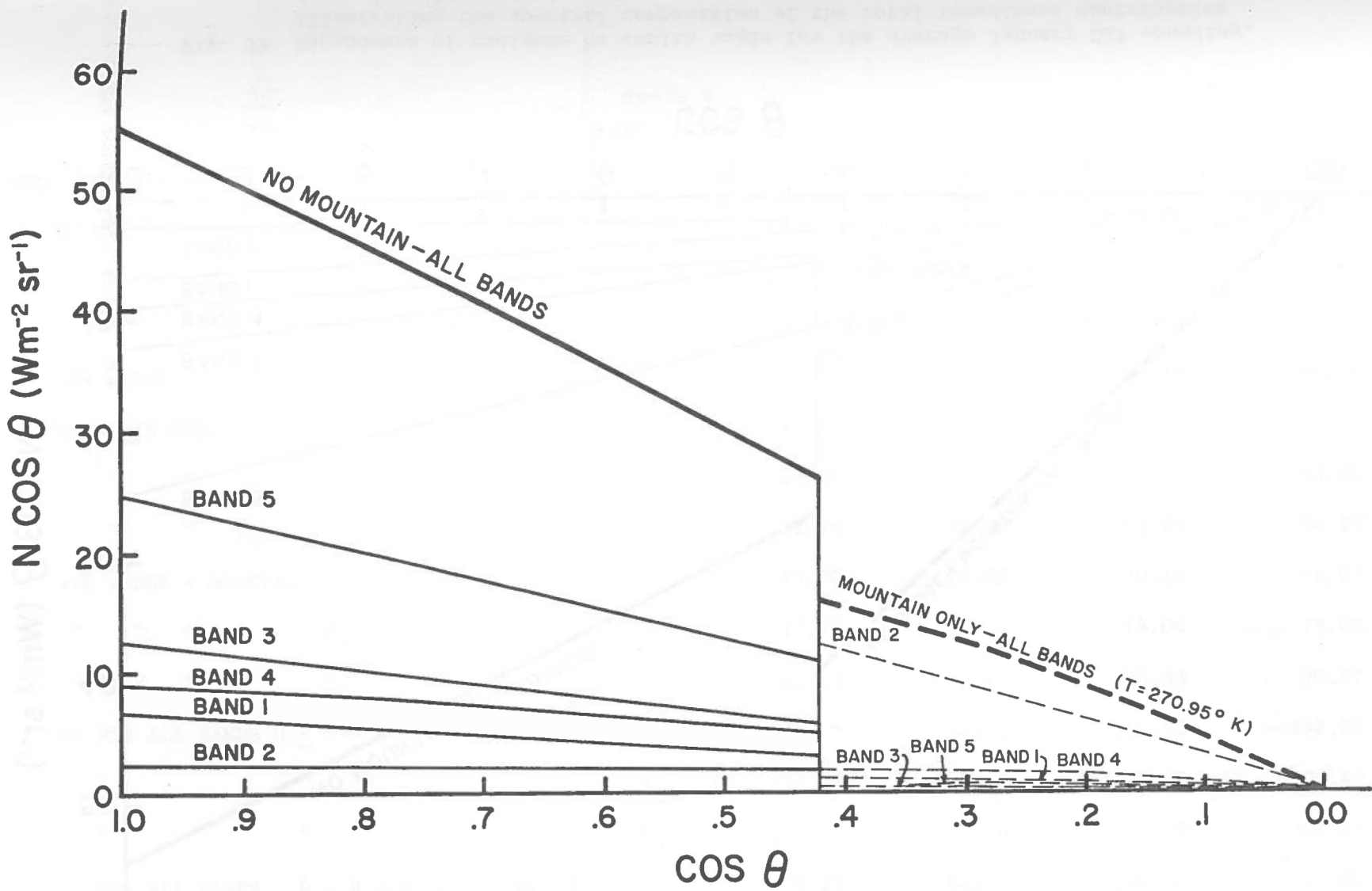


Fig. 38 Dependence of radiance on zenith angle for the average January GJT sounding, illustrating the spectral composition of the irradiance contribution from radiating sidewalls.

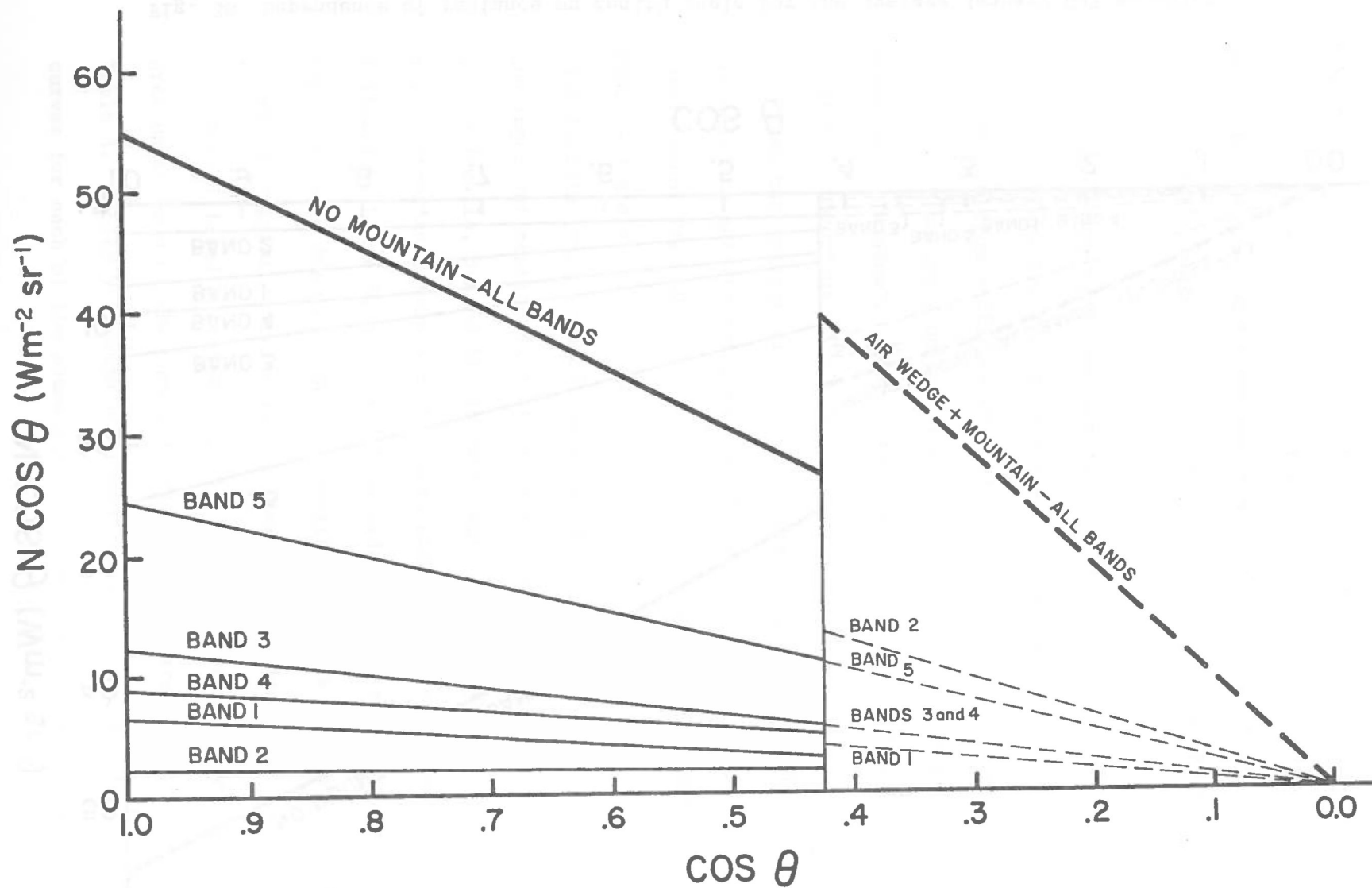


Fig. 39 Dependence of radiance on zenith angle for the average January GJT sounding, illustrating the spectral composition of the total irradiance contribution from sidewalls and air wedge.

Fig. 39 Dependence of radiance on zenith angle for the average January GJT sounding, illustrating the spectral composition of the total irradiance contribution from sidewalls and air wedge.

Table 8
Irradiances

Area under listed curves	Irradiance Wm^{-2}			
	JAN AVG	JAN -3S	JUL AVG	JUL -3S
1. NO MOUNTAIN ALL BANDS	186.97	172.68	310.84	286.33
2. " " " $0 \leq \theta \leq \theta_r$	149.76	138.39	246.24	227.38
3. " " " $\theta_r \leq \theta \leq 90^\circ$	37.21	34.29	64.59	58.96
4. AIR WEDGE	29.46	26.55	48.39	46.48
5. MOUNTAIN ONLY T_1	15.85	17.77	21.79	23.18
6. " " T_2	23.26	25.79	30.66	32.61
7. " " T_3	32.78	36.06	41.64	44.29
8. AIR WEDGE + MOUNTAIN T_1	45.30	44.32	70.18	69.67
9. " " " " T_2	52.72	52.34	79.04	79.09
10. " " " " T_3	62.23	62.61	90.03	90.77
11. NO MTN ALL BANDS $0 \leq \theta \leq \theta_r$ + AIR WEDGE + MTN T_1	195.06	182.71	316.42	297.04
12. " " " " " T_2	202.48	190.73	325.29	306.47
13. " " " " " T_3	211.99	201.00	336.27	318.15
14. NO MTN ALL BANDS $0 \leq \theta \leq \theta_r$ + AIR WEDGE	179.22	164.94	294.63	273.86

θ_r is the zenith angle from valley center to ridgetop. For winter soundings this angle is 65.02° ; for the summer soundings it is 64.59° .

Table 9
Average January Grand Junction Sounding
Area Ratios from Figure 32 (column variable/row variable)

	1	2	3	4	5	6	7	8	9	10	11	12	13	14
1	1.00	1.25	5.02	6.35	11.80	8.04	5.70	4.13	3.55	3.00	0.96	0.92	0.88	1.04
2	0.80	1.00	4.02	5.08	9.45	6.44	4.57	3.31	2.84	2.41	0.77	0.74	0.71	0.84
3	0.20	0.25	1.00	1.26	2.35	1.60	1.14	0.82	0.71	0.60	0.19	0.18	0.18	0.21
4	0.16	0.20	0.79	1.00	1.86	1.27	0.90	0.65	0.56	0.47	0.15	0.15	0.14	0.16
5	0.08	0.11	0.43	0.54	1.00	0.68	0.48	0.35	0.30	0.25	0.08	0.08	0.07	0.09
6	0.12	0.16	0.63	0.79	1.47	1.00	0.71	0.51	0.44	0.37	0.12	0.11	0.11	0.13
7	0.18	0.22	0.88	1.11	2.07	1.41	1.00	0.72	0.62	0.53	0.17	0.16	0.15	0.18
8	0.24	0.30	1.22	1.54	2.86	1.95	1.38	1.00	0.86	0.73	0.23	0.22	0.21	0.25
9	0.28	0.35	1.42	1.79	3.33	2.27	1.61	1.16	1.00	0.85	0.27	0.26	0.25	0.29
10	0.33	0.42	1.67	2.11	3.93	2.68	1.90	1.37	1.18	1.00	0.32	0.31	0.29	0.35
11	1.04	1.30	5.24	6.62	12.31	8.39	5.95	4.31	3.70	3.13	1.00	0.96	0.92	1.09
12	1.08	1.35	5.44	6.87	12.78	8.70	6.18	4.47	3.84	3.25	1.04	1.00	0.96	1.13
13	1.13	1.42	5.70	7.20	13.38	9.11	6.47	4.68	4.02	3.41	1.09	1.05	1.00	1.18
14	0.96	1.20	4.82	6.08	11.31	7.70	5.47	3.96	3.40	2.88	0.92	0.89	0.85	1.00

Key to Variables:

- | | |
|--|---|
| 1 = Area under "NO MOUNTAIN-ALL BANDS" curve | 8 = Variable 4 + variable 5 |
| 2 = " " " " " " " " for $0 \leq \theta \leq \theta_r$ | 9 = Variable 4 + variable 6 |
| 3 = " " " " " " " " for $\theta_r \leq \theta \leq 90^\circ$ | 10 = Variable 4 + variable 7 |
| 4 = Area under "AIR WEDGE ONLY" curve | 11 = Variable 2 + variable 4 + variable 5 |
| 5 = Area under "MOUNTAIN ONLY-T ₁ " curve | 12 = Variable 2 + variable 4 + variable 6 |
| 6 = " " " " T ₂ " curve | 13 = Variable 2 + variable 4 + variable 7 |
| 7 = " " " " T ₃ " curve | 14 = Variable 2 + variable 4 |

Table 10
 Dry January Grand Junction Sounding
 Area Ratios from Figure 33 (column variable/row variable)

	1	2	3	4	5	6	7	8	9	10	11	12	13	14
1	1.00*	1.25	5.04	6.50	9.72	6.70	4.79	3.90	3.30	2.76	0.95	0.91	0.86	1.05
2	0.80	1.00	4.04	5.21	7.79	5.37	3.84	3.12	2.64	2.21	0.76	0.73	0.69	0.84
3	0.20	0.25	1.00	1.29	1.93	1.33	0.95	0.77	0.66	0.55	0.19	0.18	0.17	0.21
4	0.15	0.19	0.77	1.00	1.49	1.03	0.74	0.60	0.51	0.42	0.15	0.14	0.13	0.16
5	0.10	0.13	0.52	0.67	1.00	0.69	0.49	0.40	0.34	0.28	0.10	0.09	0.09	0.11
6	0.15	0.19	0.75	0.97	1.45	1.00	0.72	0.58	0.49	0.41	0.14	0.14	0.13	0.16
7	0.21	0.26	1.05	1.36	2.03	1.40	1.00	0.81	0.69	0.58	0.20	0.19	0.18	0.22
8	0.26	0.32	1.29	1.67	2.49	1.72	1.23	1.00	0.85	0.71	0.24	0.23	0.22	0.27
9	0.30	0.38	1.53	1.97	2.95	2.03	1.45	1.18	1.00	0.84	0.29	0.27	0.26	0.32
10	0.36	0.45	1.83	2.36	3.52	2.43	1.74	1.41	1.20	1.00	0.34	0.33	0.31	0.38
11	1.06	1.32	5.33	6.88	10.28	7.08	5.07	4.12	3.49	2.92	1.00	0.96	0.91	1.11
12	1.10	1.38	5.56	7.18	10.73	7.39	5.29	4.30	3.64	3.05	1.04	1.00	0.95	1.16
13	1.16	1.45	5.86	7.57	11.31	7.79	5.57	4.54	3.84	3.21	1.10	1.05	1.00	1.22
14	0.96	1.19	4.81	6.21	9.28	6.39	4.57	3.72	3.15	2.63	0.90	0.86	0.82	1.00

* variables defined in Table 9

Table 11
Average July Grand Junction Sounding
Area Ratios from Figure 34 (column variable/row variable)

	1	2	3	4	5	6	7	8	9	10	11	12	13	14
1	1.00 *	1.26	4.81	6.42	14.26	10.14	7.46	4.43	3.93	3.45	0.98	0.96	0.92	1.05
2	0.79	1.00	3.81	5.09	11.30	8.03	5.91	3.51	3.12	2.74	0.78	0.76	0.73	0.84
3	0.21	0.26	1.00	1.33	2.96	2.11	1.55	0.92	0.82	0.72	0.20	0.20	0.19	0.22
4	0.16	0.20	0.75	1.00	2.22	1.58	1.16	0.69	0.61	0.54	0.15	0.15	0.14	0.16
5	0.07	0.09	0.34	0.45	1.00	0.71	0.52	0.31	0.28	0.24	0.07	0.07	0.06	0.07
6	0.10	0.12	0.47	0.63	1.41	1.00	0.74	0.44	0.39	0.34	0.10	0.09	0.09	0.10
7	0.13	0.17	0.64	0.86	1.91	1.36	1.00	0.59	0.53	0.46	0.13	0.13	0.12	0.14
8	0.23	0.28	1.09	1.45	3.22	2.29	1.69	1.00	0.89	0.78	0.22	0.22	0.21	0.24
9	0.25	0.32	1.22	1.63	3.63	2.58	1.90	1.13	1.00	0.88	0.25	0.24	0.24	0.27
10	0.29	0.37	1.39	1.86	4.13	2.94	2.16	1.28	1.14	1.00	0.28	0.28	0.27	0.31
11	1.02	1.28	4.90	6.54	14.52	10.32	7.60	4.51	4.00	3.51	1.00	0.97	0.94	1.07
12	1.05	1.32	5.04	6.72	14.93	10.61	7.81	4.64	4.12	3.61	1.03	1.00	0.97	1.10
13	1.08	1.37	5.21	6.95	15.43	10.97	8.07	4.79	4.25	3.74	1.06	1.03	1.00	1.14
14	0.95	1.20	4.56	6.09	13.52	9.61	7.07	4.20	3.73	3.27	0.93	0.91	0.88	1.00

* variables defined in Table 9

Table 12
 Dry January Grand Junction Sounding
 Area Ratios from Figure 35 (column variable/row variable)

	1	2	3	4	5	6	7	8	9	10	11	12	13	14
1	1.00*	1.26	4.86	6.16	12.35	8.78	6.46	4.11	3.62	3.15	0.96	0.93	0.90	1.05
2	0.79	1.00	3.86	4.89	9.81	6.97	5.13	3.26	2.87	2.50	0.77	0.74	0.71	0.83
3	0.21	0.26	1.00	1.27	2.54	1.81	1.33	0.85	0.75	0.65	0.20	0.19	0.19	0.22
4	0.16	0.20	0.79	1.00	2.00	1.43	1.05	0.67	0.59	0.51	0.16	0.15	0.15	0.17
5	0.08	0.10	0.39	0.50	1.00	0.71	0.52	0.33	0.29	0.26	0.08	0.08	0.07	0.08
6	0.11	0.14	0.55	0.70	1.41	1.00	0.74	0.47	0.41	0.36	0.11	0.11	0.10	0.12
7	0.15	0.19	0.75	0.95	1.91	1.36	1.00	0.64	0.56	0.49	0.15	0.14	0.14	0.16
8	0.24	0.31	1.18	1.50	3.00	2.14	1.57	1.00	0.88	0.77	0.23	0.23	0.22	0.25
9	0.28	0.35	1.34	1.70	3.41	2.43	1.79	1.14	1.00	0.87	0.27	0.26	0.25	0.29
10	0.32	0.40	1.54	1.95	3.92	2.78	2.05	1.30	1.15	1.00	0.31	0.30	0.29	0.33
11	1.04	1.31	5.04	6.39	12.81	9.11	6.71	4.26	3.76	3.27	1.00	0.97	0.93	1.08
12	1.07	1.35	5.20	6.59	13.22	9.40	6.92	4.40	3.87	3.38	1.03	1.00	0.96	1.12
13	1.11	1.40	5.40	6.84	13.72	9.76	7.18	4.57	4.02	3.50	1.07	1.04	1.00	1.16
14	0.96	1.20	4.65	5.89	11.81	8.40	6.18	3.93	3.46	3.02	0.92	0.89	0.86	1.00

* variables defined in Table 9

rows 2 and 3, 80% of the area under the NO MOUNTAIN--ALL BANDS curve comes from zenith angles less than the zenith angle to the ridge; 20% from zenith angles greater than this angle. In row 4, the air wedge contains 16% of the irradiance represented under the NO MOUNTAIN--ALL BANDS curve. Row 12 shows that the mountain valley floor (assuming radiating sidewalls at temperature T_2) has 8% more irradiance than an equivalent surface on flat terrain. The effect of the enhanced irradiance varies with the temperature of the sidewalls (Cols. 11-13, 104% to 113%). Other ratios that may be of interest can be obtained from the tables.

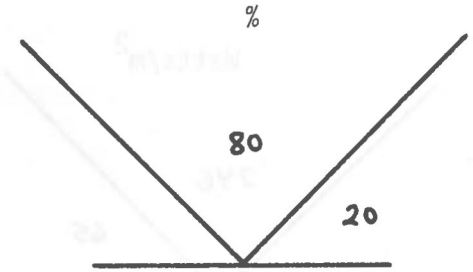
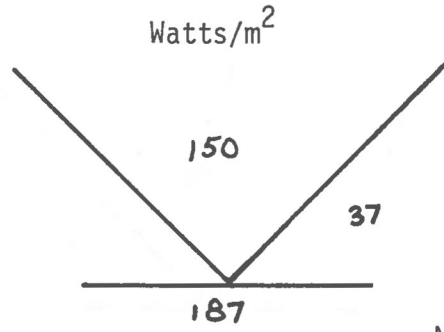
B. Components of IR Radiation Budget at the Surface

From the irradiance calculations in the previous sections we can summarize the components of the downward IR irradiance at the surface for January and July average soundings as depicted in Figs. 40 and 41 below. The surface energy budget can then be determined assuming that the valley floor is at the same temperature as the base of the sounding (850 mb) and is radiating as a black body. The resulting upward irradiance can be determined by using Fig. 42. The complete IR energy balances are then as shown in Tables 13 and 14.

In Table 13 energy budgets are presented for the January average and dry soundings. Upward irradiance in both cases is 292 W m^{-2} , figured on the basis of black body radiation at the temperature of the base of the sounding (-2.15°C). For the average January sounding, downward irradiance at the surface over flat terrain is calculated to be 187 W m^{-2} . Using the "winter standard valley", comparable irradiances are 195 W m^{-2} for the case with cold sidewalls, 202 W m^{-2} for the case

IRRADIANCES

comes



ains

urve.

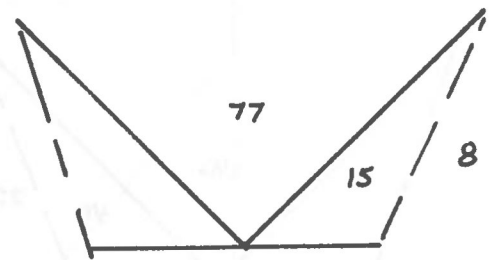
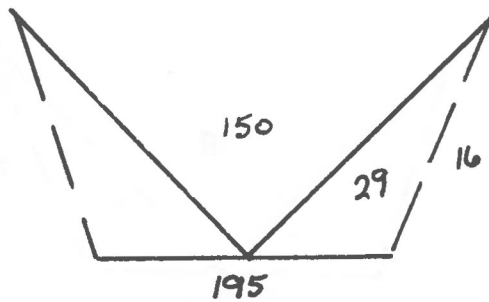
walls

e on

e

ratios

No Valley



Valley with side T 20 C ◀ bottom T

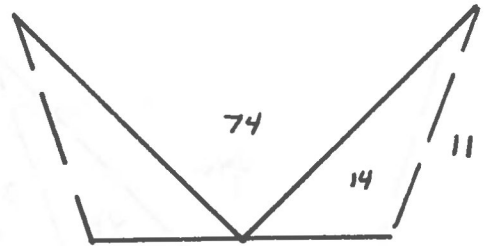
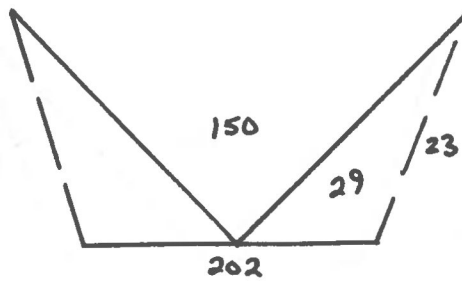
can

ace

41

that

inding



Valley with side T = bottom T

nergy

verage

,

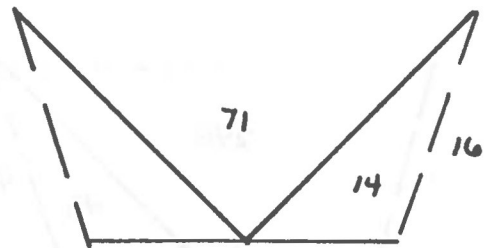
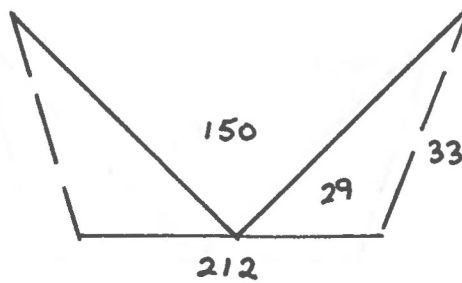
of the

g,

ed to

rradiances

he case



Valley with side T 20 C ▶ bottom T

Fig. 40 Irradiance contributions--January average sounding. Left column is in irradiance units, right column in percentages. Contribution of air wedge, radiating sidewalls, etc. shown in schematic view.

IRRADIANCES

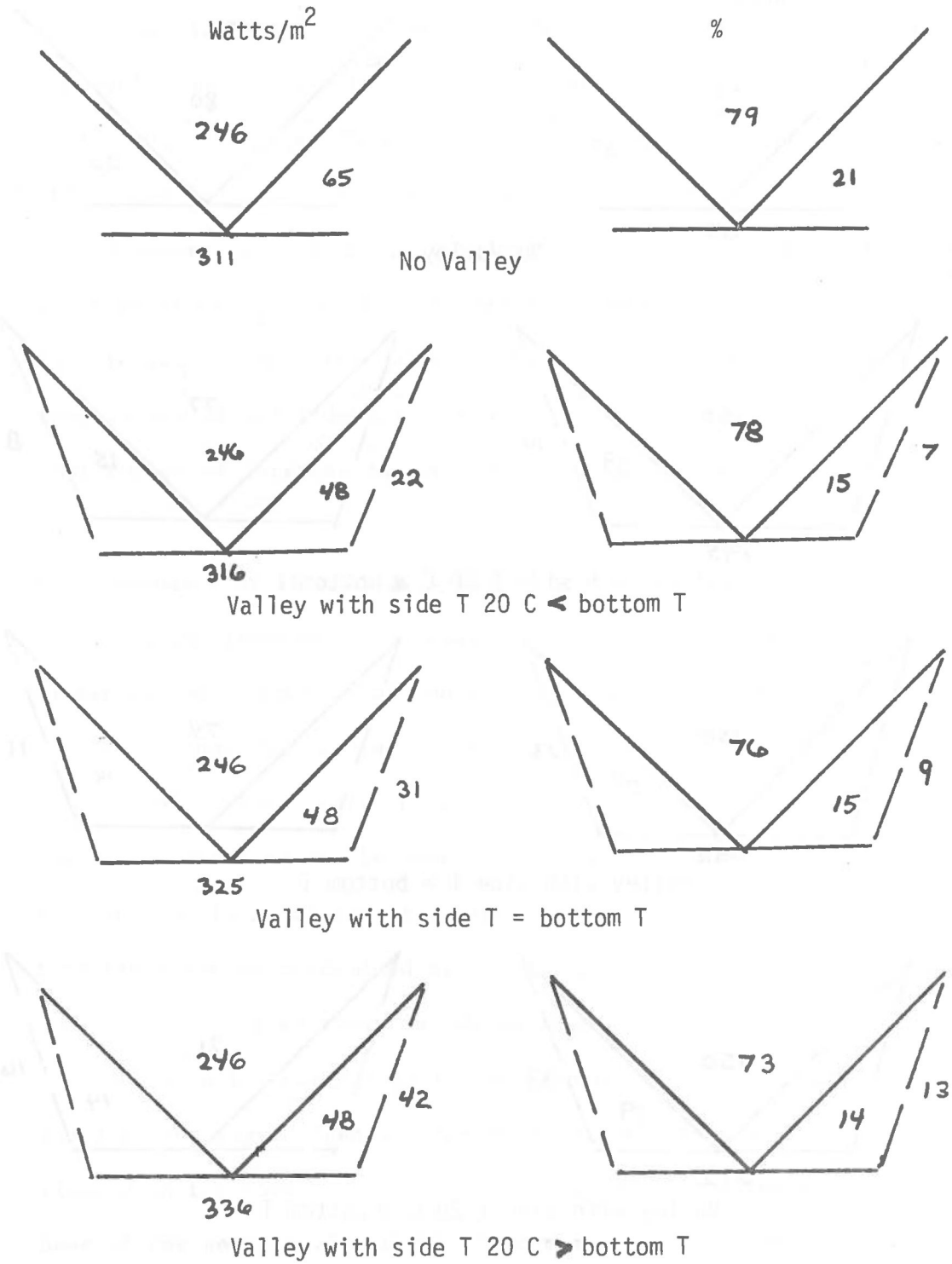


Fig. 41 Irradiance contributions--July average sounding. Left column is in irradiance units, right column in percentages. Contribution of air wedge, radiating sidewalls, etc. shown in schematic view.

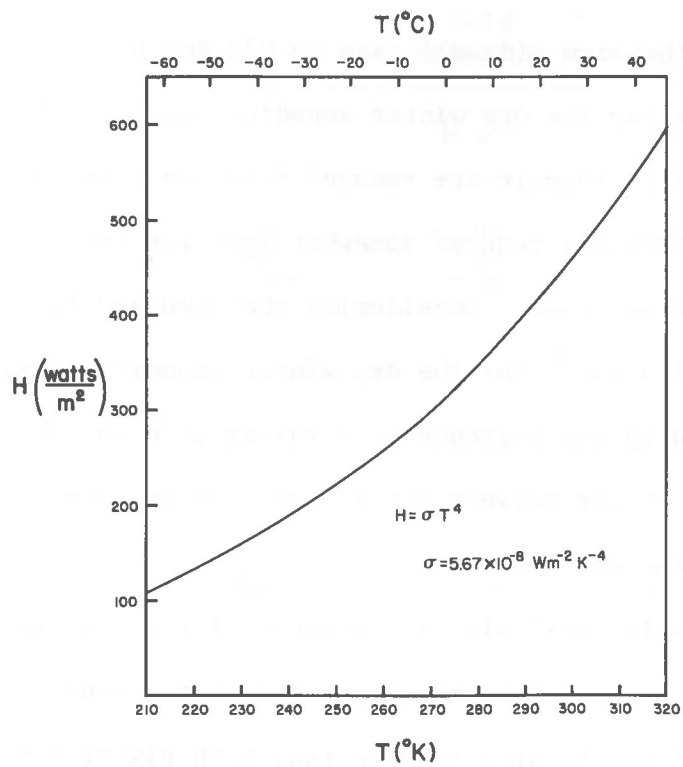


Fig. 42 Upward blackbody irradiance as a function of temperature.

with sidewalls at -2.15°C , and 212 W m^{-2} for the case with warm sidewalls. Thus downward irradiances are enhanced over the flat terrain case by 4 to 13%. Since net radiation is the difference between the upward and downward irradiances, H_{net} over flat terrain is 105 W m^{-2} . Net irradiances are lower than this for all of the valley cases, ranging from 76% of this figure for the warm sidewall case to 92% for the cold sidewall case.

Considering the dry winter sounding, downward irradiances over both flat and valley terrain are reduced from those of the average winter sounding. They are reduced somewhat less for the valley cases than for the flat terrain case. Considering the downward irradiance over flat terrain of 173 W m^{-2} for the dry winter sounding downward irradiances are enhanced by the presence of a valley by 6 to 16%. Net radiation values also differ between the average and dry soundings, being somewhat higher for the dry case.

The results of Table 14, presented for the summer soundings, are qualitatively similar to those for the winter soundings in Table 13. Values of H_{\uparrow} and H_{\downarrow} are, as expected, much higher for the summer case. Values of H_{net} are also higher by 6 to 15% for the summer cases. When the valley results for net radiation are compared to net radiation over flat terrain the summer ratios are quite comparable to the winter ratios. Downward irradiance ratios, however, are somewhat lower for the summer cases--ranging from 1.02 to 1.11 as compared to 1.04 to 1.16.

C. Radiative Cooling in Valley Atmosphere

Upward, downward and net irradiance calculations of the preceding sections have been calculated for a single point on the surface of the center of the valley floor. In order to determine IR atmospheric

ls. Thus
 13%.
 d
 re
 s
 both
 for
 at
 es
 a
 ewhat
 re
 .
 se.
 then
 over
 ratios.
 mmer
 ding
 the

Table 13. Infrared Radiation Energy Budget at Valley Bottom - January

	JAN AVG			
	No Valley	Cold Sidewalls	Valley	Warm Sidewalls
	$W m^{-2}$	$W m^{-2}$	$W m^{-2}$	$W m^{-2}$
H_{\uparrow}	292	292	292	292
H_{\downarrow}	187	195	202	212
H_{net}	105	97	90	80
$H_{\downarrow}/H_{\downarrow}$ (No Valley)	1.00	1.04	1.08	1.13
% of H_{net} (No Valley)	100%	92%	86%	76%
	JAN -3S			
H_{\uparrow}	292	292	292	292
H_{\downarrow}	173	183	191	201
H_{net}	119	109	101	91
$H_{\downarrow}/H_{\downarrow}$ (No Valley)	1.00	1.06	1.10	1.16
% of H_{net} (No Valley)	100%	92%	85%	76%

Table 14. Infrared Radiation Energy Budget
at Valley Bottom - July

JUL AVG				
	No Valley	Cold Sidewalls	Valley	Warm Sidewalls
	$W m^{-2}$	$W m^{-2}$	$W m^{-2}$	$W m^{-2}$
H↑	422	422	422	422
H↓	<u>311</u>	<u>316</u>	<u>325</u>	<u>336</u>
H _{net}	111	106	97	86
H↓/H↑ (No Valley)	1.00	1.02	1.05	1.08
% of H _{net} (No Valley)	100%	95%	87%	77%
JUL -3S				
H↑	422	422	422	422
H↓	<u>286</u>	<u>297</u>	<u>306</u>	<u>318</u>
H _{net}	136	125	116	104
H↓/H↑ (No Valley)	1.00	1.04	1.07	1.11
% of H _{net} (No Valley)	100%	92%	85%	76%

cooling rates at points in the atmosphere above the valley floor, H_{net} calculations would be required at various points in the atmosphere. Since H_{net} is the difference between $H\uparrow$ and $H\downarrow$ at the same level, these individual components should be calculated. The $H\downarrow$ for levels above the valley atmosphere will be unchanged from the flat terrain case. Within the valley atmosphere, however, $H\downarrow$ will be larger than corresponding values over flat terrain. At the valley floor the difference between flat terrain and valley downward irradiances will be a maximum or nearly a maximum, but this difference, even for the relatively extreme cases of steep walled valleys and heated sidewalls, is only 16%. For the dry January sounding this will result in an increase to 201 Wm^{-2} from the flat terrain case of 173 Wm^{-2} . The upward irradiance in the atmosphere within the valley will likewise be increased above the flat terrain case due to the effect of elevated radiating sidewalls, at least for the case of constant temperature up the sidewall. A minor increase of $H\uparrow$ above the ridgetop level will similarly be caused by sidewall radiation. This increase will diminish slowly with height. As a result of the changes in both $H\uparrow$ and $H\downarrow$, a slight change in cooling rate relative to the flat terrain case is possible but significant changes are not envisioned. Consequently, no attempt has been made to calculate cooling rates from detailed calculations in a valley.

V. SUMMARY AND CONCLUSIONS

Infrared radiation components in mountain valleys were investigated theoretically using a radiative transfer computer program in which radiances were calculated for different spectral bands and for different atmospheres and viewing angles. First, in the case of a linear valley, transmissivities between various points on the valley sidewalls and the center of the valley floor were determined. Using this linear valley model and assuming that the valley surfaces radiated as ideal blackbodies, spectral radiances were calculated for individual points within the valley for specified viewing angles. In the calculations an isothermal winter atmosphere having the same temperature as the valley surfaces was utilized. An analysis of the spectral radiances showed that two spectral intervals were particularly important in allowing radiation transfer between valley surfaces. One band corresponded to the water vapor continuum or atmospheric "window" at 7.8 to 13.4 microns and the other was in a "small window", at 16.3 to 20.2 microns, between the CO₂ and rotational water absorption bands. Radiation from the sidewalls in other spectral bands is effectively attenuated by the small transmittances along the beam paths due to absorption by atmospheric water vapor and CO₂.

The above analysis resulted in partitioning of the IR spectrum into 5 separate bands which were utilized in all subsequent work. The bands, designated as Bands 1 through 5, correspond to the water vapor band at 4.4 to 7.8 microns, the water vapor continuum at 7.8 to 13.4 microns, the CO₂ band at 13.4 to 16.3 microns, the small window at 16.3 to 20.2 microns, and the rotational water band at 20.2 to 48.8 microns, respectively.

A further analysis of the linear valley model calculations showed that 32 to 38% of black body radiation transmitted at one point reached the receptor point for path lengths between 1.45 and 2.25 km. For longer path lengths of 3 to 9 km, only 16 to 29% of the radiation was transferred. The great proportion of transferred radiation came through the atmospheric windows.

The preceding analysis was useful in gaining a preliminary view of the magnitude and nature of radiative interactions between radiating valley surfaces. In addition to this component, however, the radiation at a point on a valley surface will include a contribution from the adjacent atmosphere. In order to gain an appreciation of the magnitude of this contribution in various spectral intervals and for selected viewing angles, flat terrain calculations were made for 4 horizontally homogeneous atmospheres. The atmospheric soundings were obtained from upper air data statistics for Grand Junction, Colorado and included January and July average and dry soundings. The dry soundings were obtained from dew point statistics by adjusting the dew point values of the average sounding downwards by 3 standard deviations. This analysis allowed a determination of the fraction of energy arriving at the ground from various viewing angles coming from different layers of the atmosphere. Most of the radiance reaching the surface in bands 1, 3, and 5 comes from layers very close to the surface. By contrast, significant percentages of the radiance in bands 2 and 4 come from higher levels of the atmosphere, since transmittance is larger in these bands. For the dry soundings more of the radiation reaching the surface in all bands comes from higher in the atmosphere. Given the 4 soundings, in which

temperature and water vapor content decrease with height, the fraction of energy received at the surface from a given layer in the atmosphere is higher for higher zenith angles. The effect of zenith angle is particularly pronounced for the higher zenith angles. Transmittances are so low in bands 1, 3, and 5 that their contribution to radiances at the surface comes essentially from the lowest 100 meters of the atmosphere. This analysis, while conducted for flat terrain, suggests that the atmospheric structure (temperature and moisture profiles) within a valley will be much more important in reckoning the contribution to radiances and irradiances at the valley floor than the structure above the valley.

The effects of mountain valley terrain on surface radiance and irradiance fields were calculated for an idealized, circularly-symmetrical, flat-bottomed mountain valley. In particular, the radiances at the center of the valley floor were presented as a function of viewing angle for five spectral intervals and four atmospheres. Use of the circularly-symmetrical valley allowed comparison of the various components making up the surface radiance field, including the effect of atmospheric radiation at elevation angles above the surrounding ridgetops, atmospheric radiation from the air wedge within the valley, and the effect of the radiating sidewalls on the surface radiance field for several different sidewall temperatures. For comparison with these components calculations were also made of the equivalent radiance field over flat terrain. The circular symmetry of the idealized valley cross-section further allowed a simple angular integration to be performed resulting in calculations of downward

irradiance at the center of the valley floor. The resulting irradiances were compared with corresponding irradiances over flat terrain and the downward irradiances were found to be somewhat higher in the case of the mountain valley. The magnitude of the effect of the radiating sidewalls was largest when the valley volume contained small quantities of water vapor and when the sidewalls were warm relative to the air within the valley. The largest relative effect was, therefore, seen in dry winter soundings. In such cases the downward irradiances at valley center can be 6 to 16% higher than those over flat terrain. The highest value obtained corresponds to the effect of a sidewall that is 20° C warmer than the temperature at the base of the sounding. Even when the sidewalls are 20° C less than the temperature at the base of the sounding the downward irradiance is enhanced by 6% over the case of flat terrain. In accordance with this result a sharp discontinuity in the radiance field occurred at the critical zenith angle of the ridgetop. For zenith angles greater than this critical angle the downward radiance field was significantly enhanced over the flat terrain case. The effect of the atmosphere within the valley at zenith angles greater than the critical angle (called the "air wedge" in the analysis) also provides an important component of the surface irradiance. This component comes mainly from spectral bands 5, 3, and 4 where transmittances are low. The component from the radiating sidewalls, on the other hand, comes through bands 2 and 4 where atmospheric transmittance is high.

For the dry winter sounding, where the relative effect of radiating sidewalls was most important, values of downward irradiance varied from 183 W m^{-2} for cold sidewalls to 201 W m^{-2} for warm sidewalls. These

irradiances may be compared to the downward irradiance of 173 W m^{-2} calculated over flat terrain. If we assume that the surface is radiating as a black body at the temperature of the base of the sounding we may calculate an upward irradiance of 292 W m^{-2} . By considering the difference between upward and downward irradiances we arrive at net loss of 109 W m^{-2} for the cold sidewall case and 91 W m^{-2} for the warm sidewall case. These compare to 119 W m^{-2} for the flat terrain case. Thus the effect of the sidewalls is to decrease net radiation by 8 to 24%, resulting in a decrease of the cooling rate at the surface. This effect, of course, will be somewhat smaller for valleys shallower than the modeled valley where sidewalls sloped upwards at 31° , and for more realistic, non-circularly-symmetrical valleys.

2

adiating
may
differ-
s of
ewall
; the
effect,
e modeled
tic,

VI. REFERENCES

- Bignell, K. J., 1970: The Water-Vapor Intra-red Continuum, Quart. J. Roy. Meteor Soc., 96, 390-403.
- Bushnell, R. H., 1977: Letters to the Editor - Radiation Constants. Bull. Amer. Meteor Soc., 58, 258-259.
- Chief of Naval Operations, 1966: Selected Level Temperatures and Dew Points for the Northern Hemisphere. NAVAIR 50-1C-52.
- Cox, S. K., 1973: Infrared Heating Calculations with a Water Vapor Pressure Broadened Continuum. Quart. J. Roy. Meteor Soc., 99, 669-679.
- Cox, S. K., M. C. Polifka, K. Griffith, A. Rockwood, D. Starr, 1976: Radiative Transfer Computational Routines For Atmospheric Science Applications. Department of Atmospheric Science, Colorado State University Fort Collins. August 1, 1976, 75 pp.
- Elsasser, W. M., and M. F. Culbertson, 1960: Atmospheric Radiation Tables, Meteorological Monographs, 4, 43pp.
- Paltridge, G. W., and C.M.R. Platt, 1976: Radiative Processes in Meteorology and Climatology, Developments in Atmospheric Science, 5, Elsevier Scientific Publishing Company, New York, 318 pp.
- Smith, W. L., 1969: A polynomial Representation of Carbon Dioxide and Water Vapor Transmission, ESSA Technical Report NESC 47, 20 pp.
- Staley, D. O., and G. M. Jurica, 1970: Flux Emissivity Tables for Water Vapor, Carbon Dioxide and Ozone, J. Appl. Meteor. 9, 365-372.
- Widger, W. K., Jr., 1968: A Note on the Wien Displacement Law. Bull. Amer. Meteor. Soc., 49, 724-725.
- Widger, W. K., Jr., and M. P. Woodall, 1976: Integration of the Planck Blackbody Radiation Function, Bull. American Meteor Soc., 57, 1217-1219.

APPENDIX A
Standard Soundings

1. VAIL DEC ISO

Isothermal sounding constructed utilizing approximate temperature and mixing ratio values obtained from December 1975 Vail tethered balloon data. The sounding was used for calculating transmissivity within the valley from a point at the center of the valley floor to any arbitrary point on the sidewall of any arbitrary-shaped valley. Details of the sounding are listed below in Table A1.

Table A1
VAIL DEC ISO

Pressure (mb)	Temperatures (°C)	Mixing Ratio (gm/kg)
655	-5.	4.5
680	-5.	4.5
700	-5.	4.5
715	-5.	4.5
725	-5.	4.5
730	-5.	4.5
735	-5.	4.5
740	-5.	4.5
745	-5.	4.5
750	-5.	4.5

2. NAVAIR Soundings

January and July averages and standard deviations of temperatures and dewpoints at standard levels above Grand Junction, Colorado, were used to construct reference atmospheres for use in calculations. The data for standard levels came from NAVAIR 50-1C-52: "Selected Level Temperatures and Dew Points For The Northern Hemisphere." Average soundings, dry soundings and saturated soundings were used for both months. The "dry" soundings were constructed using the average temperature soundings, but utilizing dew point temperatures that were 3 standard deviations below normal. Interpolations were used to calculate temperatures at pressures between the standard levels (i.e., the soundings were "EXTENDED"). The surface pressure at Grand Junction was taken to be 850 mb.

2.1 NAVAIR JAN GJT AVG.: Average January Grand Junction sounding.

Shown below in Table A2 is a listing of this sounding. The sounding is plotted in Figure A1.

Table A1
NAVAIR GJT JAN AVG

Pressure (mb)	Temperature (Deg C)	Mixing Ratio (gm/kg)
850	-2.150	2.400
845	-2.315	2.375
840	-2.480	2.350
835	-2.645	2.325
830	-2.810	2.300
825	-2.975	2.275
820	-3.140	2.250
815	-3.305	2.225
810	-3.470	2.200
805	-3.635	2.175
800	-3.800	2.150
750	-5.400	1.900
700	-7.030	1.700
650	-10.300	1.400
600	-14.000	1.100
550	-18.000	.800
500	-22.240	.600
450	-27.300	.300
400	-33.000	.140
350	-39.700	.080
300	-47.250	.050
250	-52.000	.000
200	-57.380	.000
150	-59.000	.000
100	-61.000	.000

Precipitable Water: .617 cm

NAVAIR JAN GJT -321 017 January Grand Junction Sounding
 Table A1 lists the sounding. Figure A1 provides a
 sounding

NAVAIR JAN GJT AVG

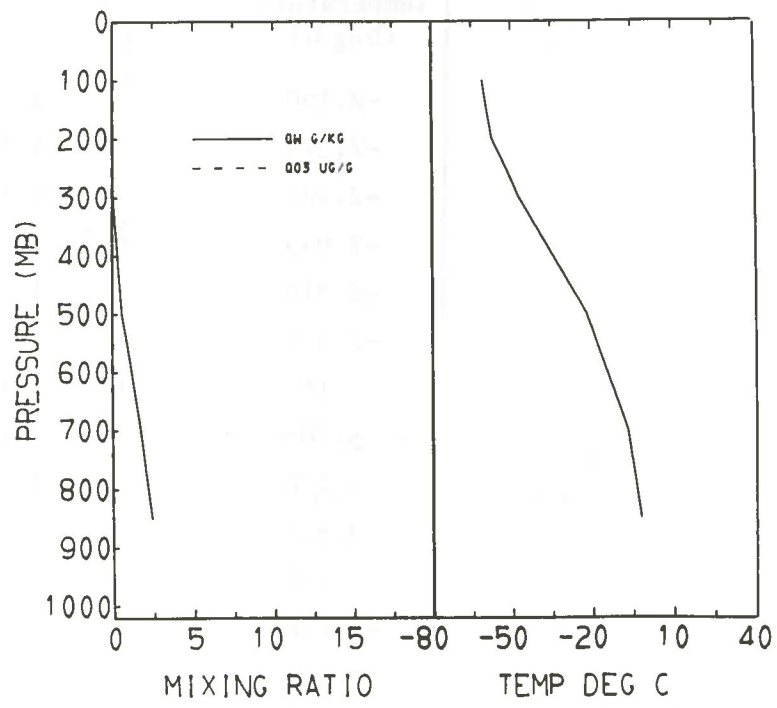


Fig. A1 Average January Grand Junction sounding

2.2 NAVAIR JAN GJT -3S: Dry January Grand Junction Sounding

Table A3 lists the sounding; Figure A2 provides a plot of the sounding.

Table A3
NAVAIR GJT JAN -3S

Pressure (mb)	Temperature (Deg C)	Mixing Ratio (gm/kg)
850	-2.150	1.200
845	-2.315	1.194
840	-2.480	1.188
835	-2.645	1.182
830	-2.810	1.176
825	-2.975	1.170
820	-3.140	1.164
815	-3.305	1.158
810	-3.470	1.152
805	-3.635	1.146
800	-3.800	1.140
750	-5.400	1.070
700	-7.030	1.000
650	-10.300	.800
600	-14.000	.600
550	-18.000	.460
500	-22.240	.320
450	-27.300	.190
400	-33.000	.100
350	-39.700	.062
300	-47.250	.025
250	-52.000	.000
200	-57.380	.000
150	-59.000	.000
100	-61.000	.000

Precipitable Water: .346 cm

the

NAVAIR JAN GJT -3S

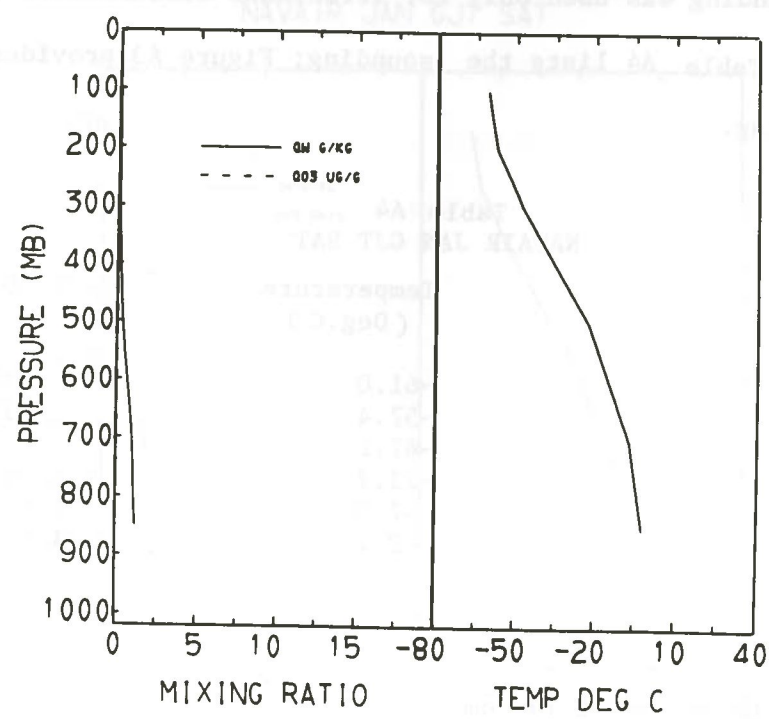


Fig. A2 Dry January Grand Junction sounding.

2.3 NAVAIR JAN GJT SAT: Saturated January Grand Junction Sounding

This sounding was used only for irradiance calculations for flat terrain. Table A4 lists the sounding; Figure A3 provides a plot of the sounding.

Table A4
NAVAIR JAN GJT SAT

Pressure (mb)	Temperature (Deg.C)	W H2O (gm/kg)
100.0	-61.0	.001
200.0	-57.4	.001
300.0	-47.2	.150
500.0	-22.2	1.300
700.0	-7.0	3.200
850.0	-2.2	3.700

Precipitable water: 1.143 cm

NAVAIR JUL GJT SAT: Average July Grand Junction sounding

NAVAIR JAN GJT SAT: Average January Grand Junction sounding

NAVAIR JAN GJT SAT

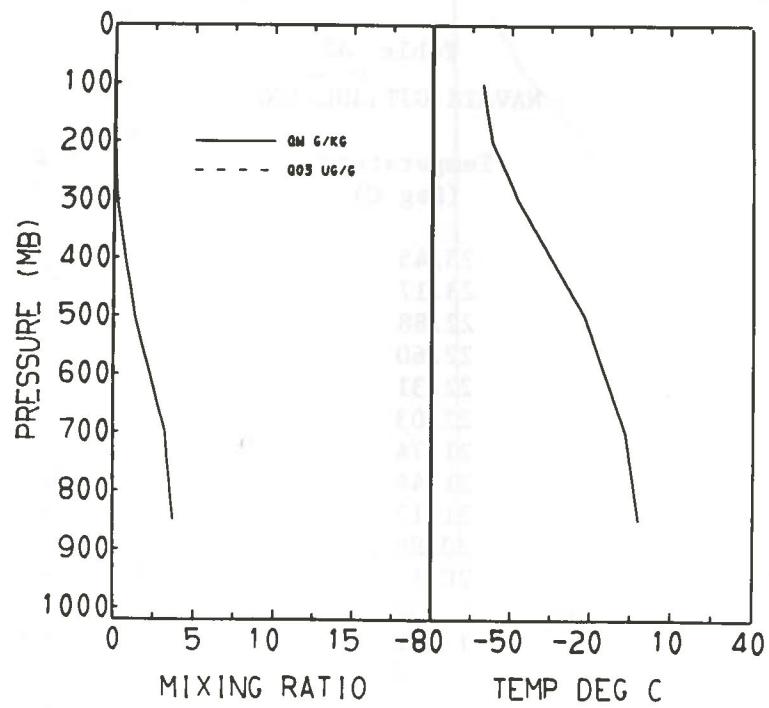


Fig. A3 Saturated January Grand Junction sounding.

2.4 NAVAIR JUL GJT AVG: Average July Grand Junction Sounding.

Table A5 lists the sounding; Figure A4 provides a plot of the sounding.

Table A5
NAVAIR GJT JUL AVG

Pressure (mb)	Temperature (Deg C)	Mixing Ratio (gm/kg)
850	23.45	7.30
845	23.17	7.25
840	22.88	7.20
835	22.60	7.15
830	22.31	7.10
825	22.03	7.05
820	21.74	7.00
815	21.46	6.95
810	21.17	6.90
805	20.89	6.85
800	20.60	6.80
750	17.30	6.40
700	14.06	6.00
650	9.10	4.80
600	3.90	3.90
550	-2.00	3.00
500	-8.13	2.20
450	-13.60	1.60
400	-19.70	1.20
350	-26.50	.54
300	-34.40	.20
250	-43.30	.10
200	-53.79	.05
150	-59.10	.00
100	-66.13	.00

Precipitable water: 2.110 cm

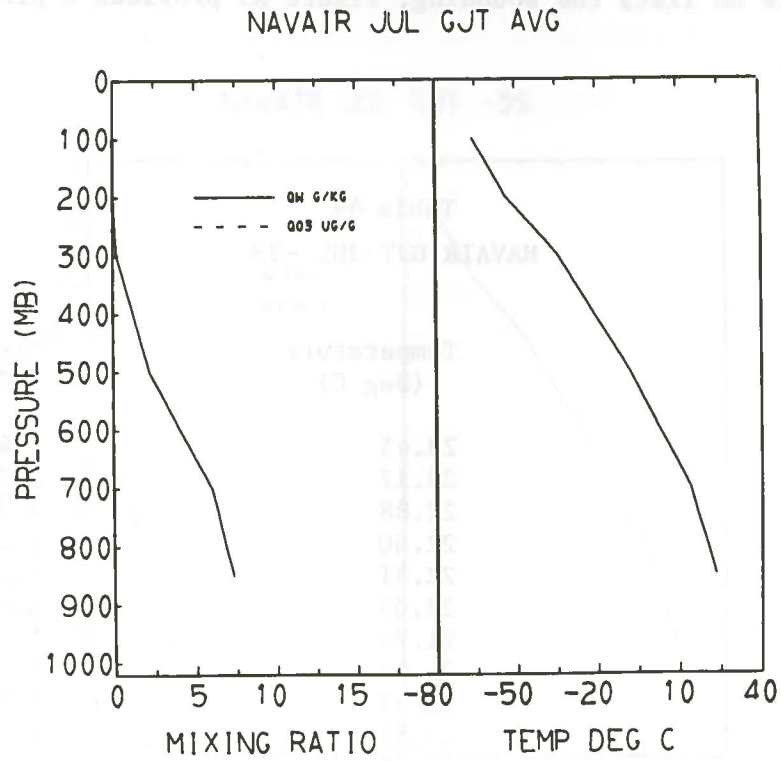


Fig. A4 Average July Grand Junction sounding.

2.5 NAVAIR JUL GJT -3S: Dry July Grand Junction sounding.

Table A6 lists the sounding; Figure A5 provides a plot of the sounding.

Table A6
NAVAIR GJT JUL -3S

Pressure (mb)	Temperature (Deg C)	Mixing Ratio (gm/kg)
850	23.45	5.400
845	23.17	5.350
840	22.88	5.300
835	22.60	5.250
830	22.31	5.200
825	22.03	5.150
820	21.74	5.100
815	21.46	5.050
810	21.17	5.000
805	20.89	4.950
800	20.60	4.900
750	17.30	4.400
700	14.06	4.000
650	9.10	3.200
600	3.90	2.500
550	-2.00	1.900
500	-8.13	1.400
450	-13.60	1.000
400	-19.70	.700
350	-26.50	.320
300	-34.40	.110
250	-43.30	.050
200	-53.79	.025
150	-59.10	.000
100	-66.13	.000

Precipitable water: 1.430 cm.

NAVAIR JUL GJT -3S

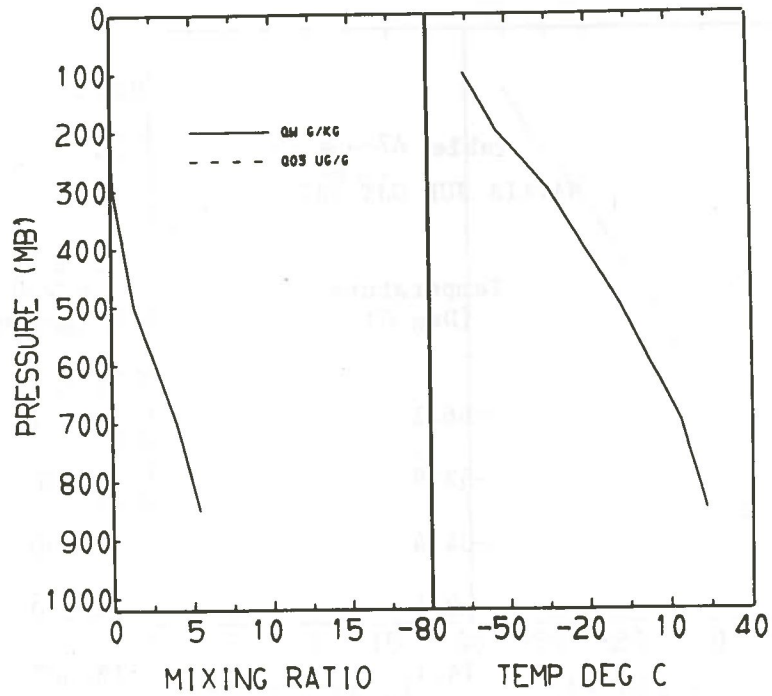


Fig. A5 Dry July Grand Junction sounding.

2.6 NAVAIR JUL GJT SAT: Saturated July Grand Junction Sounding.

This sounding was used only for irradiance calculations for flat terrain. Table A7 lists the sounding; Fig. A6 provides a plot of the sounding.

Table A7
NAVAIR JUL GJT SAT

Pressure (mb)	Temperature (Deg C)	W H2O (gm/kg)
100.0	-66.1	.001
200.0	-53.8	.100
300.0	-34.4	.700
500.0	-8.1	4.200
700.0	14.1	15.000
850.0	23.5	22.100

Precipitable water: 5.344 cm.

Precipitable water: 1.430 cm.

NAVAIR JUL GJT SAT

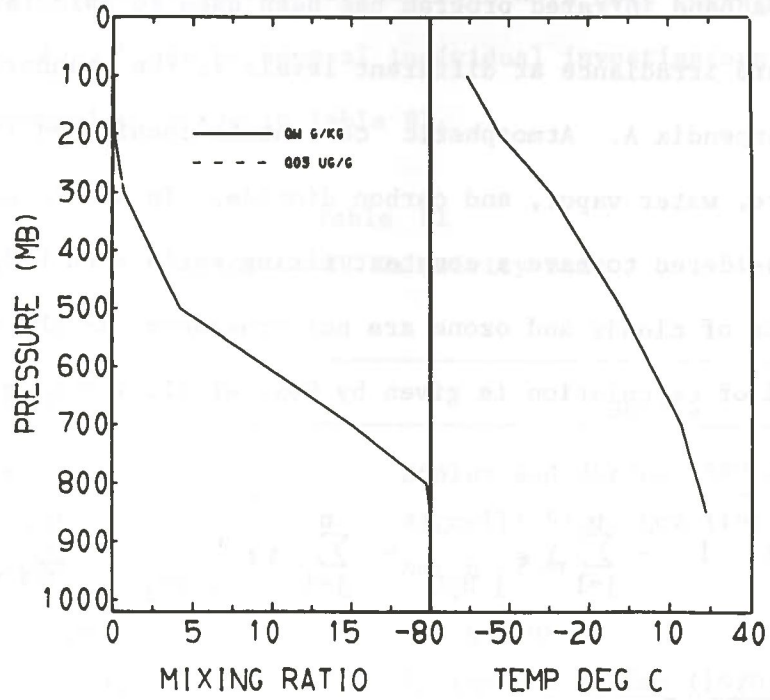


Fig. A6 Saturated July Grand Junction sounding.

APPENDIX B
Computer Programs

1. Irradiance Program.

A broadband infrared program has been used to calculate upward and downward irradiance at different levels in the standard atmospheres given in Appendix A. Atmospheric components considered include temperature, water vapor, and carbon dioxide. In all reference atmospheres CO₂ is considered to have a constant mixing ratio with height of .486 gm/kg. The effects of clouds and ozone are not considered in the calculations. The method of calculation is given by Cox, et al. (1976) and is summarized below:

$$H(P) = H_0 \left[1 - \sum_{j=1}^n \Delta \epsilon_j \text{ H}_2\text{O} - \sum_{j=1}^n \Delta \epsilon_j \text{ CO}_2 + \sum_{j=1}^n \Delta \epsilon_j \text{ overlap} \right] + \sum_{j=1}^n \left\{ H_j \left[\Delta \epsilon_j \text{ H}_2\text{O} + \Delta \epsilon_j \text{ CO}_2 - \Delta \epsilon_j \text{ overlap} \right] \right\}$$

where H(P) represents the upward or downward irradiance at pressure level P, and H₀ is the emitted radiance of the background surface. For calculations of upward irradiance, H(P)↑, the background surface is the earth and we assume H₀ = σT_{SFC}^4 . For calculations of downward irradiance, H(P)↓, the background surface is outer space and we assume H₀ = 0.

The first term in the expression represents the transmitted term, i.e., the contribution to H(P) from the background surface. The second term represents the contribution to irradiance originating from emissions from within the atmospheric layers themselves, where:

$$H_j = \sigma T_j^4 \quad \text{and } j \text{ is the layer index.}$$

The $\Delta \epsilon_j$ are emissivity increments for individual layers.

The increments are due to water vapor, carbon dioxide and a correction term due to the overlap between CO₂ and H₂O bands. The actual gaseous emissivity data used in the calculations have been determined empirically for the various bands by several individual investigators. This information is summarized below in Table B1.

Table B1
Sources of IR Emissivity Data

Band	Source
H ₂ O 6.3 micron	Staley and Jurica (1970)
H ₂ O Continuum	Bignell(1970), Cox (1973)
H ₂ O Rotational	Smith (1960)
CO ₂ 14.7 micron	Smith (1969)
CO ₂ - H ₂ O overlap	Staley and Jurica (1970)

Collision broadening is accounted for in the program; details can be obtained from Cox, et al. (1976). Computations of upward and downward irradiances at various levels in the atmosphere enable layer cooling rates to be calculated using the formula:

$$\frac{\Delta T}{\Delta t} = \frac{g}{C_P} \frac{\Delta H_{net}}{\Delta P} \quad \text{where } H_{net}(P) = H \uparrow (P) - H \downarrow (P)$$

2. Radiance Program.

The program used to calculate radiances within a mountain valley was adapted from PROGRAM RADLON, described by Cox, et al. (1976). A brief description of PROGRAM RADLON and the modifications necessary to enable us to utilize this program for mountain valley calculations follows:

The program is a general spectral infrared radiative transfer program in which the user is required to input a specific atmosphere, a viewing zenith angle (θ), and the wavenumber limits of the specific band (or bands) of interest. The specific atmospheres used with this program were listed in Appendix A. Pressure, temperature, specific humidity, and CO₂ profiles were specified. The effects of ozone were ignored. The CO₂ mixing ratio was assumed constant (.486 gm/kg) with height. Radiance calculations were made for the 5 distinct bands listed below in Table B2.

Table B2
Spectral Intervals used in Calculations

Bands	Wavelength Interval (μ)	Wavenumber Interval (cm^{-1})	
1	4.4-7.8	1285-2265	H ₂ O 6.3 micron
2	7.8-13.4	745-1285	H ₂ O Continuum
3	13.4-16.3	615-745	CO ₂
4	16.3-20.2	495-615	Small window
5	20.2-48.8	205-495	H ₂ O Rotational

Radiances were calculated using the numerical integration:

$$N_{\nu}(\theta, P) = - \int_P^{P_0} B_{\nu, \theta}(T) \frac{\partial \tau_{\nu}}{\partial \rho} d\rho - B_{\nu, \theta}(T) \int_P^{P_0} \frac{\partial \tau_{\nu}}{\partial \rho} d\rho$$

where $B(T)$ is the Planck radiation function, τ_{ν} is transmissivity defined by

$$\tau_{\nu} = \pi \tau_{\nu_i} \quad \text{for } i = 1, n, \text{ and where } n \text{ is the total number of absorbers.}$$

The integration across the spectral bands is accomplished as follows:

$$N_{\nu_1 \text{ to } \nu_2}(\theta, P) = \sum_{j=1}^m N_{\nu_j}(\theta, P) \Delta \nu \quad \text{where } m = \frac{\nu_2 - \nu_1}{10}$$

The program uses empirical spectral absorption data for spectral intervals of 10 cm^{-1} from the authors listed below in Table B3.

Table B3
Sources of IR Emissivity Data

Band	Source
H ₂ O 6.3 micron	Elsasser and Culbertson (1960)
H ₂ O continuum	Bignell (1970)
H ₂ O rotational	Smith (1964) for $u \leq 5 \text{ cm}$ Elsasser and Culbertson (1960) for $u > 5 \text{ cm}$
CO ₂ 14.7 micron	Smith (1969) for $u \leq 500 \text{ cm}$ Elsasser and Culbertson (1960) for $u > 500 \text{ cm}$

The effects of collision broadening were handled using the scheme described by Cox, et al. (1976). Doppler broadening effects were disregarded.

The two major modifications required to adapt PROGRAM RADLON to handle our mountain valley calculations were: (1) modifications to allow the pressure integration limits to be reversed so that the integration could

proceed downward from the top of the atmosphere, and (2) a modification to allow Bignell's (1970) continuum absorption data to be properly meshed with the absorption data for bands on either side of the continuum.

The program was developed in the spectral range as follows:

$$k_{\text{eff}}(\lambda) = \frac{k_{\text{cont}}(\lambda) + k_{\text{band}}(\lambda)}{1 + \frac{k_{\text{cont}}(\lambda)}{k_{\text{band}}(\lambda)}}$$

The program uses analytical spectral absorption data for spectral

intensity of I_0 from the surface layer using in units of

the total number of absorbers

of the total number of absorbers

of the total number of absorbers

of the total number of absorbers

of the total number of absorbers

of the total number of absorbers

of the total number of absorbers

Wavelength (microns)	Source
0.2 - 0.4	Platz and Chubb (1961)
0.4 - 0.6	Bignell (1970)
0.6 - 0.8	Bignell (1970) $\pm 2\%$
0.8 - 1.0	Platz and Chubb (1961) $\pm 2\%$
1.0 - 1.2	Platz and Chubb (1961) $\pm 2\%$
1.2 - 1.4	Platz and Chubb (1961) $\pm 2\%$
1.4 - 1.6	Platz and Chubb (1961) $\pm 2\%$
1.6 - 1.8	Platz and Chubb (1961) $\pm 2\%$
1.8 - 2.0	Platz and Chubb (1961) $\pm 2\%$
2.0 - 2.2	Platz and Chubb (1961) $\pm 2\%$
2.2 - 2.4	Platz and Chubb (1961) $\pm 2\%$
2.4 - 2.6	Platz and Chubb (1961) $\pm 2\%$
2.6 - 2.8	Platz and Chubb (1961) $\pm 2\%$
2.8 - 3.0	Platz and Chubb (1961) $\pm 2\%$
3.0 - 3.2	Platz and Chubb (1961) $\pm 2\%$
3.2 - 3.4	Platz and Chubb (1961) $\pm 2\%$
3.4 - 3.6	Platz and Chubb (1961) $\pm 2\%$
3.6 - 3.8	Platz and Chubb (1961) $\pm 2\%$
3.8 - 4.0	Platz and Chubb (1961) $\pm 2\%$
4.0 - 4.2	Platz and Chubb (1961) $\pm 2\%$
4.2 - 4.4	Platz and Chubb (1961) $\pm 2\%$
4.4 - 4.6	Platz and Chubb (1961) $\pm 2\%$
4.6 - 4.8	Platz and Chubb (1961) $\pm 2\%$
4.8 - 5.0	Platz and Chubb (1961) $\pm 2\%$
5.0 - 5.2	Platz and Chubb (1961) $\pm 2\%$
5.2 - 5.4	Platz and Chubb (1961) $\pm 2\%$
5.4 - 5.6	Platz and Chubb (1961) $\pm 2\%$
5.6 - 5.8	Platz and Chubb (1961) $\pm 2\%$
5.8 - 6.0	Platz and Chubb (1961) $\pm 2\%$
6.0 - 6.2	Platz and Chubb (1961) $\pm 2\%$
6.2 - 6.4	Platz and Chubb (1961) $\pm 2\%$
6.4 - 6.6	Platz and Chubb (1961) $\pm 2\%$
6.6 - 6.8	Platz and Chubb (1961) $\pm 2\%$
6.8 - 7.0	Platz and Chubb (1961) $\pm 2\%$
7.0 - 7.2	Platz and Chubb (1961) $\pm 2\%$
7.2 - 7.4	Platz and Chubb (1961) $\pm 2\%$
7.4 - 7.6	Platz and Chubb (1961) $\pm 2\%$
7.6 - 7.8	Platz and Chubb (1961) $\pm 2\%$
7.8 - 8.0	Platz and Chubb (1961) $\pm 2\%$
8.0 - 8.2	Platz and Chubb (1961) $\pm 2\%$
8.2 - 8.4	Platz and Chubb (1961) $\pm 2\%$
8.4 - 8.6	Platz and Chubb (1961) $\pm 2\%$
8.6 - 8.8	Platz and Chubb (1961) $\pm 2\%$
8.8 - 9.0	Platz and Chubb (1961) $\pm 2\%$
9.0 - 9.2	Platz and Chubb (1961) $\pm 2\%$
9.2 - 9.4	Platz and Chubb (1961) $\pm 2\%$
9.4 - 9.6	Platz and Chubb (1961) $\pm 2\%$
9.6 - 9.8	Platz and Chubb (1961) $\pm 2\%$
9.8 - 10.0	Platz and Chubb (1961) $\pm 2\%$

The effect of collision broadening was handled using the method described

in Platz et al. (1970). Doppler broadening was also included.

The two major modifications are applied to model PROGRAM FATHOM to

allow for accurate mixing calculations using (1) coefficients to allow

the effect of collision broadening to be restored so that the integration could

be performed with greater accuracy.

The effect of collision broadening is restored so that the integration could

be performed with greater accuracy.

The effect of collision broadening is restored so that the integration could

3. Blackbody Flux Program

The Planck blackbody functions are defined as follows:

$$B_{\lambda}(T) d\lambda = C_1 \lambda^{-5} [\exp(C_2/\lambda T) - 1]^{-1} d\lambda$$

$$B_{\nu}(T) d\nu = C_3 \nu^3 [\exp(C_4 \nu/T) - 1]^{-1} d\nu$$

The energy emitted by a black body of temperature T within a discrete spectral band can be determined by integrating the Planck blackbody function between the limits of the band. The integral thus determined can be visualized as representing an area under the blackbody curve as shown in Fig. B1.

The integrations

$$B(T) = C_1 \int_{\lambda_1}^{\lambda_2} \left\{ \lambda^{-5} [\exp(C_2/\lambda T) - 1]^{-1} \right\} d\lambda \quad \text{and}$$

$$B(T) = C_3 \int_{\nu_1}^{\nu_2} \left\{ \nu^3 [\exp(C_4 \nu/T) - 1]^{-1} \right\} d\nu$$

can be accomplished using a scheme described by Widger and Woodall (1976) and Bushnell (1977). See also Widger (1968). Following is a copy of the Widger and Woodall HP-65 Program that accomplishes the integration. This integration scheme was used to determine the amount of energy emitted by valley sidewalls (assuming they radiate as blackbodies) within certain spectral intervals.

HP-65 User Instructions

Title PLANCK RADIATION FUNCTION INTEGRAL Page 1 of 1

Programmer W. K. WIDGER, JR. Date 7/2/75

PLANCK RADIATION INTEGRAL

STEP	INSTRUCTIONS	INPUT DATA/UNITS	KEYS	OUTPUT DATA/UNITS
1	INSERT PROGRAM		<input type="text"/> <input type="text"/>	
2	ν (WAVE NUMBER)	cm^{-1}	<input type="text"/> <input type="text"/>	
3	T (TEMPERATURE)	(K)	D <input type="text"/>	$X = C_2\nu/T$
4			f REG <input type="text"/>	
5	Δn (# REITERATIONS)		<input type="text"/> <input type="text"/>	
6	$x = C_2\nu/T$		A <input type="text"/>	$\sum_n \exp -nx$
	OPTIONS: { TO CHECK CONVERGENCE: $\left\{ \begin{matrix} 1 \\ x \end{matrix} \right.$ OR FOR FURTHER Δn ITERATIONS	(one)	<input type="text"/> <input type="text"/>	$\int_0^x [x^3/\exp x]$
			A <input type="text"/>	$\int_0^\infty [x^3/\exp x]$
			R/S <input type="text"/>	$\int_0^\infty [x^3/\exp x]$
7	$\sum \exp -nx () = \int_0^x [x^3/(\exp x - 1)] dx$		<input type="text"/> <input type="text"/>	
8	T	(K)	E <input type="text"/>	$[B(T)]_\nu^\infty$
	-----	-----	<input type="text"/> <input type="text"/>	WATTS $\text{CM}^{-2}\text{STER}^{-1}$
	$[B(T)]_\nu^\infty = C_1 C_2^{-4} T^4 \int_0^x [x^3/(\exp x - 1)] dx$		<input type="text"/> <input type="text"/>	
	$\int_0^x \frac{x^3}{\exp x - 1} dx = \sum_{n=1}^\infty \exp(-nx) (x^3 n^{-1} + 3x^2 n^{-2} + 6x n^{-3} + 6n^{-4})$		<input type="text"/> <input type="text"/>	
	REITERATIONS (Δn) AT LEAST ADEQUATE FOR 10 SIGNIF. FIGURES		<input type="text"/> <input type="text"/>	
X	0.1 0.2 0.3-0.4 0.5 0.6 0.7 0.8		<input type="text"/> <input type="text"/>	
Δn	101 65 50 35 30 25 22		<input type="text"/> <input type="text"/>	
X	0.9-1.4 1.5-1.9 2.0-2.9 3.0-3.9 4.0-4.9 5.0-9.9 10.0-24.9 ≥ 25.0		<input type="text"/> <input type="text"/>	
Δn	20 15 10 8 6 4 3 1		<input type="text"/> <input type="text"/>	
		89	<input type="text"/> <input type="text"/>	

SWITCH TO W PRGM PRESS F PRGM TO CLEAR MEMORY

KEY ENTRY	CODE SHOWN	COMMENTS	KEY ENTRY	CODE SHOWN	COMMENTS	REGISTERS	
LBL	23	COMPUTES $\int_0^x \frac{x^3}{(exp x - 1)} dx$	LN	07	exp -nx	R1 <u>x =</u> <u>C₂V/T</u>	
A	11		⊗	71	exp -nx()		
STO 1	33 01	X = C ₂ V/T	STO	33	Σ exp -nx()	R2 <u>Δn</u> <u>(# REITER.)</u>	
g R ↓	35 08	Δn (# REITERATIONS)	⊕	61			
STO 2	33 02		4	04			
LBL	23	SHIFTS Δn	g	35	Δn - 1	R3 <u>n</u>	
B	12	TO REG 8	DSZ	83			
RCL 2	34 02	Δn	GTO	22	NEXT		
STO 8	33 08		C	13	ITERATION		
LBL	23	REITERATION	RCL 4	34 04	Σ exp -nx() = $\int_0^x \frac{x^3}{(exp x - 1)} dx$	R4 <u>Σ →</u> $\int_0^x \frac{x^3}{(exp x - 1)} dx$	
C	13	SUB-PROGRAM	R/S	84	READOUT Σ		
I	01	ONE	GTO	22	RELOADS REG 8		
STO	33	n → n + 1	B	12	AND REPEATS (2Δn)	R5	
⊕	61			RTN	24	ENDS PROGRAM A	
3	03		LBL	23	COMPUTES		
RCL 1	34 01	x	D	14	x = C ₂ V/T	R6	
3	03	3	÷	81	V/T		
g	35	x ³	1	01	C ₂ = 1.438833	R7	
y ^x	05			⊙		83	
RCL 3	34 03	n	70 4	04			
÷	81	x ³ /n	3	03			
RCL 1	34 01	x	8	08			
RCL 3	34 03	n	8	08			
÷	81	x/n	3	03			
f ⁻¹	32	x ² /n ²	3	03			
√	09			⊗	71	C ₂ V/T = x	
3	03	3	RTN	24	READOUT X	R8 <u>Δn</u>	
⊗	71	3x ² /n ²	LBL	23	COMPUTES B(T) =		
⊕	61	x ³ /n + 3x ² /n ²	E	15	C ₁ C ₂ ⁻⁴ T ⁴ Σ exp -nx()	R9	
RCL 1	34 01	x	4	04		LABELS	
6	06	6	g	35	T ⁴ Σ exp -nx()	A $\int_0^x \frac{x^3}{(exp x - 1)} dx$	
⊗	71	6x	y ^x	05			B Δn → REG 8
RCL 3	34 03	n	⊗	71			C Σ (S.P.)
3	03	3	2	02			D X = C ₂ V/T
g	35	n ³	⊙	83			E C ₁ C ₂ ⁻⁴ T ⁴ Σ
y ^x	05			7	07		0
÷	81	6x/n ³	7	07	C ₁ /C ₂ ⁴ = 2.778649 x 10 ⁻¹³	1	
⊕	61	x ³ /n + 3x ² /n ² + 6x/n ³	8	08			2
6	06	6	6	06			3
RCL 3	34 03	n	4	04			4
4	04	4	9	09			5
g	35	n ⁴	EEX	43		6	
y ^x	05			CHS	42		7
÷	81	6/n ⁴	1	01		8	
⊕	61	(x ³ /n) + 3x ² /n ² + (6x/n ³) + (6/n ⁴)	⊗	71		9	
RCL 1	34 01	x	RTN	24	READOUT	FLAGS	
RCL 3	34 03	n			C ₁ C ₂ ⁻⁴ T ⁴ $\int_0^x \frac{x^3}{(exp x - 1)} dx$ = [B(T)] _∞	1	
⊗	71	nx					2
CHS	42	-nx					
f ⁻¹	32						

APPENDIX C

INTERIM PROGRESS REPORT

January 31, 1977

Note - Corrections to Table 3 have been made since the issuance of the original report. The water vapor mixing ratio of the sounding has also been corrected.

INVESTIGATE COMPONENTS OF NET RADIATION IN A MOUNTAIN VALLEY

INTERIM PROGRESS REPORT

January 31, 1977

Cooperative Agreement No. 16-629-CA

between

Colorado State University

and

U. S. Forest Service, RMFRES

This report documents the progress made in a theoretical study of the infrared radiation component of the surface energy budget in mountain valley topography.

An infrared radiative transfer program has been modified and utilized to simulate the transfer of infrared radiation through a valley atmosphere. Atmospheric constituent and temperature profiles, spectral bandpass, and viewing geometry may be specified in this program. Radiance and transmissivity values for various viewing angles, various spectral intervals, and at various levels in the model atmosphere constitute the output of the model.

The program can calculate values of radiance for any model atmosphere. We have chosen to use the following atmosphere:

isothermal: -5°C

surface pressure: 750 mb

CO_2 mixing ratio constant: .486 gm/kg

water mixing ratio: 4.5 gm/kg

A data tape has been created for this model atmosphere containing radiance and transmissivity values for zenith viewing angles of 0, 60, 65, 70, 75, 80, and 85° at 10 cm^{-1} spectral intervals from 210 cm^{-1} to 2260 cm^{-1} (i.e., from ~ 4.42 to 47.6μ). Values are calculated at pressure levels of 655, 680, 700, 715, 725, 730, 735, 740, and 745 mb as shown in Figure 1 and Table 1 below. Note that given an azimuth angle and pressure level we can determine the distance between the surface (750 mb) and the pressure level along the azimuth θ .

Using this data and assuming the initial symmetrical valley shape shown in Figure 2--namely a flat-bottomed valley with sides of constant slope and of infinite length capable of orientation in any arbitrary

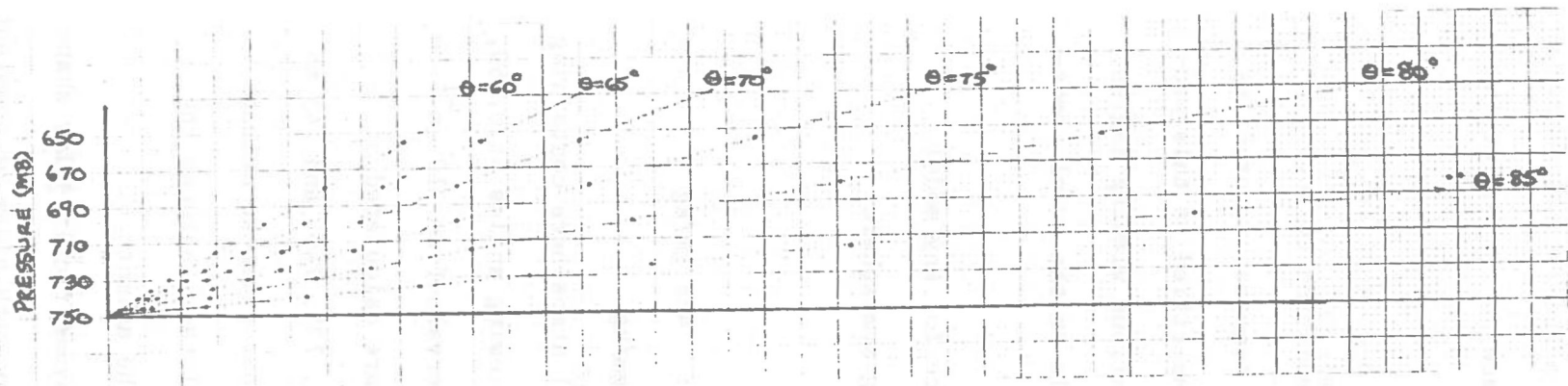


Figure 1. Grid showing radiance and transmissivity calculation points.

PRESSURE LEVEL (mb)	HEIGHT (M AGL)	From Surface distance (km) along zenith angle θ_1 to pressure level					
		$\theta = 60^\circ$	$\theta = 65^\circ$	$\theta = 70^\circ$	$\theta = 75^\circ$	$\theta = 80^\circ$	$\theta = 85^\circ$
655	1063	2.13	2.52	3.11	4.11	6.12	12.20
680	769	1.54	1.82	2.25	2.97	4.43	8.83
700	542	1.08	1.28	1.58	2.09	3.12	6.21
715	375	.75	.89	1.10	1.45	2.16	4.30
725	266	.53	.63	.78	1.03	1.53	3.05
730	212	.42	.50	.62	.82	1.22	2.43
735	159	.32	.38	.46	.61	.91	1.82
740	105	.21	.25	.31	.41	.61	1.21
745	53	.11	.12	.15	.20	.30	.60
750	0	—	—	—	—	—	—

Table 1. Calculation Point Data for Full Grid.

azimuth--we can choose points on the valley sidewall corresponding to the data points available and investigate the transmissivity of the atmosphere between the points as a function of wavelength.

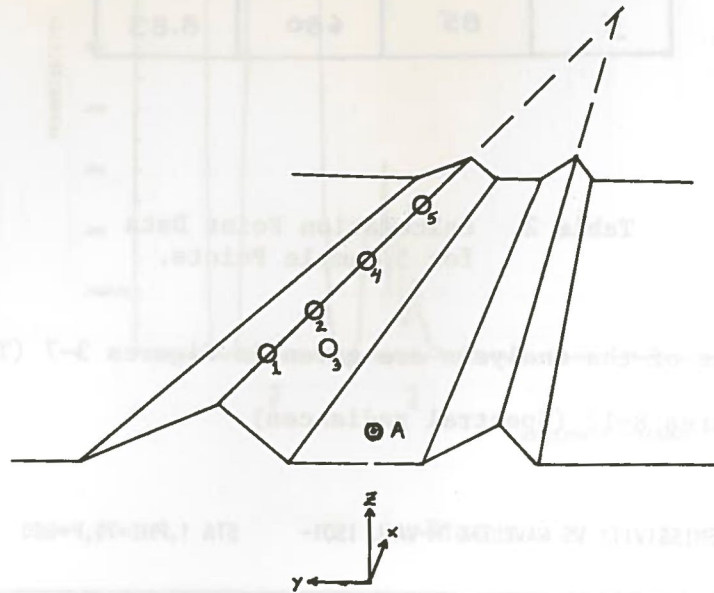


Figure 2. Idealized valley configuration with calculation points indicated.

Here, for example, we choose the point A to be in the center of the valley and the receptor points (1, 2, 3...5) to be along the sidewalls at varying distances and zenith angles from point A (Table 2).

POINT NUMBER	ZENITH ANGLE θ ($^{\circ}$)	PRESSURE LEVEL (mB)	DISTANCE From A (km)
1	70	680	2.25
2	75	680	2.97
3	75	715	1.45
4	80	680	4.43
5	85	680	8.83

Table 2. Calculation Point Data for 5 Sample Points.

The results of the analysis are given in Figures 3-7 (Transmissivities) and Figures 8-12 (Spectral radiances).

TRANSMISSIVITY VS WAVELENGTH-VAIL 1S01- STA 1, PHI=70, P=680

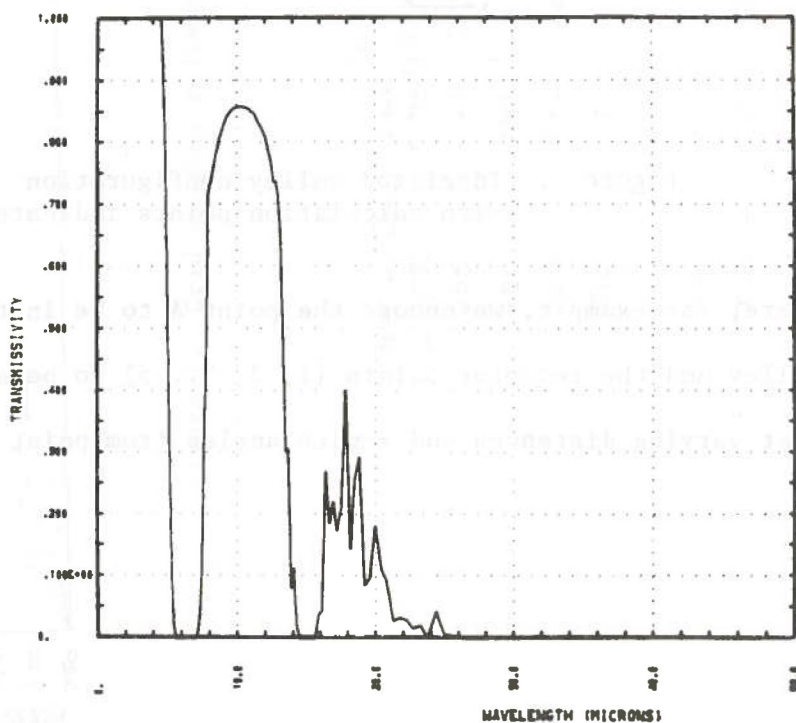


Figure 3.

TRANSMISSIVITY VS WAVELENGTH-VAIL 1S01- STA 2,PHI=75,P=680

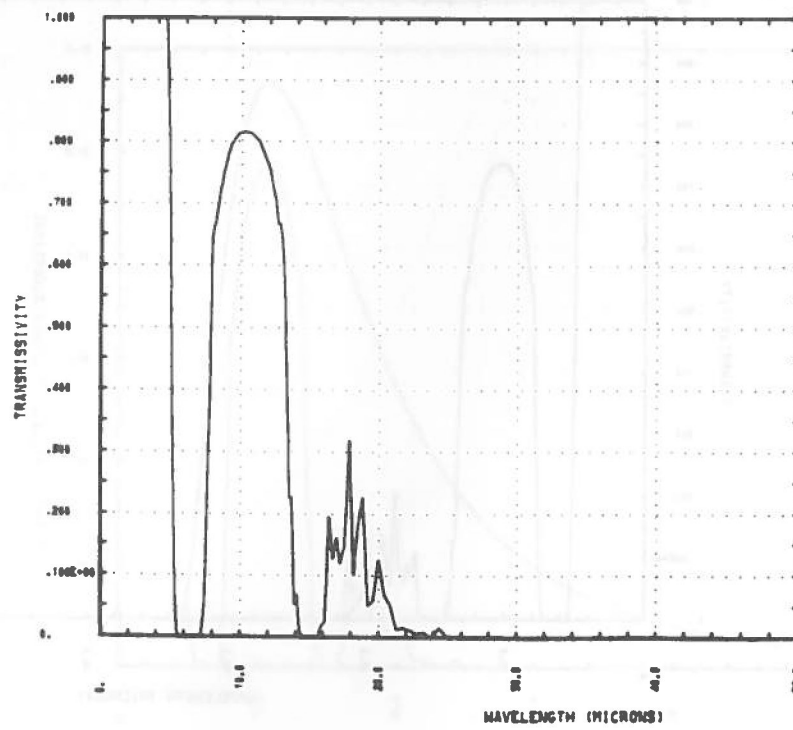


Figure 4.

TRANSMISSIVITY VS WAVELENGTH-VAIL 1S01- STA 3,PHI=75,P=715

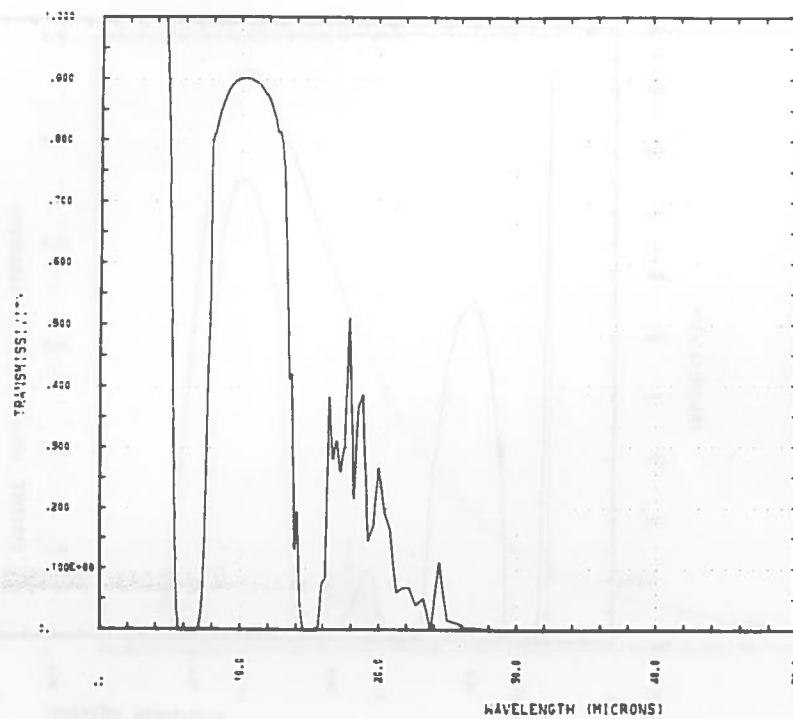


Figure 5.

TRANSMISSIVITY VS WAVELENGTH-VAIL 1S01- STA 4, PHI=80, P=680

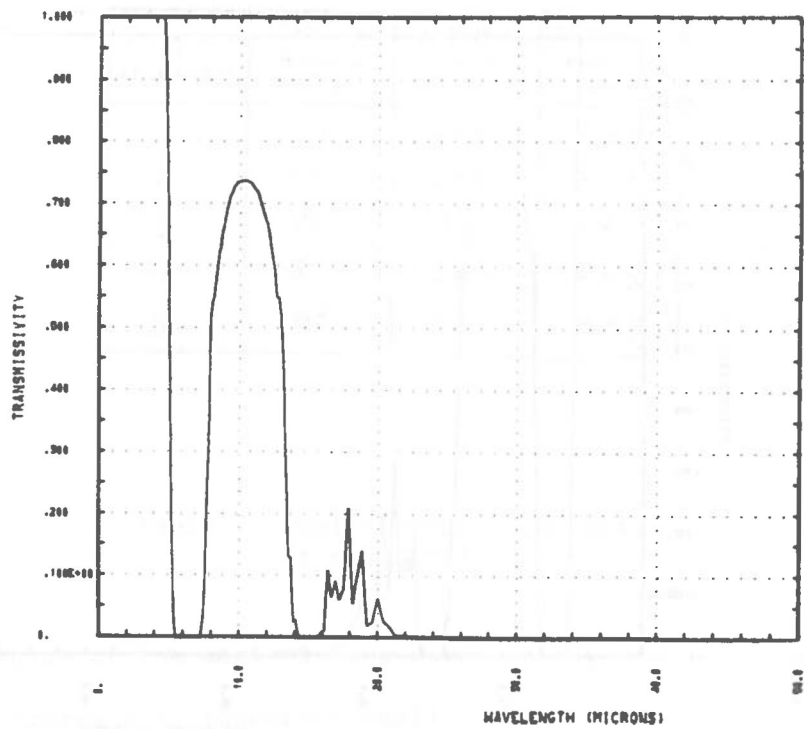


Figure 6.

TRANSMISSIVITY VS WAVELENGTH-VAIL 1S01- STA 5, PHI=85, P=680

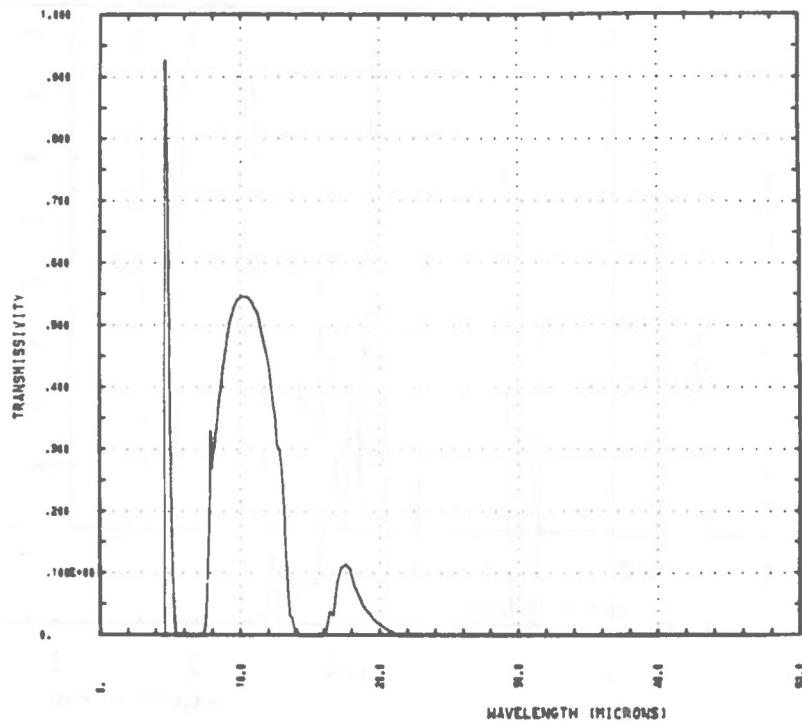


Figure 7.

BLACK BODY (A) AND SFC RADIANCE (B)-VAIL ISO1-STA 1, PHI=70, P=680

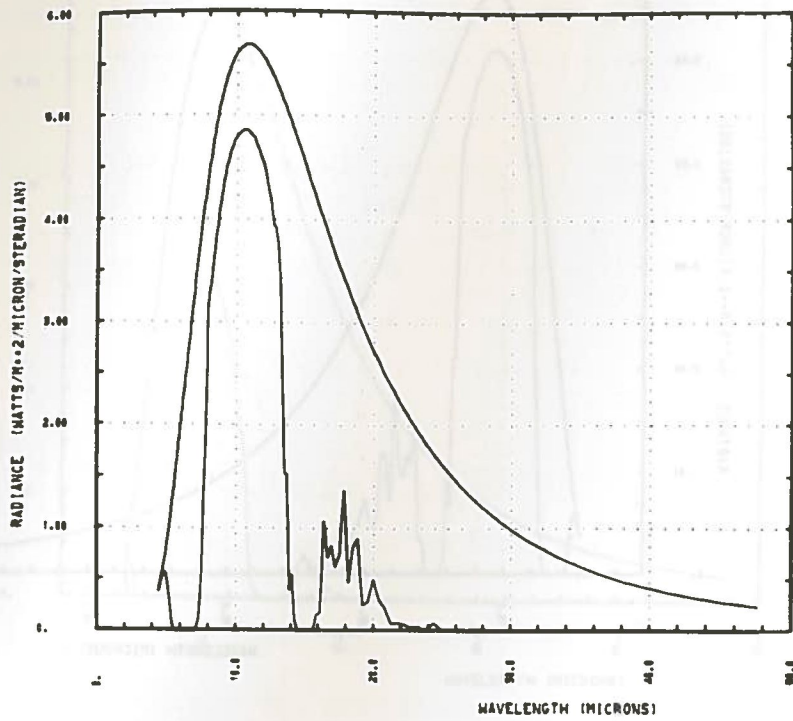


Figure 8.

BLACK BODY (A) AND SFC RADIANCE (B)-VAIL ISO1-STA 2, PHI=75, P=680

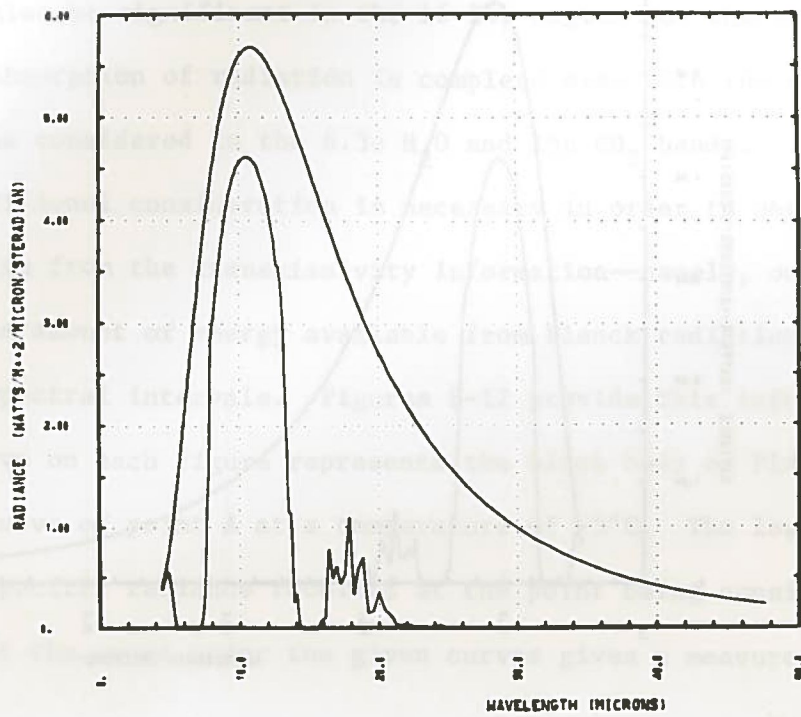


Figure 9.

BLACK BODY (A) AND SFC RADIANCE (B)-VAIL ISO1-STA 3, PHI=75, P=715

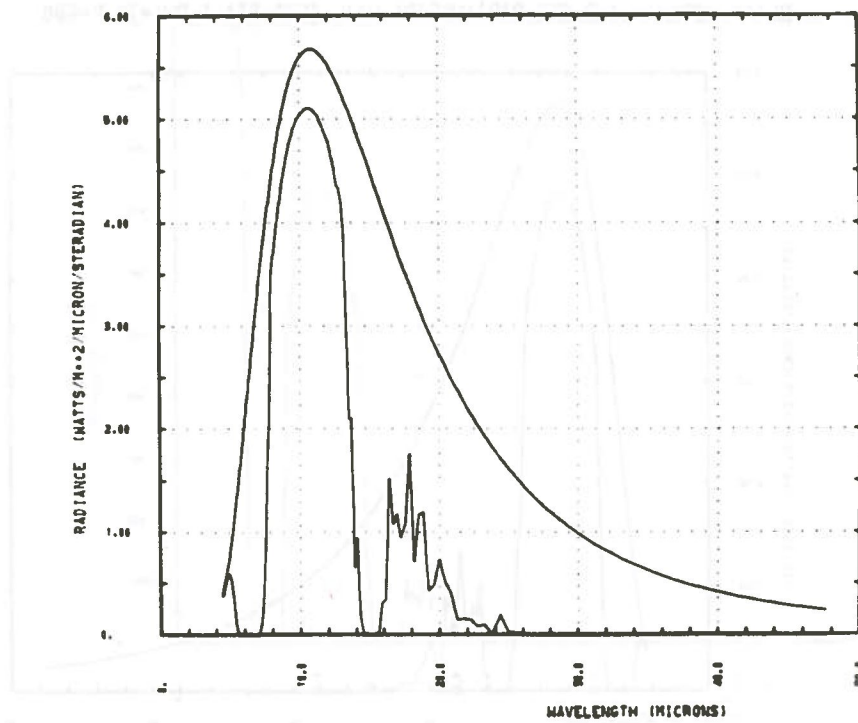


Figure 10.

BLACK BODY (A) AND SFC RADIANCE (B)-VAIL ISO1-STA 4, PHI=80, P=680

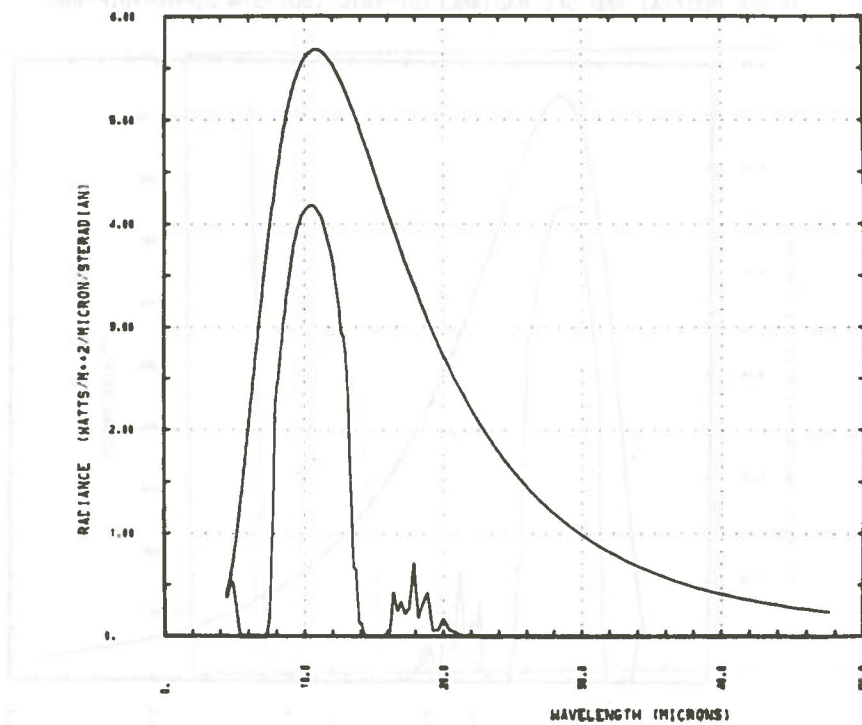


Figure 11.

BLACK BODY (A) AND SFC RADIANCE (B)-VAIL 1501-STA 5, PHI=85, P=680

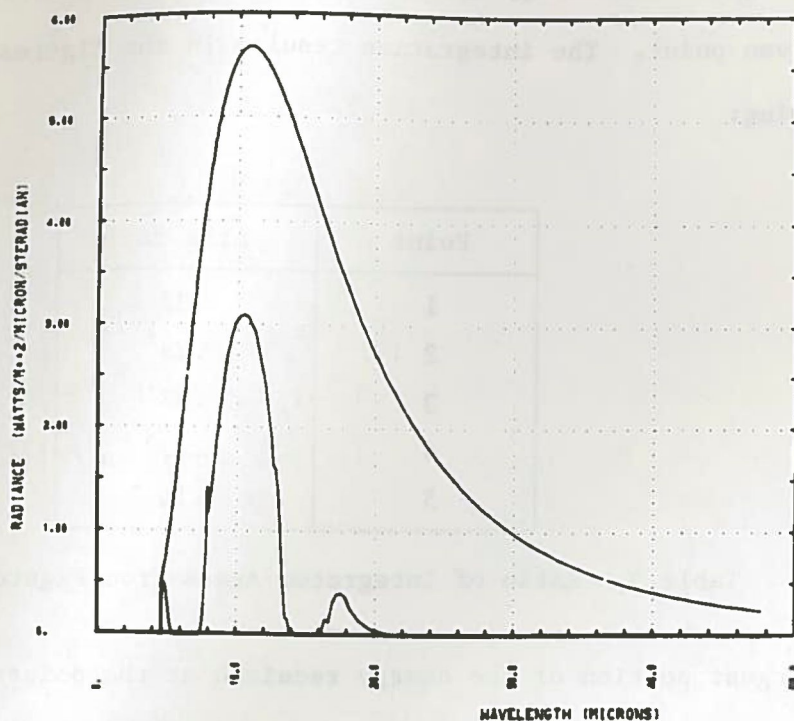


Figure 12.

Transmissivities are high in the 10μ window region. Transmissivities may also be significant in the $16-24\mu$ region for shorter path lengths. Absorption of radiation is complete even with the smaller path lengths considered in the 6.3μ H_2O and 15μ CO_2 bands.

An additional consideration is necessary in order to obtain practical results from the transmissivity information--namely, one must consider the amount of energy available from Planck radiation in the different spectral intervals. Figures 8-12 provide this information. The top curve on each figure represents the black body or Planck radiation curve of point A at a temperature of $-5^\circ C$. The lower curve shows the spectral radiance received at the point being considered. The ratio of the areas under the given curves gives a measure of the

percentage of the energy transmitted from point A that is received at the given point. The integration results in the figures in Table 3, following:

Point	Area ratio
1	.32
2	.29
3	.38
4	.23
5	.16

Table 3. Ratio of Integrated Areas from Figures 3-12.

The largest portion of the energy received at the points 1-5 comes through 2 spectral intervals--the 10μ window region and the $16-22\mu$ region.

This analysis, to date, has allowed us to focus attention on the spectral intervals of importance in the valley IR radiation component problem.

BIBLIOGRAPHIC DATA SHEET		1. Report No. ATIS Paper No. 279		3. Acquisition/Accession No.	
4. Title and Subtitle Components of Infrared Net Radiation in a Mountain Valley				5. Report Date October 1977	
7. Author(s) Thomas B. McKee and C. David Whiteman				8. Performing Organization Repr. No. 279	
9. Performing Organization Name and Address Department of Atmospheric Science Colorado State University Fort Collins, Colorado 80523				10. Project/Task/Work Unit No.	
				11. Contract/Grant No. US Forest Service Cooperative Agreement 16-629-CA	
12. Sponsoring Organization Name and Address U. S. Forest Service Rocky Mountain Forest and Range Experiment Station Fort Collins, Colorado 80521				13. Type of Report & Period Covered	
				14.	
15. Supplementary Notes					
16. Abstracts The infrared components of the surface radiation budget in a mountain valley have been investigated theoretically. Calculations were based on a set of winter and summer atmospheric soundings specifying temperature and moisture content and for two valley models including a linear valley model and a circularly symmetric valley model. Radiance and irradiance calculations are compared with similar calculations for flat terrain. Downward irradiances at the valley center were shown to be higher than for flat terrain and were due to radiation from the valley sidewalls. The largest effect was obtained for a dry winter atmosphere with the sidewalls warmer than the valley bottom. Downward irradiance was increased by 16% over the flat terrain case and the net irradiance at the valley center was decreased by 24% which would lead to a decreased surface cooling. The enhanced downward irradiance came predominantly from 2 spectral intervals--the atmospheric window (7.8-13.4 μ) and a small window at 16.3 to 20.2 microns.					
17. Key Words and Document Analysis. 17a. Descriptors Infrared Radiation Atmospheric Radiation Mountain Valleys Irradiance Radiance					
17b. Identifiers/Open-Ended Terms					
17c. COSATI Field/Group					
18. Availability Statement				19. Security Class (This Report) UNCLASSIFIED	
				21. No. of Pages 102	
				20. Security Class (This Page) UNCLASSIFIED	
				22. Price	